

Binary Classification as a Phase Separation Process

Rafael Monteiro

MONTEIRODASILVA-RAFAEL@AIST.GO.JP,
RAFAEL.A.MONTEIRO.MATH@GMAIL.COM

*Mathematics for Advanced Materials - Open Innovation Laboratory,
AIST, c/o Advanced Institute for Materials Research,
Tohoku University, Sendai, Japan*

Abstract

We propose a new binary classification model called Phase Separation Binary Classifier (PSBC). It consists of a discretization of a nonlinear reaction-diffusion equation coupled with an ODE, and is inspired by fluid behavior, namely, on how binary fluids phase separate. Hence, parameters and hyperparameters have physical meaning, whose effects are carefully studied in several different scenarios.

PSBC's coefficients are trainable weights, chosen according to a minimization problem using Gradient Descent; optimization relies on a classical Backpropagation with weight sharing. The model can be seen under the framework of feedforward networks, and is endowed with a nonlinear activation function that is linear in trainable weights but polynomial in other variables, yielding a cost function that is also polynomial.

In view of the model's connection with ODEs and parabolic PDEs, forward propagation amounts to an initial value problem. Thus, stability conditions are established using the concept of Invariant regions. Interesting model compression properties are thoroughly discussed. We illustrate the classifier's qualities by applying it to the subset of numbers "0" and "1" of the classical MNIST database, where we are able to discern individuals with more than 94% accuracy, sometimes using less only about 10% of variables.

Keywords: Phase-separation, Allen-Cahn model, binary classification, statistical machine learning, reaction-diffusion systems, maximum-principles, finite-differences methods, inverse problems.

1. Introduction

In practical terms, classification is a task that humans and machines perform in many different situations: distinguishing a good fruit from a bad one, deciding whether an article is worth reading or not, classifying the content of an image, recognizing hand-written numbers, classifying a device as defective or functional, or, in summary, assigning an object X to one of the M classes $\{0, \dots, M-1\}$. In the latter case, when $M = 2$, this process is called *binary classification*, which will be the main focus of this paper.

Scientific understanding of how a classification takes place concerns to the field of Machine Learning (ML). Here we are concerned with a particular case of binary classification using empirical risk minimization, tailoring the discussion in the sequel to these goals. We refer to (Boucheron et al., 2005; Devroye et al., 1996) for a more theoretical approach to supervised learning. Terminology in the field varies, and we mostly follow (Cucker and Smale, 2002) and (Shalev-Shwartz and Ben-David, 2014), pointing out to other references along the way.

In binary classification one assumes the existence of an unknown map $h : \mathcal{X} \rightarrow \{0, 1\}$, conveniently called *hypothesis*, that one aims to investigate and somehow reconstruct (or rather approximate) from information available only on a subset of \mathcal{X} . In other words, given a dataset (a sample) $\mathcal{D} := \{(X_{(i)}, Y_{(i)})\}_{1 \leq i \leq N_d} \subset \mathcal{X} \times \{0, 1\}$ and constraints

$$h(X_{(i)}) = Y_{(i)}, \quad (1.1)$$

one wishes to construct a map $\tilde{h} : \mathcal{X} \rightarrow \{0, 1\}$ that is a good approximation to $h(\cdot)$ in a certain sense. As such, since the constraints (1.1) are available for all $X_{(i)}$, this problem falls in the class of *supervised learning*. With regards to the quality of the aforementioned approximation, it can be measured for instance by the quantity

$$\text{Accuracy} = \frac{\text{cardinality} \left(\{i \in \{1, \dots, N_d\} \mid Y_{(i)} = \tilde{h}(X_{(i)})\} \right)}{N_d}, \quad (1.2)$$

which must then be maximized.¹

The nature of this problem allows one to write $h(\cdot) = \mathbb{1}_{\mathcal{A}}(\cdot)$, where $\mathbb{1}_{\mathcal{A}}(x) = 1$ whenever $x \in \mathcal{A}$, 0 otherwise. Hence, constructing an approximation to $h(\cdot)$ is equivalent to finding, or rather “learning”, the unknown set $\mathcal{A} = h^{-1}(\{1\})$. Once an approximation $\tilde{h} : \mathcal{X} \rightarrow \{0, 1\}$ is constructed, it can be applied to any element in \mathcal{X} in order to “predict” whether it does, or does not, belong to \mathcal{A} ; consequently, one refers to $\tilde{h}(\cdot)$ as a *predictor*. Whenever a probability measure $\mu(\cdot)$ is considered in the space $\mathcal{X} \times \{0, 1\}$, discovering \mathcal{A} is called PAC learning; cf. (Devroye et al., 1996, Chapter 12), (Cucker and Smale, 2002, Page 3).

In the form just described the problem is too complex, for the space of functions $\{g(\cdot) \mid g : \mathcal{X} \rightarrow \{0, 1\}\}$ is too big and lacks mathematical structure. In practice, one follows the heuristics of choosing a smaller space of functions $\mathcal{H} \subset \{g(\cdot) \mid g : \mathcal{X} \rightarrow \{0, 1\}\}$ where $\tilde{h}(\cdot)$ is sought for. We call \mathcal{H} a *hypothesis space*, whose choice has substantial consequences on properties and quality of the constructed approximations; cf. (Cucker and Smale, 2002, §3).

We briefly describe one of the techniques developed to construct the map $\tilde{h}(\cdot)$, using *feedforward networks* (Goodfellow et al., 2016, Chapter 6): these are graph structures devoid of cyclic loops, as seen in the diagram in Figure 1.

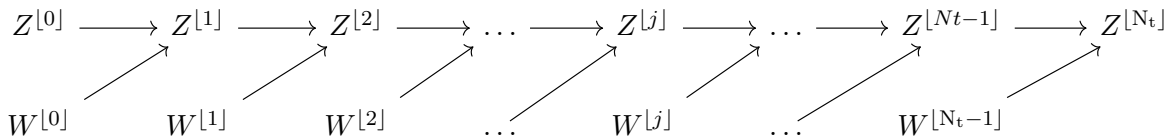


Figure 1: The forward propagation in a network with N_t layers and trainable weights $W^{[l]}$. An arrow from A to B indicates that B is a function of A .

For each $n \in \{0, \dots, N_t\}$ there exists an associated pair $(Z^{[n]}, W^{[n]}) \in \mathbb{R}^{z_n} \times \mathbb{R}^{w_n}$ referred to as a layer. When $n = 0$ and $n = N_t$, $Z^{[0]}$ and $Z^{[N_t]}$ are called respectively input layer (that receives input data from \mathcal{X}) and output layer; when $1 \leq n \leq N_t - 1$, the vectors $Z^{[n]}$ are called *hidden layers*. The variables $W^{[0]}, \dots, W^{[N_t-1]}$ are referred to as *trainable weights*, and are used for optimization purposes. Layers are all connected to each other in a hierarchical (that is, in a tree-like) fashion as

$$Z^{[n+1]} = \sigma^{[n]} \left(Z^{[n]}, W^{[n]} \right), \quad \text{for } 0 \leq n \leq N_t - 1. \quad (1.3)$$

The maps $\sigma^{[n]} : \mathbb{R}^{z_n} \times \mathbb{R}^{w_n} \rightarrow \mathbb{R}^{z_{n+1}}$ are called *activation functions* and can be endowed with different properties as differentiability, decay in the far-field, etc; cf. (Hastie et al., 2001). Last, one associates to this network a loss function $L(Z, W, Y)$ that evaluates the sequence $Z = (Z^{[0]}, \dots, Z^{[N_t]})$ and its proximity to a given label $Y \in \{0, 1\}$ at a specific parameter value $W = (W^{[0]}, \dots, W^{[N_t-1]})$. Using

1. Or minimizing the quantity $1 - \text{Accuracy} = \frac{\text{cardinality}(\{i \in \{1, \dots, N_d\} \mid Y_{(i)} \neq \tilde{h}(X_{(i)})\})}{N_d}$, called *misclassification error*; cf. (Devroye et al., 1996).

the whole dataset \mathcal{D} , these quantities make up a cost function $\text{Cost}_{\mathcal{D}}(\cdot)$ of the form

$$\text{Cost}_{\mathcal{D}}(W) = \sum_{i=1}^{N_d} \frac{L(Z_{(i)}, W, Y_{(i)})}{N_d}, \quad (1.4)$$

that one minimizes by optimization on W , as we explain next in detail.

Construction of $\tilde{h}(\cdot)$ from data is called *training* or *model fitting*, and is carried out using the network (1.3). First, one generates an initial sequence of trainable weights $W_0 := (W^{[0]}, \dots, W^{[N_t-1]})_0$ either randomly or deterministically. Then, for each pair of elements in $\mathcal{D} = \{(X_{(i)}, Y_{(i)})_{1 \leq i \leq N_d}\} \in \mathcal{X} \times \{0, 1\} = \mathbb{R}^{k_0} \times \{0, 1\}$ one sets $Z^{[0]} = X_{(i)}$ and generates a sequence $Z_{(i)} := (Z^{[0]}, \dots, Z^{[N_t]})_{(i)}$ using the feedforward network (1.3). Afterwards, W is updated using Gradient Descent,

$$W_{q+1} := W_q - \eta_q \frac{\partial \text{Cost}_{\mathcal{D}}(W)}{\partial W} \Big|_{W=W_q}, \quad q \in \mathbb{N}, \quad (1.5)$$

where W_q denotes the q -th iteration of this process.

Each iteration (1.5) to update W is called an *epoch*. The quantities η_q are positive numbers that receive the name of *learning rates* and may vary across epochs. The computation of sequences $Z_{(i)}$ is called *forward propagation*, while computing the derivatives of the cost with respect to Z and W is referred to as *backpropagation*; altogether, the algorithmic organization of this process receives the name of *Backpropagation Algorithm* (BP), and is one of the cornerstones in the field of ML (LeCun et al., 2012; Rumelhart et al., 1986); see Figure 2.

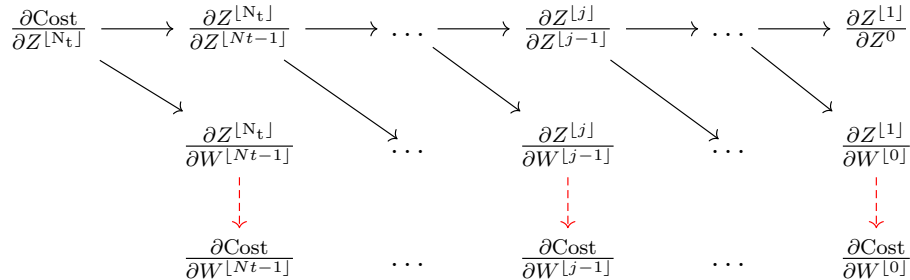


Figure 2: Classical Backpropagation algorithm. Its development was a major improvement in the design of the algorithms to perform gradient descent. Full arrows for A to B denote composition ($A \circ B$). Dashed arrows from A to B denote variable assignment ($A \leftarrow B$); see further details in Appendix B, Algorithm 2.

Once iterations satisfy a stopping criteria (like tolerance, or some threshold), a parameter W_* is obtained, and a class assignment, or *discrimination rule*, takes place, corresponding in our case to

$$\tilde{h}(X_{(i)}) := \begin{cases} 1, & \text{if } L(Z_{(i)}, W_*, 1) \leq L(Z_{(i)}, W_*, 0), \\ 0, & \text{otherwise,} \end{cases} \quad (1.6)$$

finally completing the construction of $\tilde{h}(\cdot)$. There are several challenges presented along the way though: the structure of the cost function's landscape can be very complex and in many applications optimizing with respect to W consists of a non-convex optimization problem, a difficulty that has receiving extensive attention of researchers in recent years (Choromanska et al., 2015; Sagun et al., 2016). Among other things, research has also focused on how to speed up the training process (Møller, 1993), the approximation of trainable weights evolutions of ANNs (when the number of nodes is large) using Mean Field theory (Mei et al., 2018), in finding different reformulations of the optimization process using Partial Differential Equations (Chaudhari et al., 2018), and the interplay between ML and dynamical systems (Brunton and Kutz, 2019).

It is worthwhile to emphasize that the feedforward network architecture in Figure 1 is ubiquitous in ML, appearing in Neural Networks, Convolution Neural Networks, among other models, some of which are considered analogies to the brain or human vision functioning. To what extent these models just mimic or are a faithful description of any biological processes is unclear and sometimes disputed (Mumford, 1997); in this paper, however, we shall leave these considerations aside. We propose a new ML model whose motivation stems from a physical phenomenon by no means related to Biology nor (at least in principle) “brain-like” structures, but fluids and their dynamics: our model is inspired by how binary fluids phase separate.

In full generality, the model propagates features using two variables that evolve simultaneously,

$$\frac{U_m^{[n+1]} - U_m^{[n]}}{\Delta_t^u} := \varepsilon^2 \left(U_{m+1}^{[n+1]} - 2U_m^{[n+1]} + U_{m-1}^{[n+1]} \right) + f(U_m^{[n]}; \alpha_m^{[n]}), \quad \text{for } 1 \leq m \leq N_u, \quad (1.7a)$$

$$\frac{P_j^{[n+1]} - P_j^{[n]}}{\Delta_t^p} := f(P_j^{[n]}; \beta_j^{[n]}), \quad \text{for } 1 \leq j \leq N_p, \quad (1.7b)$$

where $f(u, w) = u(1 - u)(u - w)$ and parameters $\alpha^{[l]}$ in $\beta^{[l]}$ are “trainable weights”, hence learned from data. Initial conditions $U^{[0]}$ are individuals’ features, thus forward propagation amounts to an initial value problem; note that diffusion takes place in feature space. Further details are given below.

Definition 1.1 (Phase Separation Binary Classifier - PSBC) *When a discrimination rule as in (1.6) is allied the numerical scheme (1.7), we say that we have a Phase Separation Binary Classifier, denoted in short as PSBC. As we discuss below, (1.7) falls in the class of feedforward networks, and in the sequel is also called PSBC model, whereas evolution of an initial condition is called forward propagation (see Figure 1). Whenever $\varepsilon = 0$ (resp., $\varepsilon > 0$) we refer to this classifier as non-diffusive PSBC (resp., diffusive PSBC).*

It is shown in Section 5 that the feedforward networks’ formulation (1.3) is sufficiently broad to encompass the PSBC model (1.7), then written as

$$\begin{pmatrix} U^{[n+1]} \\ P^{[n+1]} \end{pmatrix} := \sigma^{[n]} \left(U^{[n]}, W_U^{[n]}, P^{[n]}, W_P^{[n]} \right), \quad \text{with } W_U^{[n]} := \alpha^{[n]}, \quad W_P^{[n]} := \beta^{[n]}. \quad (1.8)$$

Nevertheless, when compared with some state-of-art binary classifiers there are striking differences, many of which we investigate and highlight throughout the text. For instance: the first term on the right hand side of (1.7a), a discretization of the Laplacian, consists of a diffusion operator acting on features; $f(\cdot, \cdot)$ is a nonlinear reaction term that is common in thresholding phenomena, and mostly plays a role on classification of an individual $X_{(i)}$ into one of the elements in $\{0, 1\}$. It is worth saying that the nonlinearity is the same in both systems (1.7a) and (1.7b), although their parameters $\alpha^{[l]}$ and $\beta^{[l]}$ are not, and must be optimized using the dataset \mathcal{D} .

Let’s briefly describe each variable in the PSBC, without attempting to fully elucidate their role at this point. The scalars $\Delta_t^u, \Delta_t^p > 0$ and $\varepsilon \geq 0$ are *hyperparameters* - quantities that are neither optimized, nor inputs in \mathcal{X} - and must be chosen in advance: the first two are due to time discretization, whereas the latter is a diffusion (or viscosity) term. We set $U^{[0]} = X \in \mathcal{X}$, with X representing features of an individual; thus, for each feature X_m we set $U_m^{[0]} := X_m$, $1 \leq m \leq N_u$. Note that $U^{[n]} \in \mathbb{R}^{N_u}$ for all layers, where N_u is the Euclidean dimension of \mathcal{X} . The values of $U_0^{[l]}$ and $U_{N_u+1}^{[l]}$ are imposed according to boundary conditions, which in our case are either of Neumann (Section 5) or Periodic type (Remark 6.3). A companion quantity $P^{[l]}$ follows an ODE (1.7b) with same nonlinearity as that in (1.7a) and initial condition $P_j^{[0]} = \frac{1}{2}$ for $1 \leq j \leq N_p$; it has a crucial role that we clarify in Section 3. The vectors $\alpha^{[l]} \in \mathbb{R}^{N_u}$ and $\beta^{[l]} \in \mathbb{R}^{N_p}$ contain variables that must be optimized according to a

cost function. The number N_p is either 1 or a value N_{ptt} that indicates the dimension of the subspace where $\alpha^{[\cdot]} \in \mathbb{R}^{N_u}$ lies; see discussion in Section 4.

Throughout this paper we write $U^{[\cdot]}(X; \alpha^{[\cdot]})$ to represent the flow of X through (1.7a) or, in a different terminology, we say that X is propagated by $U^{[\cdot]}$; the same holds in the case $P^{[\cdot]}(\frac{1}{2}; \beta^{[\cdot]})$ with respect to (1.7b). In addition to that, we require a normalization condition of the initial data $X \in \mathcal{X}$,

$$X \in [0, 1]^{N_u}, \quad (\text{N-C})$$

easily attained by data preprocessing. As we shall see in Section 2.1, the main reason to enforce (N-C) is assuring that at any given epoch the forward propagation takes place inside an invariant region.

In order to explain other qualities of the PSBC we need to understand the numerical scheme (1.7) and its contrasting differences to other ML models. In the next section we present a succinct discussion of nonlinear diffusion equations, on which the mathematical and physical core of the PSBC model stand.

1.1 Mathematical setting: nonlinear diffusion equations (the heart of the matter)

Clearly, the numerical scheme (1.7a) is a semi-implicit finite-differences discretization² of

$$\begin{aligned} \partial_t u(x, t) &= \varepsilon^2 \partial_x^2 u(x, t) + u(x, t)(1 - u(x, t))(u(x, t) - \alpha(x)), & x \in [0, 1], \\ \partial_x u(0, t) &= 0, \quad \partial_x u(1, t) = 0, & u(x, 0) = u_0(x), \end{aligned} \quad (1.9)$$

a nonlinear diffusion equation that describes phase separation in binary alloys and is known as *Allen-Cahn equation* (Allen and Cahn, 1979; Aronson and Weinberger, 1978; Fife, 1979). Equation (1.9) is one of the fundamental models in the theory of pattern formation; cf. (Nishiura, 2002, Chapter 4.2), (Dennis et al., 2015, IV.27).

In equation (1.9) time is represented by t , while x represents space. The scalar $u(x, t)$ denotes a macroscopic quantity that measures the relative proportion of two different species at (x, t) . The quantity $\varepsilon \geq 0$ represents a diffusive term, and for this reason we call the model diffusive (resp., non-diffusive) whenever $\varepsilon > 0$ (resp. $\varepsilon = 0$). Finally, $\alpha(\cdot) \in \mathbb{R}$ describes the medium's spatial heterogeneity, being paramount to understanding how the initial value problem associated to (1.9) evolves; see Figure 3 for some illustrative examples.

Following (Angenent et al., 1987), we begin to understand the Allen-Cahn equation by first considering $\varepsilon = 0$ and $\alpha(\cdot) \in (0, 1)$: in this case, for each $x \in [0, 1]$ the dynamics in (1.9) decouples, yielding an ODE with two stable attracting points: $u \equiv 0$ and $u \equiv 1$. These limits are attained according to the initial state; namely, assuming that $\{x \in [0, 1] \mid u(x, 0) = \alpha(x)\}$ has measure zero, we have convergence (almost everywhere) to

$$\lim_{t \rightarrow \infty} u(x, t) = \begin{cases} 1, & \text{when } u(x, 0) > \alpha(x), \\ 0, & \text{when } u(x, 0) < \alpha(x). \end{cases} \quad (1.10)$$

Interestingly, the limiting function $\lim_{t \rightarrow \infty} u(x, t)$ assumes (almost everywhere) only two values, 0 and 1, in sharp contrast with $\alpha(\cdot)$ and the initial condition $u(\cdot, 0)$, both x -dependent. If we bear in mind the previous discussion, one can imagine an initial condition $u(\cdot, 0) := v^0(\cdot)$ as features of an individual with a class tag $Y \in \{0, 1\}$, where $\alpha(\cdot)$ is a parameter measuring correlations among features; as time evolves, the quantity $\alpha(\cdot)$ - in synergy with the nonlinearity $f(\cdot)$ - acts to classify $v^0(\cdot)$ in the ‘‘correct’’ way, which amounts to satisfying $\lim_{t \rightarrow \infty} u(\cdot, t; v^0) = Y$.

2. We have omitted a spatial discretization term Δx in (1.7a), which can be recovered by redefining ε as $\frac{\varepsilon}{\Delta x}$.

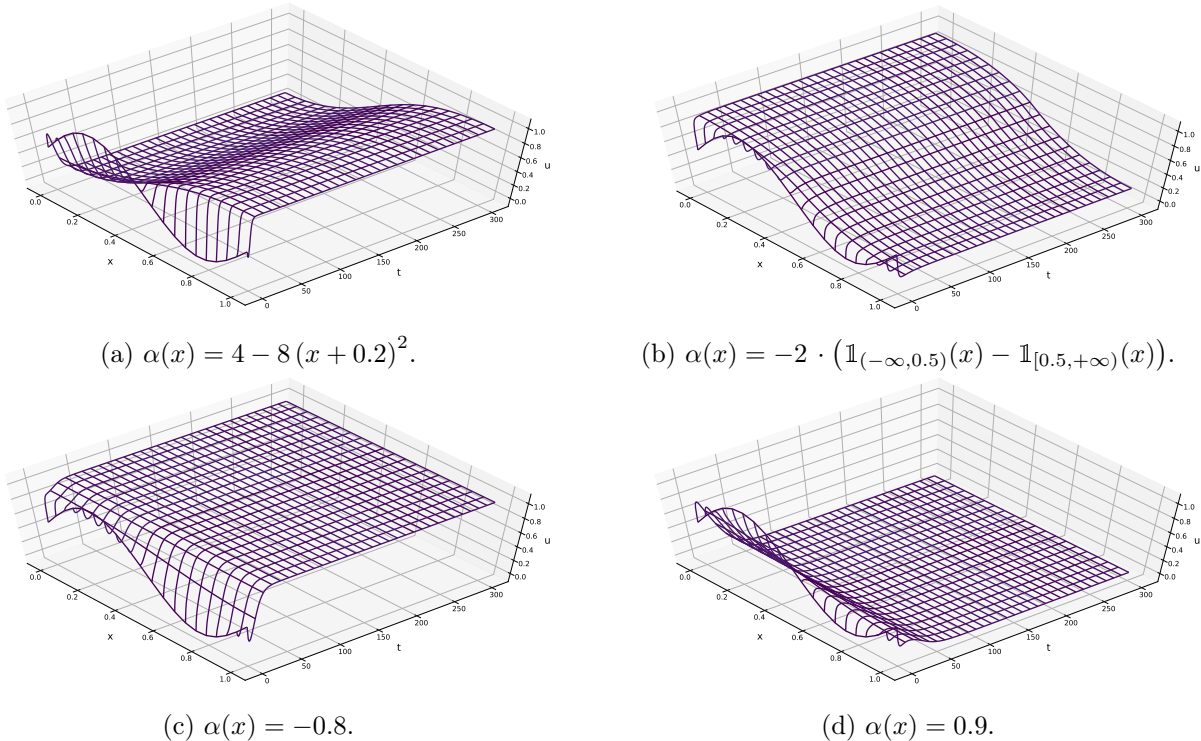


Figure 3: Numerical simulations of the Allen-Cahn equation (1.9) using (1.7a) and different parameters $\alpha(\cdot)$. The initial conditions are fixed $u(x, t = 0) = \frac{1}{2} - \frac{1}{2} \sin(\pi(2x - 1))$, on $x \in [0, 1]$ with homogeneous Neumann boundary conditions. We use an uniform spatial grid with $N_u = 20$ points; $N_t = 300$, $\Delta_t^u = 0.1$, and $\varepsilon = 0.3$.

The mathematical study of (1.9) and other nonlinear diffusion equations is extensive (Ni, 2011). Under the framework of gradient-flows, it was shown in (Chafee, 1975) that, whenever $\alpha(\cdot)$ is a constant α , the only possible limit of (1.9) are constant solutions; consequently, in the case $0 < \alpha < 1$ this result implies that the only stable solutions are $u(\cdot) \equiv 0$ and $u(\cdot) \equiv 1$. Afterwards, the interplay between geometry and dynamics was brought to the limelight in the seminal paper (Casten and Holland, 1978), where it was proven that all stable solutions are constants also in the (spatial) multidimensional case, whenever the domain is convex; cf. (Ni, 2011, Chapter 2).

There is a drastic change in the behavior of (1.9) when $\alpha(\cdot)$ is allowed to be non-homogeneous in space. In such case a larger class of stable non-constant stationary solutions can be constructed: it is shown in (Angenent et al., 1987) that for some (non-constant) $\alpha(\cdot) \in C^1([-1, 1]; \mathbb{R})$ it is possible to construct stable stationary solutions $u(\cdot)$ that display several layers separating regions where $u(\cdot)$ is either close to 0 or close to 1; see also (Rocha, 1988) and (Hale, 1988, Chapter 4, sec. 4.3.8).

Naturally, as we see the implications of the choice for $\alpha(\cdot)$ on the asymptotic behavior of (1.9), especially if we have binary classification in mind, one can think about the following inverse problem: for some fixed $T^* > 0$ (possibly $T^* = +\infty$) and given functions $v^0(\cdot)$ and $v^{T^*}(\cdot)$, is it possible to find a function $\alpha(\cdot)$ and an associated solution $u(x, t)$ to (1.9) such that

$$u(x, t) \Big|_{t=0} = v^0(x) \quad \text{and} \quad \lim_{t \uparrow T^*} u(x, t) = v^{T^*}(x)?$$

It is worth noticing that (1.9) is local but the equations to recover $\alpha(\cdot)$ are not, a common feature of inverse problems (Keller, 1976). With slightly more generality, we pose the previous question as a variational problem:³

3. Or as a dynamic programming control problem; see discussion in Section 6.11.

Problem 1.2 (Non-homogeneous α problem – continuum version) Let \mathcal{B} and \mathcal{A} be Banach spaces, and assume that for any initial conditions in $v^0 \in \mathcal{X} \subset \mathcal{B}$ and $\alpha = \alpha(\cdot) \in \mathcal{A}$ the evolution model (1.9) exists and is represented by $u(x, t; v^0)$. Given a family $\left\{ \left(v_{(i)}^0(\cdot), v_{(i)}^{T^*}(\cdot) \right) \right\}_{i \in \Gamma} \in \mathcal{X} \times \mathcal{T} \subset \mathcal{B} \times \mathcal{B}$ (possibly uncountable), find the best $\alpha(\cdot) \in \mathcal{A}$, if attainable, that minimizes

$$\lim_{t \uparrow T^*} \|u(\cdot, t; v_{(i)}^0) - v_{(i)}^{T^*}(\cdot)\|_{\mathcal{B}}. \quad (1.11)$$

Roughly speaking, the goal is that of reconstructing the heterogeneity of the media intrinsically contained in $\alpha(\cdot)$. In other words, we aim to “learn $\alpha(\cdot)$ from data”, where data consists of pairs of initial conditions $u(\cdot, t) \Big|_{t=0} = v^0(\cdot) \in \mathcal{X}$ and target functions $v^{T^*}(\cdot) \in \mathcal{T}$. Problem 1.2 poses an interesting question that motivates a closely related but discrete formulation of it in Problem 1.3, the backbone of the PSBC model.

Problem 1.3 (Non-homogeneous α problem – discrete version) Let $N_t \in \mathbb{N}$. For all $0 \leq n \leq N_t$, denote by $U^{\lfloor \cdot \rfloor}(X; \alpha^{\lfloor \cdot \rfloor}) \in \mathbb{R}^{N_u}$ the solution to the discretized PDE (1.7) (ODE, when $\varepsilon = 0$), of which $\alpha^{\lfloor \cdot \rfloor} \in \mathbb{R}^{N_u}$ is a parameter. Given a map $\mathcal{F} : \mathbb{R}^{N_u} \rightarrow \mathbb{R}^{N_u}$ and a dataset $\mathcal{D} = \{(X_{(i)}, Y_{(i)})\}_{1 \leq i \leq N_d} \subset \mathcal{X} \times \{0, 1\} \subset \mathbb{R}^{N_u} \times \{0, 1\}$, for all $0 \leq n \leq N_t - 1$ find $\alpha^{\lfloor n \rfloor} \in \mathbb{R}^{N_u}$ that minimizes

$$\text{Cost}_{\mathcal{D}}(\alpha^{\lfloor \cdot \rfloor}) = \sum_{i=1}^{N_d} \frac{1}{N_d} \left\| \mathcal{F} \left(U^{\lfloor N_t \rfloor}(X_{(i)}, \alpha^{\lfloor \cdot \rfloor}) \right) - Y_{(i)} \mathbf{1} \right\|_{\ell^2(\mathbb{R}^{N_u})}^2. \quad (1.12)$$

Let’s clarify the similarities and differences between both problems.

Clearly, if one takes the identity map $\mathcal{F}(V) = V$, minimizing (1.12) can be seen as an approximate formulation to minimization of (1.11). However, this approach does not imply high accuracy. In fact, the structure of $\mathcal{F}(\cdot)$ is non-trivial, whereby we bring the companion equation (1.7b) into play, as we shall see in Sections 2 and 3.

Unlike Problem 1.2, the target space in Problem 1.3 consists of a much simpler - binary - set that only contains the vectors $\mathbf{0}$ and $\mathbf{1}$ (respectively, vectors with only 0’s, or 1’s; see notation in Section 1.3).⁴ As we shall see, quantitative and qualitative properties of Problem 1.3 change whenever we consider a scalar model ($N_u = 1$, $N_p \in \{0, 1\}$; Sections 2 and 3), the system case ($N_u \geq 2$), a non-diffusive regime $\varepsilon = 0$ (Section 4), and a diffusive regime $\varepsilon > 0$ (Section 5). Furthermore, upon discretization we add a higher degree of flexibility to the problem by, for instance, allowing $\alpha^{\lfloor \cdot \rfloor}$ to vary over layers. In this way, finding a suitable trainable weight that minimizes (1.12) is related to problems in optimal control; see Section 6.11 for further discussion.

Remark 1.4 (The PSBC model with a single feature) In the non-diffusive PSBC with a single feature ($N_u = 1$ and $\varepsilon = 0$), its component (1.7a) can be interpreted as a discrete ODE modeling a nothing-or-all system, that is, a phenomenon of binary nature, which resembles neurons’ reaction to stimuli: depending on a threshold (in this case, denoted by $\alpha(\cdot)$), stimuli are classified as inhibitory or excitatory. An interesting discussion about mathematical modeling of nothing-or-all systems, besides further observations, can be found in (Neumann et al., 1966, pages 296-298, in “The General and Logical Theory of automata”), and in the work of Zeeman, who investigated the analogy between oscillators, catastrophe theory, and brain behavior (Zeeman, 1976).

4. We remark that this target space is simply a subset of the vector space $\ell^2(\mathbb{R}^{N_u})$ with induced topology, but not a vector space.

1.2 Outline of the paper

This paper has two main goals: first, to introduce the PSBC and second, to elaborate some of its fundamental mathematical properties, mostly by analysis of the numerical scheme (1.7) it is based upon. A glimpse at the latter and at (1.12) - which together make up the PSBC - shows that there are many parameters to be accounted for. Therefore, for pedagogical purposes, we begin by taking the whole classifier apart, gradually reassembling it piece by piece, elucidating each parameter's functionality along the way. This approach also has the secondary benefit of illustrating the use of the classifier in simple problems before stepping into more general, or rather abstract, constructions. The mathematical questions we address are mostly driven by usual difficulties in training ML models, among them: the extreme difficulty in training Deep Networks ($N_t \gg 1$) and blow up of trainable weights; in the ML literature the latter is sometimes referred to as *saturation of layers*; cf. (Glorot and Bengio, 2010).

Optimization is carried out using Stochastic Gradient Descent, which lies on the foundations of many other optimization methods and, overall, is directly amenable to quantitative mathematical investigation (see for instance Proposition 6.3). Numerically, we use the Backpropagation Algorithm and a variation of it that uses weight sharing (or parameter sharing); cf. (Nowlan and Hinton, 1992), (Goodfellow et al., 2016, Chapter 7.9).

Definition 1.5 (Weight sharing) *We say that a feedforward network (1.3) with N_t layers has weights- K -sharing property whenever*

$$W = \left(W^{[0]}, \dots, W^{[N_t-1]} \right), \quad \text{with} \quad W^{[i+j]} := W^{[i]} \quad \text{for} \quad i \in K\mathbb{Z}, \quad j \in \{0, \dots, K-1\}.$$

Weight sharing can be seen both as a model-compression, whereby a smaller set of parameter need to be physically stored, and also as a regularization technique aiming to avoid over-fitting. As we shall see in Section 4 and 6.7, this is not the only form of model compression that the PSBC relies on.

In our simulations we shall consider two somewhat extreme cases of the above scenario: weights-1-sharing, when no trainable weights are shared across layers, as in standard ANNs (see Figure 1), and weights- N_t -sharing, when all trainable weights are shared among layers (see Figure 4).⁵ Because of

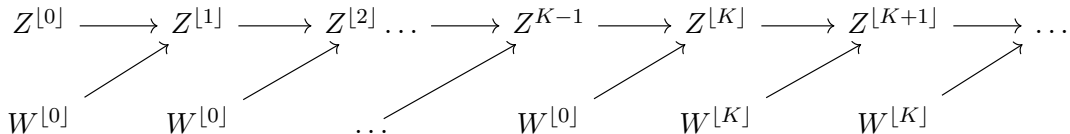


Figure 4: Forward propagation in a weights- K -sharing model with N_t layers. An arrow from A to B indicates that B is a function of A .

the Gradient Descent iteration (1.5) computing derivatives of a cost function associated to this model requires minor adaptations in the classical Backpropagation algorithm; see the diagram in Figure 5 and Appendix B.

There is an evident correspondence between forward propagation and the initial value problem associated with (1.7), therefore it is pertinent to address the model's numerical stability, which is known to depend on both spatial and temporal mesh grid size constraints. We adopt in (1.7a) a semi-implicit (parabolic) scheme in order to avoid any stability constraints on parameters Δ_t^u and Δx ,

5. In light of the previous discussion, allowing $\alpha^{[n]}$ to vary across layers $0 \leq n \leq N_t - 1$ parallels to having $\alpha(\cdot, \cdot)$ with both spatial and time dependence in the continuum model (1.9), whereas sharing $\alpha^{[0]} = \dots = \alpha^{[N_t-1]}$ across layers (weights- N_t -sharing model) seems much closer to the case investigated in (Angenent et al., 1987), where only time-independent $\alpha(\cdot)$ are considered; interestingly, the numerical behavior of $\alpha^{[j]}$ is reversed in both cases; see Section 2 and Figure 9.

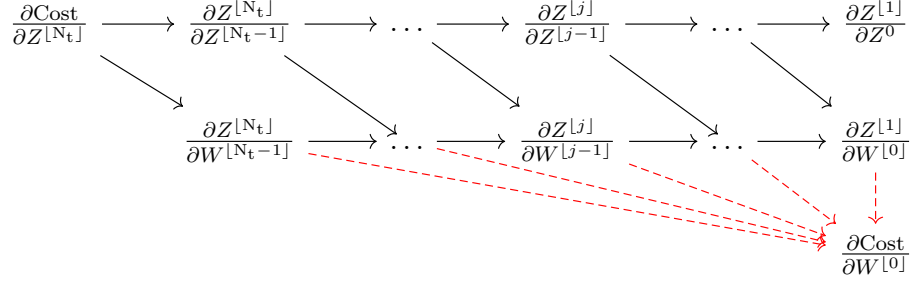


Figure 5: A diagram depicting backpropagation with weights- N_t -sharing, in which all N_t trainable weights are the same. Full arrows for A to B denote composition ($A \circ B$). Dashed arrows from A to B denote variable assignment ($A \leftarrow B$); when several dashed arrows point to the same node, values are added up before assignment. See Appendix B, Algorithm 1.

at least at the linear level:⁶ when the nonlinearity in (1.7a) is ignored the scheme is unconditionally stable. Nevertheless, when nonlinearities are included, blow-up of $U^{[l]}$ and $P^{[l]}$ (which numerically translates as a floating number overflow) is possible, and must be analyzed with care, specially if one contemplates the use of an arbitrary number of layers N_t .

In addition to all of the above concerns, forward propagation touches on the issue of global existence of the discrete dynamics (1.7). Since trainable weights may vary from layer to layer, this question becomes even more challenging, paralleling that of a numerical scheme with variable coefficients. It is proven in Proposition 5.2 (and in earlier versions of it, Proposition 2.2 and Proposition 4.7) that one can control the ℓ^∞ -norm of both $U^{[l]}$ and $P^{[l]}$ if constraints on Δ_t^u and Δ_t^p are imposed as

$$0 < \Delta_t^u \leq \frac{1}{\sqrt{3} \text{diameter}(\mathcal{P}_\alpha)^2}, \quad \text{and} \quad 0 < \Delta_t^p \leq \frac{1}{\sqrt{3} \text{diameter}(\mathcal{P}_\beta)^2}, \quad (1.14)$$

where both \mathcal{P}_α and \mathcal{P}_β are intervals constructed from the trainable weights

$$\left(W_U^{[k]}\right)_{0 \leq k \leq N_t-1} = \left(\alpha^{[k]}\right)_{0 \leq k \leq N_t-1}, \quad \text{and} \quad \left(W_P^{[k]}\right)_{0 \leq k \leq N_t-1} = \left(\beta^{[k]}\right)_{0 \leq k \leq N_t-1},$$

respectively. For that reason we shall call the restrictions (1.14) on Δ_t^u and Δ_t^p *Invariant Region Enforcing Conditions*; see Appendix D.4, in particular Lemma D.3.

In order to illustrate the PSBC, we apply it to a 1D toy problem and later on to the classical MNIST database, a benchmark dataset commonly used to assess the quality of several different ML models (Lecun et al., 1998). We concentrate our study in the subset of two digits - suggestively, we pick “0” and “1” - since we are doing binary classification; see Figure 6 and also Appendix A for further details.

As emphasized before, the PSBC has many hyperparameters, a myriad of choices that we do not intend to exhaustively cover, let alone qualitatively study: evidently, different hyperparameters yield different model’s architectures. Our main goal in fact is that of understanding how hyperparameters impact the model’s accuracy, possibly degrading or improving it. In order to do so, we perform model selection only on the learning rate, fixing all the other parameters. Afterwards, having selected a

6. Indeed, the numerical scheme (1.7a) can be seen as a particular case of

$$U^{[n+1]} = U^{[n]} + \theta \varepsilon^2 D_{N_u} U^{[n]} + (1 - \theta) \varepsilon^2 D_{N_u} U^{[n+1]} + \Delta_t^u f(U^{[n]}; \alpha^{[n]}), \quad \theta \in [0, 1], \quad (1.13)$$

If the nonlinearity is ignored ($f(\cdot; \cdot) \equiv 0$), it is known that the model is unconditionally stable when $0 \leq \theta \leq \frac{1}{2}$, that is, solution remain stable for all values of Δ_t^u ; cf (Richtmyer and Morton, 1967, pages 17-18), (Strikwerda, 1989, Section 6.3, page 147)). A similar numerical scheme has also been exploited in (Hoff, 1978) in greater generality.



Figure 6: A few examples of the subset 0 and 1 of the MNIST database containing handwritten digits. Each picture has a shape 28×28 pixels, and is stored as a matrix; see Appendix A for further information.

learning rate, model assessment is done by varying only one of the hyperparameters at the time: in Section 2 we vary the partition cardinality N_{ptt} , in Section 5 the diffusion parameter ε . In the latter case, we train the model at $\varepsilon = 0$ (non-diffusive PSBC), a choice that takes into consideration the fact that training is much cheaper (computationally) for the non-diffusive PSBC than for the diffusive PSBC, being therefore important to know whether or not model selection can be performed in a non-diffusive setting with no subsequent significant deterioration (or better, improvement) of accuracy once diffusion is added. For any given set of hyperparameters, several simulations are run so that the model’s statistical properties can be asserted; this is also done because weights have been initialized in a randomized fashion. See further discussion in Appendix A.

In short, the outline of the paper is as follows: we begin in Section 2 with a one dimensional toy problem ($N_u = 1$, $N_p = 0$; individuals have one feature) that only uses (1.7a). After understanding the virtues and failures of this simpler case, in Section 3 we include the companion reaction equation (1.7b), improving the model, that still has a single feature ($N_u = N_p = 1$). A digression to discuss model qualities and limitations in low dimensional feature spaces is done in Section 3.1. In Section 4 we naturally generalize the PSBC to encompass features in high dimension spaces ($N_u \geq 2$). In Section 5 we discuss the PSBC with diffusion, and the latter’s role in coupling features. An extensive discussion in Section 6 presents several open questions, possible directions of investigation, and more technical comments on topics addressed throughout the paper.

Last, we close the paper with an appendix, where all mathematical results are fully derived: first, we address initialization of variables and hyperparameters in Appendix A. Afterwards, in Appendix B we expose an implementation of the Backpropagation algorithm with weights- K -sharing (see Definition 1.5), besides some analytical mathematical derivations necessary for its implementation. We devote Appendix C to discrete maximum principles, a necessary tool in establishing the PSBC’s feedforward propagation. Appendix D contains the proof of all the mathematical statements in the paper.

1.3 Notation

Given a discrete Ordinary Differential Equation (ODE) or Partial Differential Equation (PDE), with initial condition X we denote the n -th iteration step by $U^{[n]} = \left(U_m^{[n]} \right)_{1 \leq m \leq N} \in \mathbb{R}^N$.

Vectors are identified with column matrices: we write $a \in \mathbb{R}^n$, as well as $a \in \mathbb{R}^{n \times 1}$. Whenever $V \in \mathbb{R}^N$ we say that $V \stackrel{\geq}{\leq} 0$ if $V_m \stackrel{\geq}{\leq} 0$ for all $1 \leq m \leq N$. As such, $V \in \mathbb{R}_+^N$ means $V \geq 0$.

We employ vector norms as

$$\|V\|_p = \left(\sum_{j=1}^N |V_m|^p \right)^{\frac{1}{p}}, \quad \text{for } 1 \leq p < \infty, \quad \text{and} \quad \|V\|_\infty = \max_{1 \leq m \leq N} |V_m|. \quad (1.15)$$

Operators will have induced norms. For instance, whenever $A : \mathbb{R}^N \rightarrow \mathbb{R}^M$ we have

$$\|A\|_{\ell^\infty(\mathbb{R}^N) \rightarrow \ell^\infty(\mathbb{R}^M)} = \max_{1 \leq i \leq M} \left(\sum_{1 \leq j \leq N} |A_{i,j}| \right);$$

see (Golub and Van Loan, 1996, Chapter 2.3.2). The identity matrix from \mathbb{R}^N to itself is $\text{Id}_N : \mathbb{R}^N \rightarrow \mathbb{R}^N$.

We write $\mathbb{G}_N := \{1, \dots, N\}$. Given the Euclidean space $E = \mathbb{R}^N$, for any vector $V \in E$, we call the support of V the set $\text{supp}(V) = \{m \in \mathbb{G}_N | V_m \neq 0\}$.

We denote by $\mathbf{1} \in E$ (resp. $\mathbf{0} \in E$) a vector with all the entries 1 (resp., 0); whenever necessary, we write $\mathbf{1}_N$ or $\mathbf{0}_N$ to indicate the dimension of the underlying space these vectors are in.

The canonical basis is defined as $e_i \in E$, $1 \leq i \leq N$. We shall further define

$$e_{\mathcal{A}} := \sum_{i \in \mathcal{A}} e_i, \quad \text{for } \mathcal{A} \subset \{1, \dots, N\} = \mathbb{G}_N. \quad (1.16)$$

Clearly, $e_{\{i\}} = e_i$, and $e_{\{1, \dots, N\}} = \sum_{i=1}^N e_i = \mathbf{1} = \mathbf{1}_N$. By abuse of notation, we shall use (1.16) for any Euclidean space, regardless of its dimension.

2. The non-diffusive PSBC with no phase: a 1D feature space study case

For now, we begin our study of the PSBC by only using the model (1.7a), discarding (1.7b). Thus, parameters are $\varepsilon = 0$ and $N_u = 1$, yielding an Euler discretization of (1.9),

$$U^{[n+1]} := U^{[n]} + \Delta_t^u f \left(U^{[n]}; \alpha^{[n]} \right), \quad U^{[0]} = X \in [0, 1], \quad \alpha^{[n]} \in \mathbb{R}, \quad (2.1)$$

where $f(u, w) = u(1-u)(u-w)$. Recall that $U^{[\cdot]}(X; \alpha^{[\cdot]})$ represents the flow of X through (2.1). As explained in Section 1.2, we must train the model with respect to the parameter $\alpha^{[n]}$, for $n \in \{0, \dots, N_t - 1\}$. Notice that this ODE can be described as a feedforward network, as seen in the diagram of Figure 1.

One of fundamental steps in dealing with (2.1) consists of showing that the model is well defined for all $0 \leq n \leq N_t$, namely, that $U^{[\cdot]}(X, \alpha^{[\cdot]})$ does not blow-up during forward propagation; the concern is legitimate since it is well known that Euler methods do not have good stability properties (Iserles, 2009, Sec. 4.2). Fortunately, we show in Proposition 2.2 that, under the normalized condition (N-C) and reasonable conditions on Δ_t^u , we can control on the growth of $\|U^{[\cdot]}(X, \alpha^{[\cdot]})\|_{\ell^\infty}$.⁷ The arguments used in the proof are very general, being later applied in the forward propagation of the full system (1.7), with or without diffusion, in Propositions 4.7 and 5.2. But first we explain why it is possible to control the growth of solution in (2.1), making a quick digression that takes us back to the Allen-Cahn equation (1.9).

7. This is quite remarkable, since the region of A-stability of the Euler equations on the the region $\{z \in \mathbb{C} | \text{Re}(z) \leq 0\}$ (Iserles, 2009, Chapter 4.2); this is a clear example of nonlinear stabilization.

2.1 A glimpse on gradient flows and invariant regions

As said above, the numerical scheme (2.1) is a discretization of the ODE

$$\frac{du}{dt} = f(u; \alpha) := u(1-u)(u-\alpha), \quad u(X, t=0) = X \in \mathbb{R}, \quad \alpha \in \mathbb{R}, \quad (2.2)$$

corresponding to (1.9) with initial condition X , and no diffusive term (i.e., $\varepsilon = 0$). The nonlinearity in (2.2) is of bistable type, with 3 stationary points: $u = 0$, $u = 1$, and $u = \alpha$ (see Figure 7a). When α varies, the qualitative behavior of the stationary points 0 and 1 change, as we can see on the phase portrait of the ODE (2.2) in Figures 7b-7c-7d.

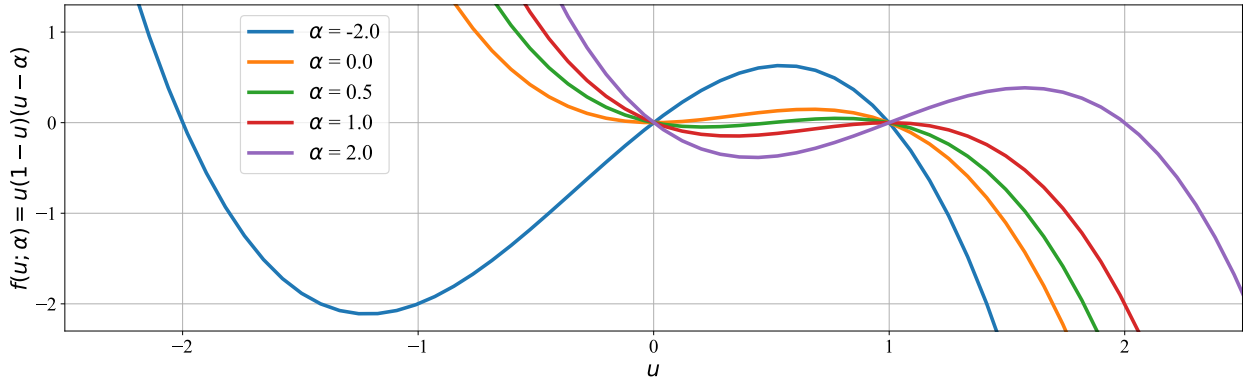
One can associate an energy functional $\mathcal{E}(u, \alpha) = -\int^u s(1-s)(s-\alpha)ds$ to (2.2), which now reads

$$\frac{du}{dt} = f(u; \alpha) := -\partial_u \mathcal{E}(u, \alpha), \quad \text{where } u(X, t=0) = X \in \mathbb{R}, \quad \alpha \in \mathbb{R}. \quad (2.3)$$

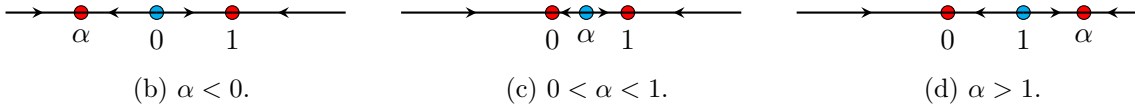
Consequently, along trajectories of (2.2) we must have

$$\frac{\partial}{\partial t} \mathcal{E}(u, \alpha) = -|\nabla_u \mathcal{E}(u, \alpha)|^2 \leq 0, \quad (2.4)$$

which can be interpreted as the rate of energy dissipated as the system evolves; these ideas and concepts can be generalized to systems and other functional spaces, and are an important tool in characterization of rate of convergence to asymptotic states; cf. (Carrillo et al., 2006, Sec. 2).



(a) Sketches of the function $f(u; \alpha) = u(1-u)(u-\alpha)$ for different values of α .



(b) $\alpha < 0$.

(c) $0 < \alpha < 1$.

(d) $\alpha > 1$.

Figure 7: Phase portraits of the ODE $\frac{d}{dt}u(t) = f(u; \alpha) = u(1-u)(u-\alpha)$, for different values of α , with red (resp., blue) circles representing stable (resp., unstable) stationary points. Notice that in all the cases presented, the lowest and largest stationary points are stable, a fact that is exploited in the search for invariant regions, as explained in Section 3.

The phase portraits in Figure 7 indicate that the lowest and the largest stationary points of (2.2) are always stable or semi-stable, regardless of the value α . In fact, using (2.4) and the structure of $\mathcal{E}(\cdot, \alpha)$, we can conclude that any interval \mathcal{I} containing the set

$$\Sigma_\alpha := [\min\{0, \alpha\}, \max\{1, \alpha\}] \quad (2.5)$$

is positively invariant with respect to (2.2), namely, whenever $x_0 \in \mathcal{I} \supset \Sigma_\alpha$ and \mathcal{I} is an interval, it holds that $u[x_0, t] \in \mathcal{I}$ for all $t \geq 0$; cf. (Hirsch and Smale, 1974, Chapter 9). Similar ideas have been applied in PDEs, as discussed in Remark D.1.

Remark 2.1 (Invariant regions and stability) *All of the above explains the existence of bounded invariant regions in the continuum model, being clear at this point that such an existence immediately implies full control of lower and upper bounds of $u(t; \cdot)$ for all $t \geq 0$. Overall, it gives some type of stability of solutions if one is not concerned with oscillatory issues.*

Unfortunately, going back to (2.1) we see that the gradient flow structure is mostly lost upon discretization although, as we show in the next proposition, it can still be exploited in searching for invariant regions. Interestingly, in virtue of numerical discretization, we shall see that the invariant set is slightly bigger than the interval Σ_α in (2.5).

Initially, observe that forward propagation of $Z^{[0]} = X$ takes place at fixed values of parameters $W^{[j]}$, with the latter getting updated at the end of each epoch using (1.5). That is, at the beginning of each epoch $Z^{[0]} = X$ is given and weights $W^{[j]}$ are fixed. With these quantities in hands, afterwards the sequence $(Z^{[0]}, \dots, Z^{[N_t]})$ is generated, and one can see the latter is the orbit of $Z^{[0]} = X$ through the dynamical system represented by the feedforward network (1.3). If we focus this discussion on (2.1), it means that one needs to translate quantitative properties of any given sequence

$$W_q^{[j]} = \left(\alpha^{[0]}, \alpha^{[1]}, \dots, \alpha^{[N_t-1]} \right)_q,$$

known at the beginning of each epoch q , to quantitative statements about the associate sequence

$$Z_q^{[j]} = \left(U^{[0]} = X, U^{[1]}, \dots, U^{[N_t]} \right)_q,$$

obtained using (2.1). This is the main idea behind the next result, which is a simpler case of Propositions 4.7.

Proposition 2.2 (Global existence of forward propagation; PSBC in the form (2.1)) *Let $N_t \in \mathbb{N} \cup \{+\infty\}$ and assume the normalization condition (N-C), i.e., $U^{[0]} := X \in [0, 1]$. Assume a given and fixed sequence $(\alpha^{[n]})_{0 \leq n \leq N_t}$, augmented by $\alpha^{[-1]} = 1$. For any $-1 \leq k \leq N_t - 1 \leq +\infty$, define*

$$L^{[k]} := \inf_{-1 \leq n \leq k} \left(\min \left\{ \alpha^{[n]}, 0 \right\} \right), \quad R^{[k]} := \sup_{-1 \leq n \leq k} \left(\max \left\{ \alpha^{[n]}, 1 \right\} \right). \quad (2.6)$$

Assume that $-\infty < L^{[N_t-1]}$ and $R^{[N_t-1]} < +\infty$, and that the Invariant Region Enforcing Condition (1.14) holds in the form

$$0 \leq \Delta_t^u \leq \frac{1}{\sqrt{3} (|L^{[N_t-1]}| + |R^{[N_t-1]}|)^2}. \quad (2.7)$$

Then, for all $0 \leq k \leq N_t$ the sequence $U^{[k]}(X, \alpha^{[k]})$ obtained using (2.1) remains bounded. In particular,

$$L^{[k-1]} - \Delta_t^u \left(M^{[k-1]} \right)^3 \leq U^{[k]}(X, \alpha^{[k]}) \leq R^{[k-1]} + \Delta_t^u M^{[k-1]} \quad (2.8)$$

holds for all $0 \leq k \leq N_t$, with $M^{[k]} := (|L^{[k]}| + |R^{[k]}|)^3$.

The quantity $R^{\lfloor N_t - 1 \rfloor}$ in (2.2) is optimal, as one can see by choosing $X = 1$, $\alpha^{\lfloor \cdot \rfloor} = 0.5$, and taking $\Delta_t^u \downarrow 0$; similar reasoning shows that $L^{\lfloor N_t - 1 \rfloor}$ is also optimal. On the other hand, given an interval containing initial conditions and trainable weights, it is unclear what is the critical maximal value Δ_t^u can take in such a way that the dynamics remains in an invariant region. The above result shows that a critical value exists, is finite, and strictly positive, although the right hand side of condition (2.7) is possibly non-optimal. It is worth noting that the maximum value of Δ_t^u yielding an invariant region may change depending on symmetry properties of the latter set, as pointed out in Remark D.5.

Corollary 2.3 *Using the same notation and under the same assumptions of Proposition 2.2, for all $0 \leq k \leq N_t$ we have $|U^{\lfloor k \rfloor}(X, \alpha^{\lfloor k \rfloor})| \leq (1 + \Delta_t^u) M^{\lfloor k - 1 \rfloor}$. In particular, when $(\alpha^{\lfloor k \rfloor})_{0 \leq k \leq N_t - 1} \in [0, 1]$, we get $M^{\lfloor \cdot \rfloor} \equiv 1$, and*

$$|U^{\lfloor k \rfloor}(X, \alpha^{\lfloor k \rfloor})| \leq 1 + \Delta_t^u, \quad \text{for all } 0 \leq k \leq N_t.$$

Proposition 2.2 says that one can control the growth of propagating of features using the trainable weights ℓ^∞ norm;⁸ a proof is found in Appendix D, relying on the technique of *invariant regions*. The result highlights some sort of stability of the PSBC, in the sense of boundedness of $U^{\lfloor \cdot \rfloor}$; see illustrative behavior in Figure 8.

Remark 2.4 (On the evolution of Invariant regions and bounds on trainable weights) *As long as the Invariant Region Enforcing Condition (1.14) holds, the invariant region in Proposition 2.2 - and consequently the bounds on $U^{\lfloor \cdot \rfloor}$ and $P^{\lfloor \cdot \rfloor}$ - do not depend on N_t . It is important to remark that these bounds may vary for different epochs, hence the result does not say how the invariant region evolves throughout the training process. Furthermore, it is not clear whether there exists an invariant region for trainable weights. Nevertheless, training relies on Gradient Descent, thereby a synergy between the ℓ^∞ -norm growth of $U^{\lfloor \cdot \rfloor}(X, \alpha^{\lfloor \cdot \rfloor})$, $P^{\lfloor \cdot \rfloor}(X, \beta^{\lfloor \cdot \rfloor})$ and that of W_U and W_P exists in virtue of the trainable weights update equation (1.5). Consequently, bounds on trainable weights can be given for a small number of epochs; see Proposition 6.3.*

Remark 2.5 (Continuum versus discrete I) *It is interesting to compare the continuum ODE (2.2) and its discretization (2.1): in the continuum model any initial condition in the interval $[0, 1]$ remains in the same interval for all $t \geq 0$, in evident contrast to the discrete dynamics of $U^{\lfloor n \rfloor}$ for all $n \in \mathbb{N}$ and different values of Δ_t^u , which can begin in the interval $[0, 1]$ but blow-up; see Figure 8 for illustrative simulations. This is a clear example in which “the numerics of the dynamics does not necessarily correspond to the dynamics of the numerics”. Observe, for instance, that whenever $0 < 1 - \alpha^{\lfloor \cdot \rfloor} \ll \Delta_t^u$ it is possible that sequences starting in $U^{\lfloor 0 \rfloor} = X > 1$ jump from the stable manifold of 1 to an unstable manifold of α , consequently converging to 0 rather than to 1; a similar issue occurs when $0 < \alpha^{\lfloor \cdot \rfloor} \ll \Delta_t^u$.*

Remark 2.6 (Continuum versus discrete II) *Physics laws get broken upon discretization: conserved quantities may not be conserved at the discrete level, symmetries may not be respected, and quantities representing functionals that should decay in time do not always decay over iterations. These*

8. Roughly speaking, Proposition 2.2 (and in special Lemma D.3) says that, given any bounded sequence $(\alpha^{\lfloor n \rfloor})_{0 \leq n \leq N_t}$, the area of the maximal interval visited by the orbit $U^{\lfloor \cdot \rfloor}(X, \alpha^{\lfloor \cdot \rfloor})$ is bounded. Clearly, when $\Delta_t^u = 0$ the orbit is always bounded, and properties of the sequence $(\alpha^{\lfloor n \rfloor})_{0 \leq n \leq N_t}$ can be overlooked in making this assertion. In contrast, it is not hard to find examples in which $\Delta_t^u > 0$, $(\alpha^{\lfloor n \rfloor})_{0 \leq n \leq N_t}$ is bounded, but the orbit blows-up ($\alpha^{\lfloor \cdot \rfloor} \equiv 0$, $X^{\lfloor 0 \rfloor} = \frac{1}{2}$, and $\Delta_t^u = 8$ will do). The bounds in (2.8) show that there are positive values of Δ_t^u for which the boundedness of orbits still holds true. The author does not believe that the bounds are optimal.

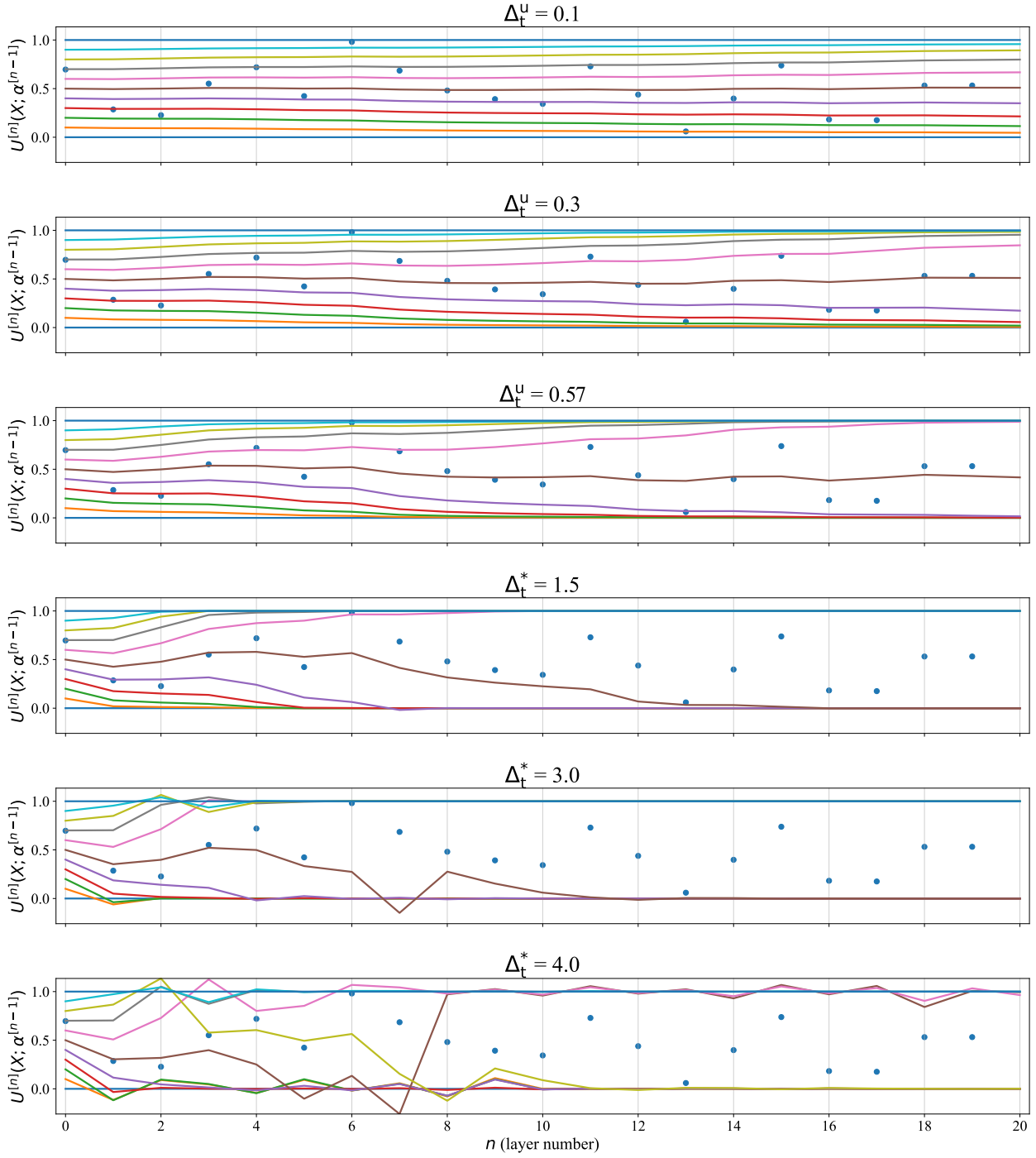


Figure 8: Orbits for the PSBC (2.1) using 10 initial conditions equally spaced in the interval $[0, 1]$. Blue dots represent the values of random weights uniformly generated in the interval $[0, 1]$ and allowed to vary across layers. Models Hyperparameters were $N_u = 1$, $N_p = 0$, and $N_t = 20$, for different values of Δ_t^u written on the top of each figure. In the first plots (from the top) the parameter Δ_t^u is below or equal the critical threshold $\Delta_t := \frac{1}{\sqrt{3}} \approx 0.57$ given by the Invariant Region Enforcing Condition (1.14); in the last three plots, in violation to the latter condition, Δ_t^u takes the value Δ_t^* . In several simulations, large values of Δ_t^u lead to blow-up of $\|U^{[1]}(X, \alpha^{[1]})\|_{\ell^\infty}$.

are still legitimate concerns when one deals with the discretization of systems with gradient flow structure, although the continuum formalism can be exploited in fruitful ways, as we illustrate in Section 2.1. Other studies also exploit model’s reaction-diffusion structure extensively, as in the use of splitting techniques in the design of numerical methods that are unconditionally stable; cf. (Eyre, 1998; Schönlieb and Bertozzi, 2011).

2.2 A toy problem with a single feature

As an initial test, we generate a dataset as a realization of independent and identically distributed (i.i.d.), uniform random variables $(X_{(i)})_{1 \leq i \leq 2000}$ in the interval $[0, 1]$, labeled according to the rule

$$Y_{(i)} := \mathbb{1}_{\{X_{(i)} \geq \gamma^*\}}(X_{(i)}). \quad (2.9)$$

Three cases have been considered in simulations:⁹ $\gamma^* = 0.6$, $\gamma^* = 0.7$, and $\gamma^* = 0.8$, with results displayed in Tables 1a and 1b. It is worth pointing out that the characteristic sets in (2.9) are particularly simple and in some cases called “rectangular boxes problems” (which are in fact *PAC learnable*, cf. (Mohri et al., 2018, Chapter 2.1)).

γ^*	Average accuracy		γ^*	Average accuracy	
	Train	Test		Train	Test
0.6	0.931 \pm 0.019	0.933 \pm 0.023	0.6	0.977 \pm 0.013	0.982 \pm 0.014
0.7	0.869 \pm 0.031	0.863 \pm 0.034	0.7	0.972 \pm 0.023	0.963 \pm 0.024
0.8	0.800 \pm 0.039	0.796 \pm 0.039	0.8	0.972 \pm 0.041	0.969 \pm 0.041

(a) Weights-1-sharing. (b) Weights- N_t -sharing.

Table 1: Some statistics for the accuracies as of the last epoch for the PSBC (2.1). The dataset obeys a train-test split of 80%-20%, and is made of 2000 points following an i.i.d. uniform distribution on $[0, 1]$ with labels (2.9). For each value of γ^* statistics were taken from a sample space of 100 simulations for each set of hyperparameters. Hyperparameters were $N_t = 20$, $N_p = 0$, $\Delta_t^u = 0.1$ (initial), patience = $+\infty$, and learning rates $0.1 + 0.08 \cdot (0.93)^{\text{epoch}}$. For a table with accuracy at best epoch, see Supplementary material, Table 1.

Our simulations comprise parameters of both weights-1-sharing and weights- N_t -sharing type. Training is performed using Gradient-descent and the Backpropagation algorithm. The number of layers is fixed at $N_t = 20$ and the cost function that must be minimized reads as

$$\text{Cost}_{\mathcal{D}}(W) = \frac{1}{2N_d} \sum_{i=1}^{N_d} \left| U^{[N_t]}(X_{(i)}; \alpha^{[N_t-1]}) - Y_{(i)} \right|^2, \quad (2.10)$$

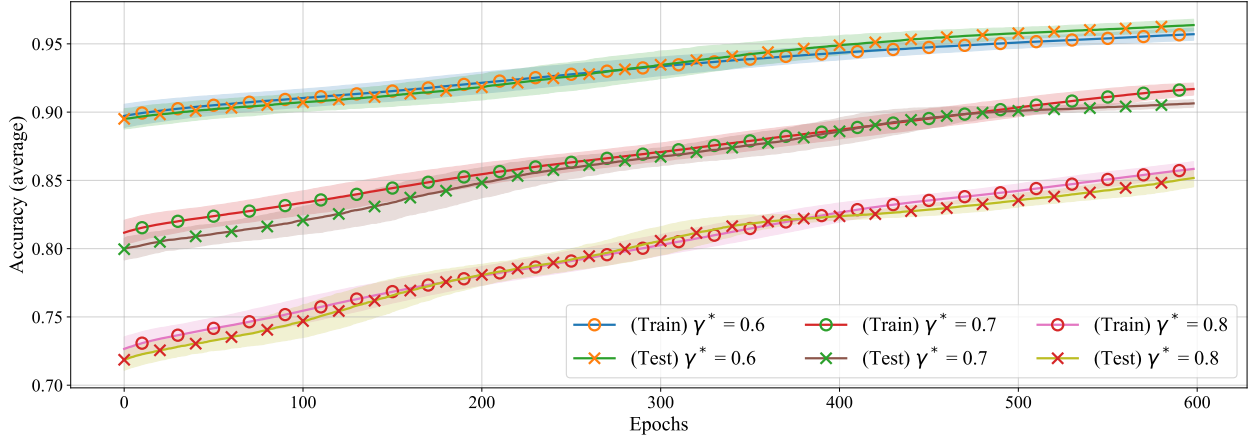
where $U^{[N_t]}(X_{(i)}; \alpha^{[L]})$ represents the initial condition propagated using (2.1). In the end, once $\alpha^{[L]}$ is chosen, we obtain a prediction map,

$$h \left(U^{[N_t]}(X_{(i)}; \alpha) \right) = \begin{cases} 1, & \text{if } U^{[N_t]}(X_{(i)}; \alpha^{[N_t-1]}) \geq \frac{1}{2}, \\ 0, & \text{otherwise;} \end{cases} \quad (2.11)$$

cf. (1.6).

From the point of view of mathematical modeling, a PSBC in the form (2.9) with weights- N_t -sharing, where $\alpha^{[L]}$ is the same over different layers, corresponds to an Euler discretization of the autonomous model $\frac{du}{dt} = f(u; \gamma^*)$. In contrast, allowing $\alpha^{[n]}$ to vary across layers (as it is the case in weights-1-sharing parameters) is closer to a non-autonomous model, that is, allowing $\alpha = \alpha(x, t)$ in (1.9). When both models are compared, a surprising thing happens:

9. We ignore the cases $\gamma^* = 0.5$ and $\gamma^* = 0.9$: the former due to the PSBC’s initialization of trainable weights (see Appendix A), which would immediately give good accuracy results; the latter, because this class is too skewed.



(a) Evolution of accuracy for the PSBC (2.1) with weights-1-sharing.

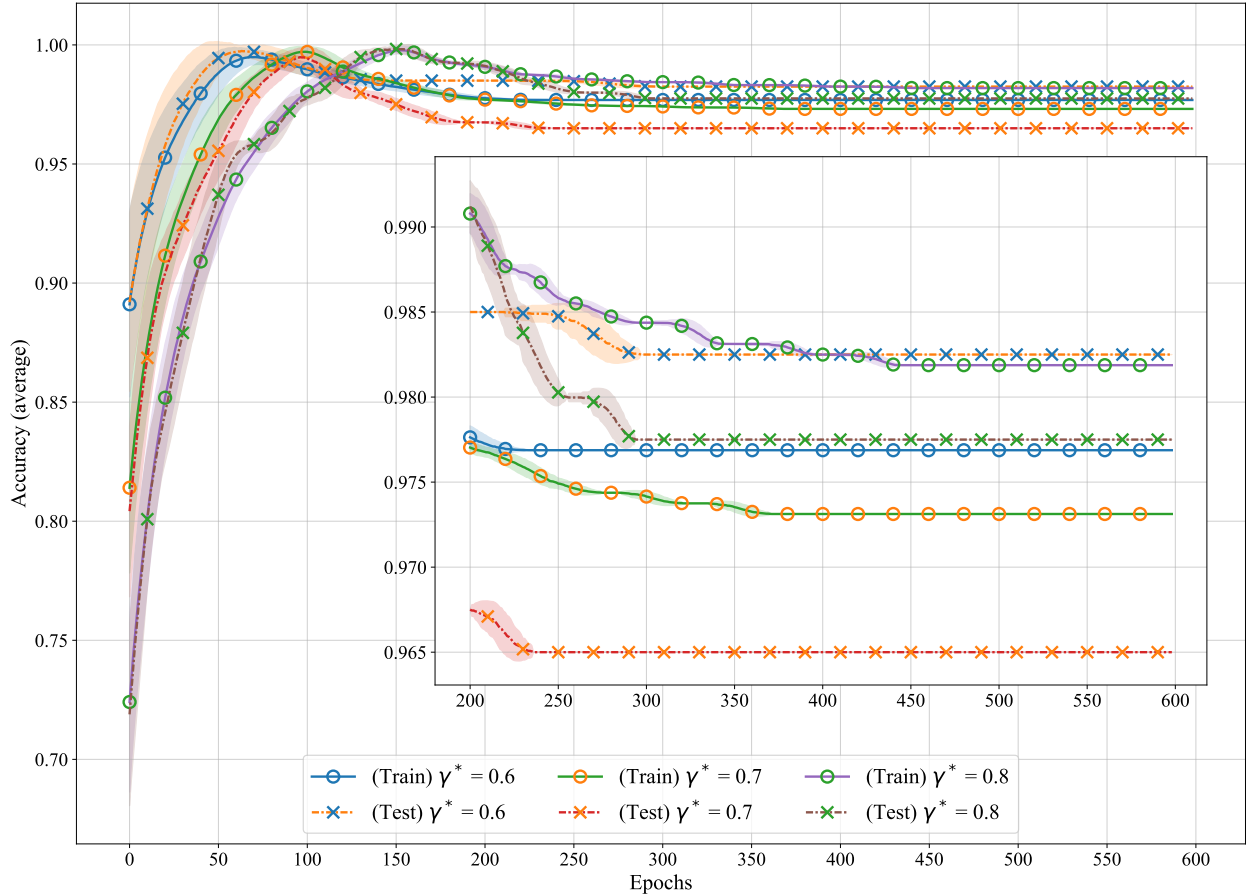
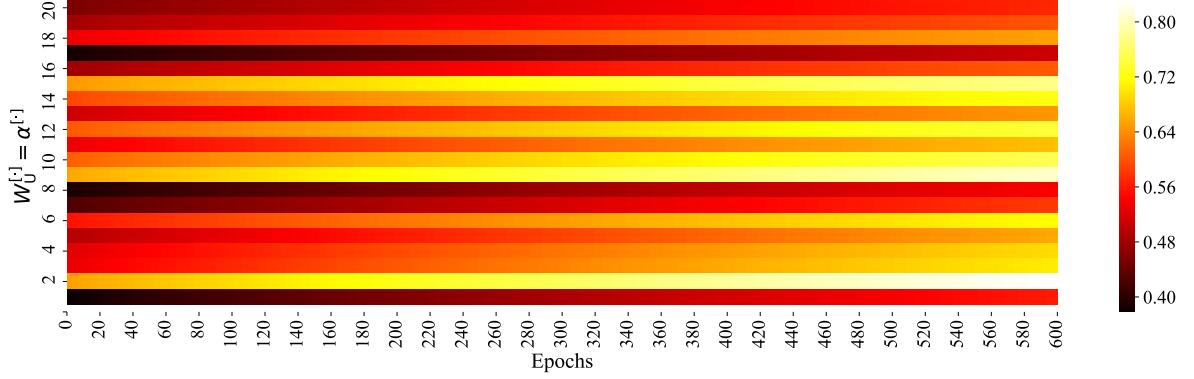
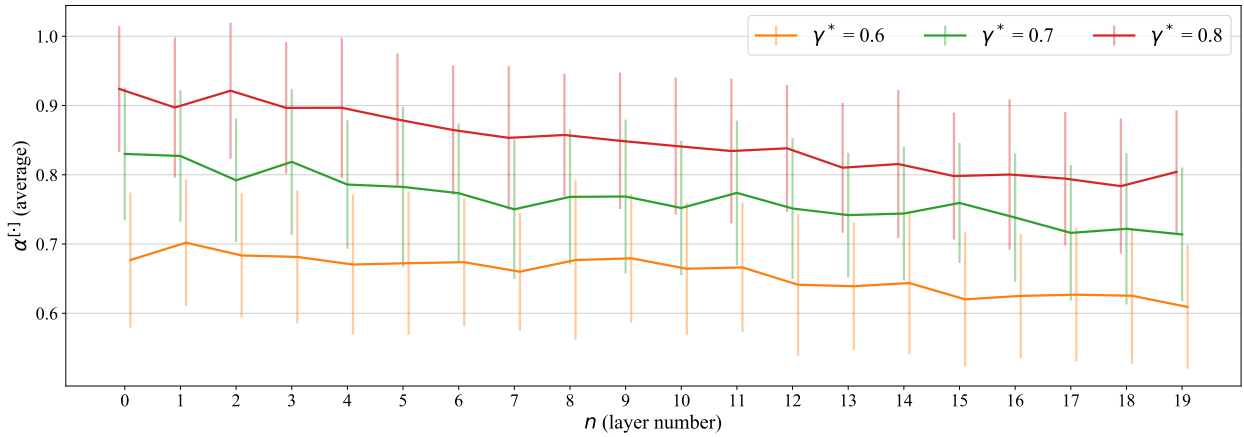

 (b) Evolution of accuracy for the PSBC (2.1) with weights- N_t -sharing.

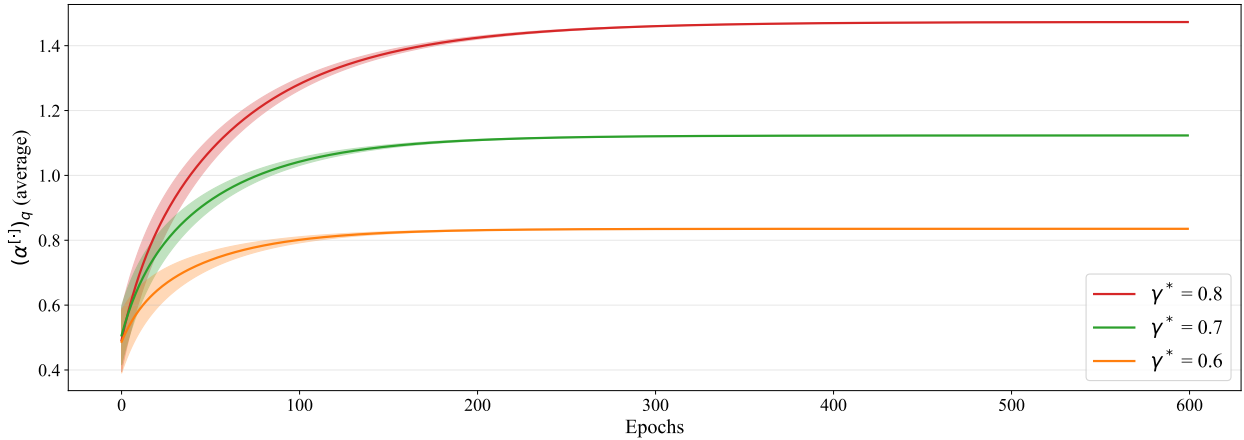
Figure 9: Evolution of accuracy throughout epochs for the PSBC (2.1). The dataset was partitioned using a train-test split of 80%-20%, and is made of 2000 points following an i.i.d. uniform distribution on $[0, 1]$ with labels (2.9). For each value of γ^* statistics were taken from a sample space of 100 simulations for each set of hyperparameters. Hyperparameters were $N_t = 20$, $N_p = 0$, $\Delta_t^u = 0.1$ (initial), patience = $+\infty$, and learning rates $0.1 + 0.08 \cdot (0.93)^{\text{epoch}}$. In both figures, shaded areas with the same colors as lines denote 1 standard deviation.



(a) Heatmap of trainable weights $\alpha^{l,j}$ over epochs in a realization of the PSBC (2.1) with weights-1-sharing.



(b) Average value of trainable weights $\alpha^{l,j}$ at the last epoch, for a PSBC (2.1) with weights-1-sharing. Vertical bars with the same colors as lines denote 1 standard deviation.



(c) Evolution over epochs of trainable weights $\alpha^{l,0} = \dots = \alpha^{l,N_t-1}$ in a PSBC (2.1) with weights- N_t -sharing. Note that $\alpha^{l,j}$ accumulates in values that are different from the true parameters γ^* defined by the label (2.9). Shaded areas with the same colors as lines denote 1 standard deviation.

Figure 10: Some statistics for trainable weights for the PSBC (2.1). The dataset obeys a train-test split of 80%-20%, and is made of 2000 points following an i.i.d. uniform distribution on $[0,1]$ with labels (2.9). For each value of γ^* statistics in (b) and (c) were computed from a sample space of 100 simulations for each set of hyperparameters. Hyperparameters were $N_t = 20$, $N_p = 0$, $\Delta_t^u = 0.1$ (initial), patience = $+\infty$, and learning rates $0.1 + 0.08 \cdot (0.93)^{\text{epoch}}$.

- (i) Our simulations indicate that as n increases towards N_t the values of $\alpha^{[n]}$ with weights-1-sharing accumulate around the true values of γ^* ; see Figure (10b).
- (ii) In contrast, the model with weights- N_t -sharing, where parameters satisfy $\alpha^{[0]} = \dots = \alpha^{[N_t-1]}$, do not converge to the true value of γ^* ; see Figure 10c.

Intriguingly, in spite of this strange behavior, both models give good results, as Tables 1a and 1b show. However, one should read the results both models provide with caution: as we can see in Figure 9, the accuracy at the very beginning is already above 70% in all the cases, and in some of them above 90%. The explanation for that is simple, as we observe first in an idealized case, using weights- N_t -sharing case: for an initial guess $\tilde{\gamma}$, all $X_{(i)} > \tilde{\gamma}$ must evolve towards 1 (its correct label) and, similarly, values for which $X_{(i)} < \tilde{\gamma}$ must evolve towards 0 (its correct label); now, if we fix $\alpha^{[0]} = \dots = \alpha^{[N_t-1]} = 0.5$, our errors will be close to 10% ($\gamma^* = 0.6$), 20% ($\gamma^* = 0.7$), and 30% ($\gamma^* = 0.8$). In reality, as discussed in Appendix A, each trainable weight is initialized as Normal variables with small variance, centered around 0.5, which is not far from the idealized scenario we have just contemplated. In conclusion, the result is not exceptional, neither unexpected; it should be said that the model performs far better than these “expected” figures, as Tables 1a and 1b show.

Let’s see then a different case: we consider i.i.d. uniform random variables $\{X_{(i)}\}_{1 \leq i \leq 2000}$ in the interval $[0, 1]$, now labeled as

$$Y_{(i)} = \mathbb{1}_{\{z \leq \gamma^*\}}(X_{(i)}). \quad (2.12)$$

If we look at Table 2a, it becomes clear that the model is not performing well. Understanding the source of the error is the key point that leads to an improvement we introduce in Section 3, whose results we anticipate in Table 2b.

γ^*	Average accuracy		γ^*	Average accuracy	
	Train	Test		Train	Test
0.6	0.515 ± 0.109	0.49 ± 0.12	0.6	0.965 ± 0.043	0.967 ± 0.042
0.7	0.618 ± 0.093	0.607 ± 0.103	0.7	0.964 ± 0.058	0.963 ± 0.059
0.8	0.705 ± 0.086	0.69 ± 0.097	0.8	0.947 ± 0.076	0.939 ± 0.073

(a) Without phase ($N_p = 0$).

(b) With phase ($N_p = 1$).

Table 2: Comparison between the accuracy in two versions of the PSBC, as evaluated at the last epoch: (a) in the form (2.1) without phase ($N_p = 0$), and (b) in the form (3.4) with phase ($N_p = 1$), that will be discussed in the next section. The dataset obeys a train-test split of 80%-20%, and is made of 2000 points following an i.i.d. uniform distribution on $[0, 1]$ with labels (2.12). For each value of γ^* statistics were computed from a sample space of 100 simulations for each set of hyperparameters. Hyperparameters were $N_t = 20$, weights- N_t -sharing, $\Delta_t^u = 0.1$ (initial), patience = $+\infty$, and learning rates $0.1 + 0.08 \cdot (0.93)^{\text{epoch}}$. For a table with accuracy at best epoch, see Supplementary material, Table 2.

The main reason for the poor accuracy stems from the fact that the PSBC in the form (2.1) cannot learn labels (2.12):¹⁰ in fact, whenever (X, Y) and (\tilde{X}, \tilde{Y}) satisfy $X > \gamma^* \geq \tilde{X}$ (which implies that $Y = 0$ and $\tilde{Y} = 1$), at least one of them is wrongfully classified. We prove this claim by first showing that $U^{[N_t]}(X; \alpha^{[N_t-1]})$ is monotonic with respect to X .

Proposition 2.7 (Monotonicity yields “unlearnable” classes - PSBC in the form (2.1)) *Fix any $0 \leq \Delta_t^u < \frac{1}{10}$ and $0 < \gamma^* < 1$. Then, there exists no parameter $\alpha^{[l]} \in [0, 1]^{N_t}$ for the PSBC in the*

10. The exact conditions under which learning cannot happen are given in Proposition 2.7.

form (2.1) that can separate all data X and \tilde{X} labeled as

$$Y = \mathbb{1}_{\{z \leq \gamma^*\}}(X), \quad \text{and} \quad \tilde{Y} = \mathbb{1}_{\{z \leq \gamma^*\}}(\tilde{X}).$$

In particular, $X \geq \tilde{X}$ implies that $U^{\lfloor n \rfloor}(X; \alpha^{\lfloor n \rfloor}) \geq U^{\lfloor n \rfloor}(\tilde{X}; \alpha^{\lfloor n \rfloor})$ for all $0 \leq n \leq N_t$.

With $X > \gamma^* \geq \tilde{X}$ and under the assumptions of the Proposition 2.7, we prove the claim as follows: assume that both individuals are correctly classified using the discrimination rule (2.11). Consequently, one should have that $U^{\lfloor N_t \rfloor}(X; \alpha^{\lfloor N_t - 1 \rfloor}) < \frac{1}{2} \leq U^{\lfloor N_t \rfloor}(\tilde{X}; \alpha^{\lfloor N_t - 1 \rfloor})$, which violates Proposition (2.7).

The main conclusion out of this discussion is that the model (2.2) strongly depends on label assignment.¹¹ This is a serious issue that we will repair in the next section.

Remark 2.8 (Unlearnable classes and hyperplane separation) *In light of Proposition 2.7, one can assert the existence of an $\tilde{\alpha} \in \mathbb{R}$ such that for all $X > \tilde{\alpha}$ (resp., $X < \tilde{\alpha}$) we have $U^{\lfloor N_t \rfloor}(X; \alpha^{\lfloor N_t - 1 \rfloor}) > \frac{1}{2}$ (resp., we have $U^{\lfloor N_t \rfloor}(X; \alpha^{\lfloor N_t - 1 \rfloor}) < \frac{1}{2}$); moreover, in virtue of (2.11), such an individual is predicted to belong to the class 1 (resp. 0). Therefore, classification takes place as a hyperplane separation of initial conditions (which, in 1D, consist of semi-infinite intervals). We highlight that the PSBC classifies dynamically, for all the features it acts upon evolve according to (2.1), thus differing from other models like Margin Classifiers (Bishop, 2006, Chapter 7).*

3. The non-diffusive PSBC with phase: a 1D feature space study case

As shown in Proposition 2.7, there exists a monotonicity dependence between features and labels, yielding a label-dependent model. This section is devoted to removing this liability, which we achieve at the expense of introducing more variables in the model. First, we recall two linear maps from the real line \mathbb{R} to itself,

$$\mathcal{S}^{(0)}(u) = u, \quad \mathcal{S}^{(1)}(u) = 1 - u, \quad u \in \mathbb{R}. \quad (3.1)$$

Observe that $\mathcal{S}^{(1)}(0) = 1$ and $\mathcal{S}^{(1)}(1) = 0$, that is, $\mathcal{S}^{(1)}(\cdot)$ flips the interval $[0, 1]$, whereas $\mathcal{S}^{(0)}(\cdot)$ is simply the identity map. Such properties convey all that is needed: we choose $\mathcal{S}^{(0)}(\cdot)$ when no relabeling is needed, otherwise we choose $\mathcal{S}^{(1)}(\cdot)$ and flip the labels, applying the previous model to $\mathcal{S}^{(1)}(U^{\lfloor \cdot \rfloor}; \alpha^{\lfloor \cdot \rfloor})$. Figuring out when to use either of these maps involves the construction of a homotopy,

$$\mathcal{S}^{(p)}(u) := (1 - p) \mathcal{S}^{(0)}(u) + p \mathcal{S}^{(1)}(u), \quad (3.2)$$

reducing matters to that of “learning” the homotopy parameter p . We do this by use of the very same equation (2.2), setting

$$\frac{dp}{dt} = f(p; \beta) := p(1 - p)(p - \beta), \quad p(0) = \frac{1}{2}. \quad (3.3)$$

where p has the desired properties as long as we learn the parameter β appropriately. In the end, going back to the continuum model, fixing the labels consists of obtaining

$$\lim_{t \rightarrow \infty} \mathcal{S}^{(p(t))}(u(X_{(i)}, t; \alpha)) = Y_{(i)},$$

achieved according to the asymptotic behavior of $p(t)$ as $t \rightarrow \infty$.

11. Constraining $\alpha^{\lfloor \cdot \rfloor}$ to the interval $[0, 1]$ seems far-fetched, specially after the remarks that follows Figure (10), which assert that parameters do not necessarily reflect what we expect from the continuum model that (2.1) discretizes. Nevertheless, it explains in a consistent way the drawbacks of the model in this simple form.

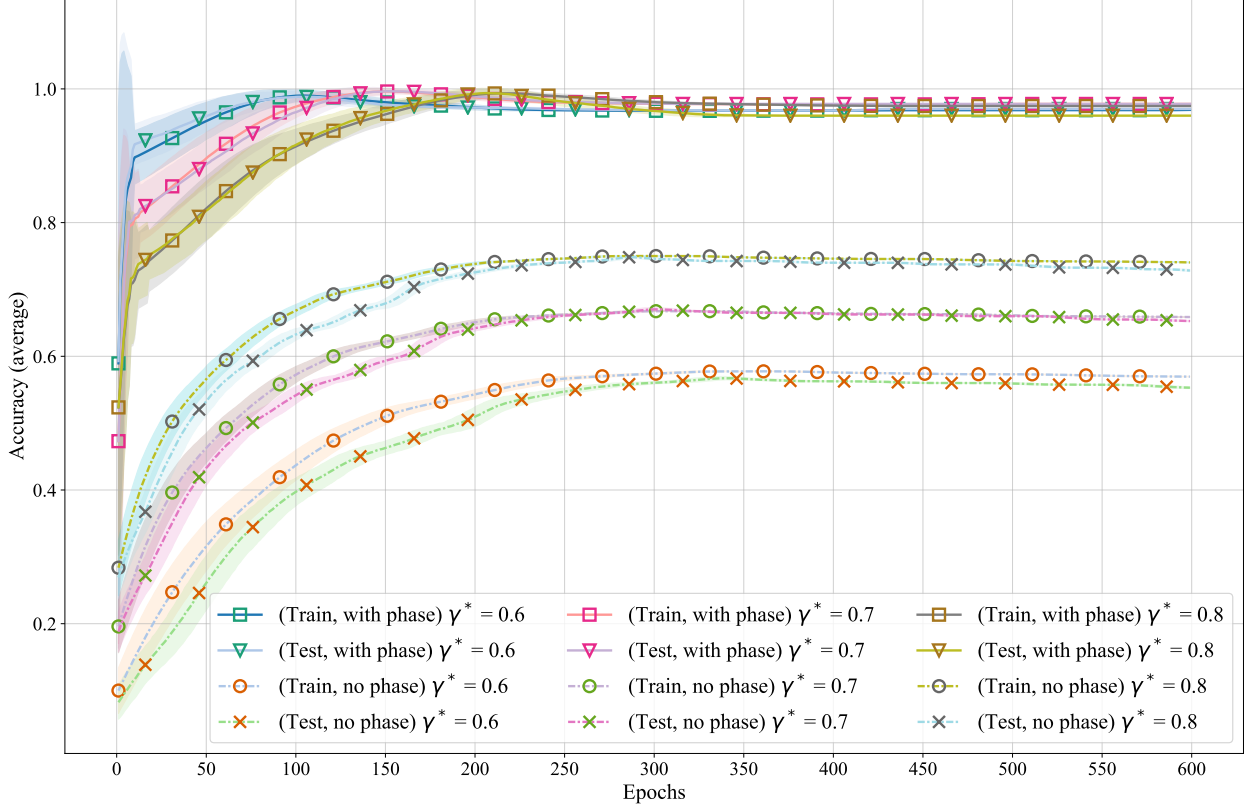


Figure 11: Comparative evolution of accuracy in two applications of the PSBC with weights- N_t -sharing: without phase (PSBC (2.1); $N_p = 0$), and with phase (PSBC (3.4); $N_p = 1$). The dataset obeys a train-test split of 80%-20%, and is made of 2000 points following an i.i.d. uniform distribution on $[0, 1]$ with labels (2.12). For each value of γ^* statistics were computed from a sample space of 100 simulations for each set of hyperparameters. Shaded areas with the same colors as lines denote 1 standard deviation. Hyperparameters were $N_t = 20$, $\Delta_t = 0.1$ and learning rates $0.1 + 0.08 \cdot (0.93)^{\text{epoch}}$.

Note that the initial data in (3.3) is artificially created, therefore in order to learn β one must introduce some coupling between $U^{[\cdot]}$ and $P^{[\cdot]}$: first, we introduce

$$\begin{aligned} U^{[n+1]} &= U^{[n]} + \Delta_t f(U^{[n]}; \alpha^{[n]}), & U^{[0]} &= X, \\ P^{[n+1]} &= P^{[n]} + \Delta_t f(P^{[n]}; \beta^{[n]}), & P^{[0]} &= \frac{1}{2}, \end{aligned} \quad (3.4)$$

and rewrite the cost function as

$$\text{Cost}_{\mathcal{D}}(W) = \frac{1}{2N_d} \sum_{i=1}^{N_d} \left| \mathcal{S}^{(P^{[N_t]})} \left(U^{[N_t]} \left(X_{(i)}; \alpha^{[N_t-1]} \right) \right) - Y_{(i)} \right|^2 \quad (3.5)$$

where $W = (W_U, W_P) = (\alpha^{[\cdot]}, \beta^{[\cdot]})$ and $P^{[N_t]} = P^{[N_t]} \left(\frac{1}{2}; \beta^{[N_t-1]} \right)$. Note that both $U^{[\cdot]}$ and $P^{[\cdot]}$ are forward propagated using (3.4) without coupling between them. However, the cost function introduces interaction between parameters $\alpha^{[\cdot]}$ and $\beta^{[\cdot]}$. The results of the coupled model are more accurate than the previous model, as anticipated in Table 2b and shown in Figure 11. With regards to the forward propagation, global existence can be proven and stated along the lines of Proposition 2.2; we postpone its statement to the next section, where an extension of the PSBC to systems is proposed.

3.1 Interlude: low dimensional feature spaces

It was pointed out in Remark 2.8 that, in virtue of Proposition 2.7, the PSBC in its earlier form (2.1) works as a margin classifier, classifying individuals as if doing hyperplane separation. On the other hand it is conceivable that the introduction of (1.7b) does not change this “margin classifier” approach, but simply relabels the tags in each of these hyperplanes, foreshadowing insurmountable difficulties the model might present in face of more complex labeling rules. This is indeed the case: consider for instance $(X_{(i)})_{1 \leq i \leq 2000}$ as a realization of i.i.d. uniform random variables in the interval $[0, 1]$, with

$$Y_{(i)} := \mathbb{1}_{[\gamma^*, \beta^*]}(X_{(i)}), \quad \text{for fixed } 0 < \gamma^* < \beta^* < 1. \quad (3.6)$$

The PSBC gives poor results, as shown in Table 3. Observe that this is not only a model limitation, but a limitation shared with other well known models like ANNs (with 1 or 2 hidden layers): only when the hidden layer of an ANN contains 3 or more nodes the ANN average performance is better than that of the PSBC.

Hidden* nodes	Average accuracy					
	ANN*		KNN - 3		PSBC	
	Train	Test	Train	Test	Train	Test
1	0.5736 ± 0.124	0.58 ± 0.1004	0.9994	0.9944	0.6822 ± 0.0028	0.653 ± 0.0037
2	0.6343 ± 0.2206	0.6382 ± 0.2128				
3	0.723 ± 0.204	0.7225 ± 0.196				
4	0.8415 ± 0.2013	0.8412 ± 0.1994				
5	0.884 ± 0.1275	0.877 ± 0.139				
6	0.8822 ± 0.1255	0.8745 ± 0.1352				
7	0.9909 ± 0.0068	0.9915 ± 0.0054				
8	0.9829 ± 0.0159	0.9853 ± 0.0146				
9	0.9777 ± 0.0383	0.9775 ± 0.0354				
10	0.9195 ± 0.2197	0.9198 ± 0.2166				

Table 3: Comparison among PSBC, ANNs and KNN with 3 neighbors. The dataset obeys a train-test split of 80%-20%, and is made of 2000 points following an i.i.d. uniform distribution on $[0, 1]$ with labels (3.6). ANN’s statistics were computed from 10 simulations for each number of hidden nodes, represented in the first column. PSBC’s statistics were computed from 10 simulations for each set of hyperparameters, using the model with phase (that is, in the form (3.4)) with parameters $N_t = 20$, weights- N_t -sharing, $\Delta_t^u = 0.1$ (initial), and patience = $+\infty$; learning rates were chosen according to Appendix A. There is no standard deviation for KNNs because the model is deterministic.

There are no issues with either of these models, but simply a lack of sufficient features to construct a good predictor. This is not a surprise, for the PSBC in the form (3.4) has a limited number of variables (in the case of a 1D model, for instance, the weights- N_t -sharing model uses only 2 trainable weights), which is definitely not enough to separate all types of points. In similar situations, non-parametric models - like KNN ¹² - may perform better (model accuracy for a KNN with 2 neighbors was also above 99% in both training and test set).

It is known that when feature space have an insufficient amount of features, one can extend it by constructing new features; for instance a simple construction $Z_{(i)} = 0.5 + 2 \cdot (X_{(i)} - 0.5)^2$ puts the pairs $(Z_{(i)}, Y_{(i)})$ in the form of Section 2’s toy problem, on which the PSBC performs much better (in fact,

¹². K Nearest Neighbors; see for instance (Hastie et al., 2001, Section 2.3.2 or Chapter 13).

it gives 100 % accuracy in both training and test set). Still, regardless of the model in use, figuring out how to map features to a different feature space involves engineering and modeling.

All the above remarks illustrate how low dimensional feature spaces can be detrimental to the model's accuracy. On the other hand, specially if we keep the Remark 2.8 in mind, it is conceivable that the model performs better in higher dimensional feature spaces for, intuitively, it is much simpler to separate points in a high dimensional space than in a low dimensional space. We shall dwell on these matters in the next section, showing that the PSBC is endowed with model compression properties, allowing trainable weights to be parametrized by less variables than the dimension of the feature space. We illustrate such properties by applying the PSBC to the MNIST database, whose features lie in \mathbb{R}^{784} .

4. The non-diffusive PSBC: the system of ODEs case

It is natural to extend the PSBC in the form (3.4) and cost (3.5) to cases in which features lie in a high dimensional feature space, where $U \in \mathbb{R}^{N_u}$ for any $N_u \geq 1$. Let us briefly recall the perspective adopted in Section 2.1: considering a map $\mathcal{E} : \mathbb{R}^{N_u} \times \mathbb{R} \rightarrow \mathbb{R}$, we describe the dynamics (of features) as a gradient flow,

$$\frac{dU}{dt} = -\nabla_U \tilde{\mathcal{E}}(U, \alpha). \quad (4.1)$$

The choice of $\tilde{\mathcal{E}}(\cdot; \cdot)$ is important, and we shall conveniently adopt

$$\tilde{\mathcal{E}}(U, \alpha) = \sum_{i=1}^{N_u} \mathcal{E}(U_i; \alpha), \quad (4.2)$$

where $\mathcal{E}(\cdot; \cdot)$ is given in Section 2.1. Numerically, matters are reduced to an Euler discretization, yielding a system of ODEs in vector form

$$U^{[n+1]} = U^{[n]} + \Delta_t^u f(U^{[n]}; \alpha^{[n]} \mathbf{1}), \quad U^{[0]} = X \in \mathbb{R}^{N_u}, \quad (4.3a)$$

$$P^{[n+1]} = P^{[n]} + \Delta_t^p f(P^{[n]}; \beta^{[n]}), \quad P^{[0]} = \frac{1}{2} \in \mathbb{R}, \quad (4.3b)$$

with notation $(f(U; V))_m = f(U_m; V_m)$.

Adopting (4.2) brings about immediate consequences:

- (i) On the downside, there are no interactions between features. Furthermore, the model now has 2^{N_u} stationary points, all of which can be stable with respect to the (continuum) dynamical system. Nevertheless, one should not neglect the presence of the cost function, that will adapt the trainable weights according to initial inputs and make some of these stationary points more preferable than others.
- (ii) On the upside, no interactions between features imply that (4.1) is decoupled in the variable U . Overall, decoupling allows for the ℓ^∞ -norm of U to be controlled using a ‘‘tensorized’’ version of the maximum principle (that is, we are consider maximum principles as applied to each entry U_m). Consequently, in this fashion invariant regions are more easily found and constructed as the cartesian product of each feature's invariant region.¹³

13. It is also reasonable to consider energy functions other than that in (4.2), at the expense of introducing interactions between features. In that case, proving the existence of invariant invariant regions may get more technical, possibly requiring more extensive use of the techniques in (Smoller, 1994, Chapter 14). We shall introduce coupling in the model using diffusion; see Section 5.

Remark 4.1 (Nonlocality of Back propagation and inverse problems) *Some caution is necessary with regards to decoupling of parameters and variables: although each entry of both $U^{[l]}$ and $P^{[l]}$ in (4.3) evolve independently during forward propagation, trainable weights $\alpha^{[l]}$ and $\beta^{[l]}$ are the same for all the components; thus, since the latter two weights vary over training, they affect the dynamics of $U^{[l]}$ and $P^{[l]}$. Therefore, if backpropagation is taken into account, features are not fully decoupled.*

However, if we scrutinize the model more, one immediately finds some unsatisfactory assumptions, like the presence of $\alpha^{[l]}\mathbf{1}$: in light of the previous discussion, why should we “couple” all features in such a way? In the sequel, we shall scrutinize this question extensively, studying possible ways to couple the parameters in (4.3). Upon doing that, we allow a bigger class of dynamical systems that have enough flexibility to better capture features salience.

4.1 Some auxiliary constructions: flexibilizing the number of trainable weights

Looking at the PSBC in the form (4.3) it becomes clear that constraining the trainable weights to the form $\alpha^{[l]}\mathbf{1}$ is too restrictive. Our main goal in this section consists in constructing a bigger space in which trainable weights are optimized, which we shall achieve by adding “spatial”-variability to the parameters $\alpha^{[l]}$.

Let’s first consider $\alpha^{[l]}$ as a restriction of polynomials to the grid $\mathbb{G}_N = \{1, \dots, N\}$,

$$a_m^{[n]} = p^{[n]}(m), \quad \text{for } p^{[n]}(x) = w_0^{[n]} + w_1^{[n]}x + \dots + w_k^{[n]}x^k, \quad (4.4)$$

with $m \in \mathbb{G}_N$, $k \in \mathbb{N}$, and $w_j^{[l]} \in \mathbb{R}$; this clearly encompasses the parametrization used in the PSBC (4.3) taking $k = 0$ and $\alpha^{[l]} = w_0^{[l]}\mathbf{1}$. In such a case there are $k + 1$ trainable weights¹⁴ $(w_j^{[l]})_{0 \leq j \leq k}$, where k can be much smaller than the dimension of the feature space \mathcal{X} (in striking difference to ANNs, where the number of trainable weights in the 0th layer is a multiple of the dimension of the features space). In matrix form, we write (4.4) as

$$\alpha^{[n]} := \begin{bmatrix} 1 & 1 & 1 & \dots & 1 \\ 1 & 2 & 2^2 & \dots & 2^k \\ 1 & 3 & (3)^2 & \dots & (3)^k \\ \vdots & \vdots & \vdots & \ddots & \vdots \\ 1 & N & (N)^2 & \dots & (N)^k \end{bmatrix} \cdot \begin{bmatrix} w_0^{[n]} \\ \vdots \\ w_k^{[n]} \end{bmatrix} =: \mathcal{V} \cdot \begin{bmatrix} w_0^{[n]} \\ \vdots \\ w_k^{[n]} \end{bmatrix}, \quad (4.5)$$

where the matrix $\mathcal{V} \in \mathbb{R}^{N_u \times (k+1)}$ is a Vandermonde matrix. In spite of its generality, we do not pursue this approach: first, because changes in any trainable $w_j^{[l]}$ weight disturb all the entries in $\alpha^{[l]}$, displaying some sort of non-locality; second, due to numerical stability, for Vandermonde matrices can have their ℓ^∞ norms exponentially increasing in N_u (and in many circumstances have high condition number (Gautschi, 1990), (Trefethen and Bau, 1997, Lectures 18 and 19)).

In order to avoid the pitfalls of the previous approach we shall take a different route, which begins in the following definition. However, we keep some useful ideas, in particular the parametrization of the space of trainable weights, which adds flexibility to the model while allowing the number of trainable weights in each layer to be reduced.

14. Because of aliasing, one can only discern finitely many polynomials restrictions to the grid \mathbb{G}_N ; cf. (Trefethen, 2000, Chapter 2, page 11). It implies that the number of polynomials $p^{[l]}(\cdot)$ is finite and depends on N_u .

Definition 4.2 (Partition of unity) Given $N \in \mathbb{N}$, fix $N_{\text{ptt}} \in \mathbb{G}_N = \{1, \dots, N\}$ (that is, $N_{\text{ptt}} \leq N$). We say that the set $(\pi_j)_{1 \leq j \leq N_{\text{ptt}}}$ is a cover of \mathbb{G}_N whenever

$$\bigcup_{j=1}^{N_{\text{ptt}}} \pi_j = \mathbb{G}_N, \quad \text{and} \quad \pi_j \cap \pi_l = \emptyset, \quad \text{for all } j \neq l, \quad 1 \leq j, l \leq N_{\text{ptt}}.$$

To each cover one associates a partition of unity, consisting of N_{ptt} vectors $(e_{\pi_j})_{1 \leq j \leq N_{\text{ptt}}} \subset \mathbb{R}^N$ with the property that

$$e_{\pi_j} = \sum_{l \in \pi_j} e_l \in \mathbb{R}^N, \quad \text{where} \quad \sum_{j=1}^{N_{\text{ptt}}} e_{\pi_j} = \mathbf{1} \in \mathbb{R}^N.$$

(See notation in Section 1.3.) In such case, one says that $(e_{\pi_j})_{1 \leq j \leq N_{\text{ptt}}}$ is subordinate to the cover $(\pi_j)_{1 \leq j \leq N_{\text{ptt}}}$, referring to N_{ptt} as the partition (or cover) cardinality.

With a partition of unity $(e_{\pi_j})_{1 \leq j \leq N_{\text{ptt}}}$ in hands one constructs a N_{ptt} -dimensional subspace of $\mathbb{R}^{N_{\text{u}}}$. Each element e_{π_j} has support π_j , which can yield a sparse basis whenever the ratio $\lfloor \frac{N_{\text{u}}}{N_{\text{ptt}}} \rfloor$ is small. We shall use them to write $\alpha^{[n]} = \sum_{j=1}^{N_{\text{ptt}}} w_j^{[n]} e_{\pi_j}$.

Remark 4.3 (Partitions of unity, decomposition, and segmentation) In addition to that, partitions of unity can be used to decompose the feature space in patches, within which features are coupled; in this form, the model captures correlation between different features, as discussed in Remark 4.1. Indeed, any partition of unity $e_{\pi_1}, \dots, e_{\pi_{N_{\text{ptt}}}}$ yields a decomposition of the vector space \mathbb{R}^N ,

$$u = \sum_{j=1}^{N_{\text{ptt}}} u \circledast e_{\pi_j} =: \sum_{j=1}^{N_{\text{ptt}}} \Pi_j[u], \quad (4.6)$$

since each e_{π_j} can be seen as an orthogonal projection $\text{diag}(e_{\pi_j})$; cf. (Kato, 1995, I, §7) (for notation, see the comment right above (N2)). One can consider the above decomposition as an static version of the segmentation, a technique commonly used in image processing (Shapiro and Stockman, 2001, Chapter 10); see an extended discussion in Section 6.7.

For now we shall focus on very particular types of covers, used to construct *ordered partitions*.

Definition 4.4 (Ordered covers and ordered partitions of unity) Let N_{u} to be the dimension of the feature space \mathcal{X} in (1.7). Fix $1 \leq N_{\text{ptt}} \leq N_{\text{u}}$ and define $k := \lfloor \frac{N_{\text{u}}}{N_{\text{ptt}}} \rfloor$; that is, $k \in \mathbb{Z}$ is the largest number such that $N_{\text{u}} = k \cdot N_{\text{ptt}} + R_*$, with $0 \leq R_* \leq N_{\text{ptt}} - 1$. For $1 \leq j \leq N_{\text{ptt}}$, define numbers l_j, r_j such that

$$1 =: l_1 \leq r_1 < l_2 \leq r_2 < \dots < l_{N_{\text{ptt}}} \leq r_{N_{\text{ptt}}} := N_{\text{u}},$$

with $r_j - l_j = \begin{cases} N_{\text{ptt}}, & \text{when } 1 \leq j \leq R_*, \\ N_{\text{ptt}} - 1, & \text{when } R_* + 1 \leq j \leq N_{\text{ptt}} \end{cases}$ and $l_{j+1} - r_j = 1$, for all $1 \leq j \leq N_{\text{ptt}}$.

Setting $\pi_j^* := \{l_j, l_j + 1, \dots, r_j\}$ we obtain a cover to $\mathbb{G}_{N_{\text{u}}}$ with cardinality N_{ptt} , since

$$\bigcup_{j=1}^{N_{\text{ptt}}} \pi_j^* = \{1, \dots, N_{\text{u}}\}, \quad \text{and} \quad \pi_j^* \cap \pi_{N_{\text{ptt}}-j+1}^* = \emptyset \quad \text{whenever } j \neq k.$$

We call $(\pi_j^*)_{1 \leq j \leq N_{\text{ptt}}}$ an ordered cover of $\mathbb{G}_{N_{\text{u}}}$, and its associate partition of unity $(e_{\pi_j^*})_{1 \leq j \leq N_{\text{ptt}}}$ an ordered partition of unity.

Observation 4.5 *In all numerical applications considered in this paper we shall always use ordered covers and ordered partitions.*

Now, given $N_u \in \mathbb{N}$ and $1 \leq N_{\text{ptt}} \leq N_u$, let $\pi_1^*, \dots, \pi_{N_{\text{ptt}}}^*$ be an ordered cover (with cardinality N_{ptt}) of \mathbb{G}_N , to which one associates a uniquely defined basis matrix \mathcal{B}^* ,

$$\mathcal{B}^* := \begin{bmatrix} | & | & \cdots & | \\ e_{\pi_1^*} & e_{\pi_2^*} & \cdots & e_{\pi_{N_{\text{ptt}}}^*} \\ | & | & \cdots & | \end{bmatrix}. \quad (4.7)$$

Notice that each row contains only one non-zero element, equal to 1, and the number of non-zero elements in two different columns differ by at most one. Consequently, the ℓ^∞ -norm of \mathcal{B} norm is always 1, in sharp contrast to properties of the Vandermonde matrices in (4.5).

In view of (4.7), we consider $\alpha^{[n]}$ of the form

$$\alpha^{[n]} := \sum_{j=1}^{N_{\text{ptt}}} w_j^{[n]} e_{\pi_j^*} = \mathcal{B}^* \begin{bmatrix} w_1^{[n]} \\ \vdots \\ w_{N_{\text{ptt}}}^{[n]} \end{bmatrix}, \quad \text{where } w_j^{[n]} \in \mathbb{R}, n \in \mathbb{N}. \quad (4.8)$$

As before, we define $\Pi_j^*(\alpha^{[n]}) := w_j^{[n]} e_{\pi_j^*}$.

If we bear in mind the role of (1.7b) and its variable $P^{[j]}$ in fixing labeling issues, we now take another step, allowing each cover element π_j^* to be associated with phase parameter P_j evolved using equation (4.3b). In this fashion, relabeling is also subordinate to the cover $(\pi_j^*)_{1 \leq j \leq N_{\text{ptt}}}$, which also increases the complexity of the space in which the prediction map is constructed; the quality of these approximations with respect to the ℓ^2 norm can be seen in Figure 12.

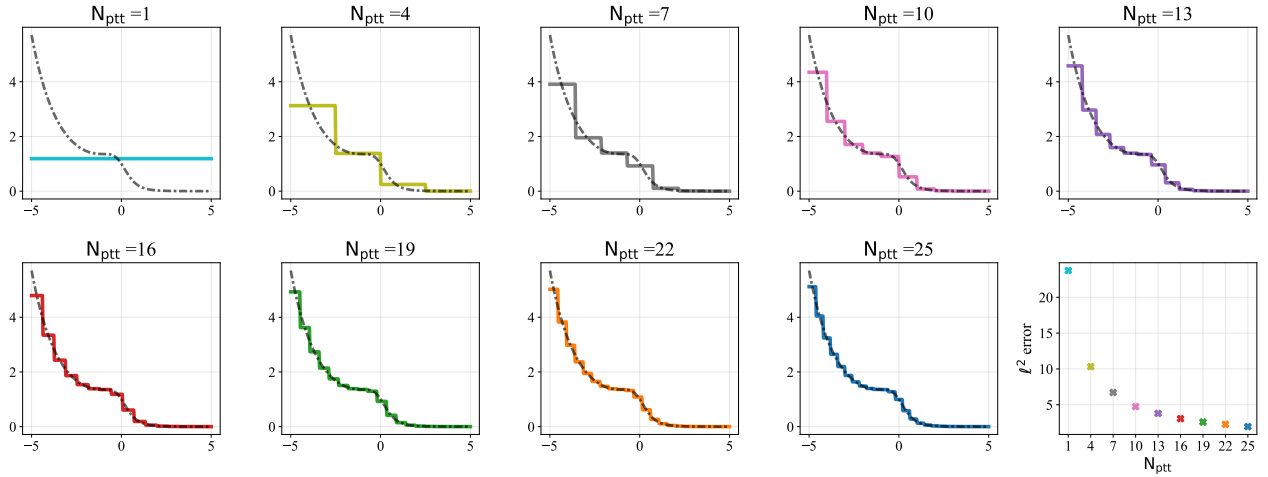


Figure 12: Approximation of $f(x) = \frac{e^{-x}}{x^2 + 1}$ in a grid $\mathbb{G}_{300} = \{1, \dots, 300\}$, using ordered partitions of unity with different partition cardinalities.

But before moving forward we must adapt the homotopy construction introduced in (3.1). We shall contemplate two different possibilities.

Definition 4.6 (Subordinate and non-subordinate models) *Given $1 \leq N_{\text{ptt}} \leq N_u$ and a basis matrix \mathcal{B}^* as in (4.7). Then, two options are available:*

(i) (**Non-subordinate phase**) Set $N_p := 1$ (hence, $P^{[\cdot]} \in \mathbb{R}$). Define

$$\widetilde{P^{[N_t]}} := P^{[N_t]} \mathbf{1}_{N_u} = \mathcal{B}^* \cdot \left(P^{[N_t]} \mathbf{1}_{N_{\text{ptt}}} \right) \in \mathbb{R}^{N_u},$$

where $P^{[\cdot]}$ evolves by (1.7b).

(ii) (**Subordinate phase**) Set $N_p := N_{\text{ptt}}$ (hence, $P^{[\cdot]} \in \mathbb{R}^{N_{\text{ptt}}}$). Define

$$\widetilde{P^{[N_t]}} := \mathcal{B}^* \cdot P^{[N_t]} = \sum_{j=1}^{N_{\text{ptt}}} P_j^{[N_t]} e_{\pi_j^*} \in \mathbb{R}^{N_u}, \quad \text{for } P^{[N_t]} = \begin{bmatrix} P_1^{[N_t]} \\ \vdots \\ P_{N_{\text{ptt}}}^{[N_t]} \end{bmatrix} \in \mathbb{R}^{N_{\text{ptt}}},$$

where $P^{[\cdot]}$ evolves by (1.7b).

Different types of layers are illustrated in Figure 13.

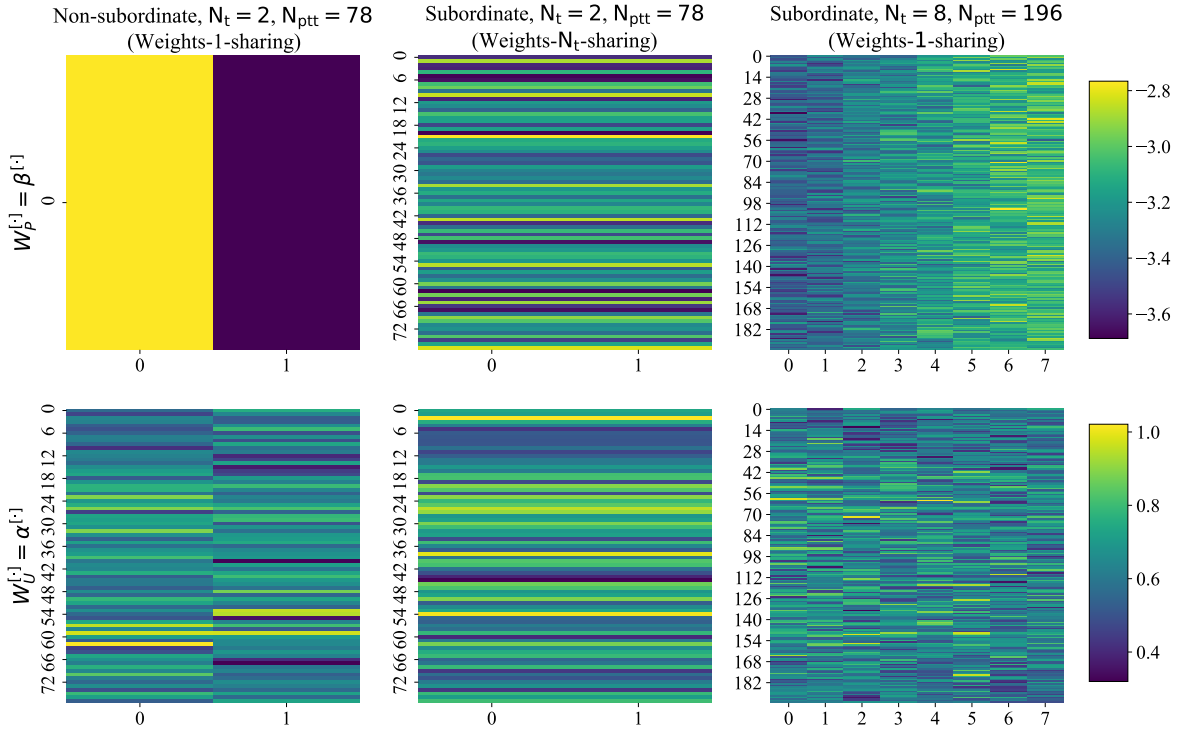


Figure 13: Heatmaps of trainable weights for different types of PSBC models trained on the MNIST database: the models on the left and middle are non-diffusive; the model on the right is diffusive, with Neumann boundary conditions (see Section 4).

Finally, we make use of the previous constructions in order to extend (4.3) as

$$U_m^{[n+1]} = U_m^{[n]} + \Delta_t^u f(U_m^{[n]}; \alpha_m^{[n]}), \quad \text{for } 1 \leq m \leq N_u, \quad (4.9a)$$

$$P_j^{[n+1]} = P_j^{[n]} + \Delta_t^p f(P_j^{[n]}; \beta_j^{[n]}), \quad \text{for } 1 \leq j \leq N_p \quad (4.9b)$$

where $N_p = 1$ (non-subordinate phase) or $N_p = N_{\text{ptt}}$ (subordinate phase). As said before, we refer to this model as the non-diffusive PSBC.

Last, for the cost function we proceed as in (3.1): we define a multidimensional version of (3.2),

$$\mathbb{R}^{N_u} \times \mathbb{R}^{N_u} \ni (p, u) \mapsto \mathcal{S}_{N_u}^{(p)}(u) := (\mathbf{1} - p) \circledast \mathcal{S}_{N_u}^{(0)}(u) + p \circledast \mathcal{S}_{N_u}^{(1)}(u). \quad (4.10)$$

where $\mathcal{S}_{N_u}^{(0)}(u) = u$, $\mathcal{S}_{N_u}^{(1)}(u) = \mathbf{1} - u$ are maps from \mathbb{R}^{N_u} to itself. The cost function is then

$$\text{Cost}_{\mathcal{D}} = \frac{1}{2N_d} \sum_{i=1}^{N_d} \left\| \mathcal{S}_{N_u}^{(\widetilde{P}^{[N_t]})} \left(U^{[N_t]}(X_{(i)}; \alpha) \right) - Y_{(i)} \mathbf{1} \right\|_{\ell^2(\mathbb{R}^{N_u})}^2, \quad (4.11)$$

where $\widetilde{P}^{[N_t]}$ is constructed according to Definition 4.6.

As noted, in the non-diffusive PSBC each feature evolves independently, without coupling (at least throughout forward propagation, for Remark 4.1 still applies). In this way, one can foresee the global existence of forward propagation, extending the results in Proposition 2.2.

Proposition 4.7 (Global existence of forward propagation, non-diffusive PSBC (4.9)) *Let $N_t \in \mathbb{N} \cup \{+\infty\}$ and $U^{[0]} := X \in [0, 1]^{N_u}$. Given two sequences of trainable weights $(\alpha^{[n]})_{0 \leq n \leq N_t-1} \in \mathbb{R}^{N_u}$ and $(\beta^{[n]})_{0 \leq n \leq N_t-1} \in \mathbb{R}^{N_p}$, augmented by $\alpha^{[-1]} := \mathbf{1} \in \mathbb{R}^{N_u}$ and $\beta^{[-1]} := \mathbf{1} \in \mathbb{R}^{N_p}$, denote by $U^{[k]}(X, \alpha^{[k]})$ and $P^{[k]}(\frac{1}{2} \mathbf{1}, \beta^{[k]})$ the values obtained using (4.9). For any fixed $1 \leq v \leq N_u$ and $-1 \leq k \leq N_t - 1$, define the quantities*

$$L_{\alpha,v}^{[k]} := \inf_{-1 \leq n \leq k} \left(\min \left\{ \alpha_v^{[n]}, 0 \right\} \right), \quad R_{\alpha,v}^{[k]} := \sup_{-1 \leq n \leq k} \left(\max \left\{ \alpha_v^{[n]}, 1 \right\} \right),$$

and assume that

$$-\infty < L_{\alpha,v}^{[N_t-1]}, \quad \text{and} \quad R_{\alpha,v}^{[N_t-1]} < +\infty.$$

Under similar assumptions, define $L_{\beta,q}^{[k]}$ and $R_{\beta,q}^{[k]}$ for all $1 \leq q \leq N_p$.

Assume the Invariant Region Enforcing Condition (1.14), holding in the form

$$0 \leq \Delta_t^u \leq \min_{1 \leq v \leq N_u} \frac{1}{\sqrt{3} \left(|L_{\alpha,v}^{[N_t-1]}| + |R_{\alpha,v}^{[N_t-1]}| \right)^2}, \quad 0 \leq \Delta_t^p \leq \min_{1 \leq q \leq N_p} \frac{1}{\sqrt{3} \left(|L_{\beta,q}^{[N_t-1]}| + |R_{\beta,q}^{[N_t-1]}| \right)^2}. \quad (4.12)$$

Then, for any $1 \leq v \leq N_u$ and $1 \leq q \leq N_p$ the sequences $U_v^{[k]}(X, \alpha^{[k]})$ and $P_q^{[k]}(X, \beta^{[k]})$ satisfy

$$\begin{aligned} L_{\alpha,v}^{[k-1]} - \Delta_t^u M_{\alpha,v}^{[k-1]} &\leq U_v^{[k]}(X, \alpha^{[k]}) \leq R_{\alpha,v}^{[k-1]} + \Delta_t^u M_{\alpha,v}^{[k-1]}, \\ L_{\beta,q}^{[k-1]} - \Delta_t^p M_{\beta,q}^{[k-1]} &\leq P_q^{[k]}(X, \beta^{[k]}) \leq R_{\beta,q}^{[k-1]} + \Delta_t^p M_{\beta,q}^{[k-1]}, \end{aligned} \quad (4.13)$$

for all $0 \leq k \leq N_t$ and $M_{(\gamma,\cdot)}^{[k]} := (|L_{(\gamma,\cdot)}^{[k]}| + |R_{(\gamma,\cdot)}^{[k]}|)^3$ for $\gamma \in \{\alpha, \beta\}$. In particular, for all $0 \leq k \leq N_t$, we have

$$|U_v^{[k]}(X, \alpha^{[k]})| \leq (1 + \Delta_t^u) M_{\alpha,v}^{[k-1]}, \quad \text{and} \quad \left| P_q^{[k]} \left(\frac{1}{2}, \beta^{[k]} \right) \right| \leq (1 + \Delta_t^p) M_{\beta,q}^{[k-1]}.$$

The previous results will be mostly used in the following way.

Corollary 4.8 *Proposition 4.7 still holds with $L_{\alpha,v}^{[k]}$ and $R_{\alpha,v}^{[k]}$ substituted respectively by $L_{\alpha}^{[k]}$ and $R_{\alpha}^{[k]}$, where*

$$L_{\alpha}^{[k]} := \inf_{-1 \leq n \leq k} \left(\min_{1 \leq v \leq N_u} \{ \alpha_v^{[n]}, 0 \} \right) \quad R_{\alpha}^{[k]} := \sup_{-1 \leq n \leq k} \left(\max_{1 \leq v \leq N_u} \{ \alpha_v^{[n]}, 1 \} \right),$$

and for similarly defined $L_{\beta}^{[k]}$ and $R_{\beta}^{[k]}$ substituting $L_{\beta,q}^{[k]}$ and $R_{\beta,q}^{[k]}$, respectively. In this case, (4.13) reads as

$$\begin{aligned} (L_{\alpha}^{[k-1]} - \Delta_t^u M_{\alpha}^{[k-1]}) \mathbf{1} &\leq U^{[k]}(X, \alpha^{[k]}) \leq (R_{\alpha}^{[k-1]} + \Delta_t^u M_{\alpha}^{[k-1]}) \mathbf{1}, \\ (L_{\beta}^{[k-1]} - \Delta_t^p M_{\beta}^{[k-1]}) \mathbf{1} &\leq P^{[k]}(X, \beta^{[k]}) \leq (R_{\beta}^{[k-1]} + \Delta_t^p M_{\beta}^{[k-1]}) \mathbf{1}. \end{aligned}$$

with $M_{\gamma}^{[k]} := (|L_{\gamma}^{[k]}| + |R_{\gamma}^{[k]}|)^3$ for $\gamma \in \{\alpha, \beta\}$.

4.2 The non-diffusive PSBC applied to the MNIST database

We illustrate the non-diffusive PSBC (4.9) by applying it to the classical MNIST database; see Appendix A and also Figure 6. Recall that we would like to predict which class a handwritten image belongs to.

Besides normalization (N-C), it is evident that further preprocessing is necessary: images are 2D, but the model is 1D. This is circumvented by flattening¹⁵ the images before using them as initial condition in the PSBC, a procedural step also used in other models, like ANNs. Evidently, in this step there is loss of information about the spatial distribution of pixels; extending the PSBC as a higher dimensional nonlinear diffusion that preserves the structure of the input space is an interesting direction of investigation (see further discussion in Section 6.9). In spite of flattening the data, the non-diffusive PSBC achieves high accuracy, highlighting in a remarkable way model compression qualities of this classifier; see Table 4 and the discussion below.

Before going further, we briefly explain how model selection is performed, pointing the reader to Appendix A for further details. Recall that in many cases hyperparameters can assume a wide range of values of which, in practice, only some are tested. Model selection is used to choose the best one among those in the latter group, according to some metric. There is in our case a secondary goal which is, nonetheless, as important: understanding the effect of varying hyperparameters, specially diffusion, in a PSBC model that has already been trained; in this section we only vary the partition number N_{ptt} , leaving the study of diffusion effect on model’s accuracy to the next one. Hence, assume a PSBC with predefined hyperparameters except for N_{ptt} , which we fix at $196 = \frac{28^2}{4}$. Then, we run a grid search (over a predefined grid) to select the learning rate using a 5-fold cross validation on train-dev sets, choosing the learning rate that achieves the highest average performance. With a learning rate in hands (and fixed), we now run the PSBC for different values of partition cardinality N_{ptt} , training on the full train-dev set (model fitting), and asserting its quality on the test set (which, we emphasize, up to this point has been untouched). The latter results are those displayed here under the labels “train” and “test”, respectively.

Table 4 concerns the study of changes in partition cardinality and their effect on model’s accuracy. Results correspond to non-diffusive PSBC models with $N_t = 2$ in two different scenarios for its phase: subordinate or non-subordinate.

When the partition cardinality increases from 196 accuracy deteriorates in both cases, although in a much faster way in weights- N_t -sharing models, in some cases degrading to below 50% accuracy, where the model is no better than simply guessing, with values similar to base rates (that is, the proportion of each class in the training and test set). There is no immediate answer to this; definitely,

15. That is, to map a matrix in $R^{N \times N}$ to a column vector $R^{N^2 \times 1}$.

Average accuracy (weights-1-sharing)				
N_{ptt}	Non-subordinate		Subordinate	
	Train	Test	Train	Test
78	0.9373 ± 0.00016	0.93627 ± 0.00015	0.93745 ± 0.0001	0.93633 ± 0.00018
87	$0.93737 \pm 9\text{e-}05$	0.93623 ± 0.0002	0.93735 ± 0.00016	0.93627 ± 0.00017
98	0.93752 ± 0.00012	0.93633 ± 0.00018	0.93749 ± 0.00018	0.9364 ± 0.00015
112	0.93743 ± 0.00011	0.9365 ± 0.00014	0.93751 ± 0.00014	0.93633 ± 0.00031
130	0.93785 ± 0.0001	0.93647 ± 0.00018	0.93784 ± 0.00018	0.93654 ± 0.00017
156	$0.93792 \pm 7\text{e-}05$	0.93654 ± 0.00017	0.93797 ± 0.00013	0.9366 ± 0.00022
196	0.9382 ± 0.00011	0.93677 ± 0.00022	0.93821 ± 0.00014	0.93677 ± 0.00024
261	$0.93839 \pm 8\text{e-}05$	0.93698 ± 0.18258	0.93838 ± 0.00019	0.93684 ± 0.00067
392	$0.9385 \pm 6\text{e-}05$	0.93694 ± 0.0	0.93852 ± 0.0	0.93694 ± 0.0
784	0.46355 ± 0.0	0.48106 ± 0.0	0.46355 ± 0.0	0.48106 ± 0.0

Average accuracy (weights- N_t -sharing)				
N_{ptt}	Non-subordinate		Subordinate	
	Train	Test	Train	Test
78	$0.93755 \pm 8\text{e-}05$	0.9364 ± 0.00015	0.9375 ± 0.0001	0.93637 ± 0.00018
87	0.93747 ± 0.0001	0.93633 ± 0.0002	0.93756 ± 0.00016	0.93623 ± 0.00017
98	0.93768 ± 0.00012	0.93643 ± 0.00018	0.93766 ± 0.00018	0.9364 ± 0.00015
112	$0.9375 \pm 7\text{e-}05$	0.93633 ± 0.00014	0.93754 ± 0.00014	0.93627 ± 0.00031
130	$0.9379 \pm 8\text{e-}05$	0.93643 ± 0.00018	0.93789 ± 0.00018	0.93654 ± 0.00017
156	$0.93807 \pm 9\text{e-}05$	0.9366 ± 0.00017	0.93806 ± 0.00013	0.93664 ± 0.00022
196	$0.93821 \pm 9\text{e-}05$	0.93684 ± 0.00022	0.93822 ± 0.00014	0.93677 ± 0.00024
261	0.84327 ± 0.18986	0.84621 ± 0.18258	0.93826 ± 0.00019	0.93714 ± 0.00067
392	0.46355 ± 0.0	0.48106 ± 0.0	0.46355 ± 0.0	0.48106 ± 0.0
784	0.46355 ± 0.0	0.48106 ± 0.0	0.46355 ± 0.0	0.48106 ± 0.0

Table 4: Comparison between average accuracy for non-subordinate and subordinate models applied to the MNIST database. A visualization of the data in this table for $N_{\text{ptt}} \leq 196$ can be seen in Figure 14; the region $N_{\text{ptt}} > 196$ has been omitted because average accuracy drops substantially, preventing standard deviation bars from being seen. Statistics were computed from a sample space of 10 simulations for each set of hyperparameters. Hyperparameters were $N_t = 2$, $\Delta_t^u = 0.1$ (initial), $\Delta_t^p = 0.1$ (initial). Learning rates were chosen according to Appendix A, at $N_{\text{ptt}} = 196$.

more simulations like that should be performed in other contexts and for other datasets. One possible explanation is that (i) all hyperparameters being the same but the partition number N_{ptt} , the model with the largest N_{ptt} has more trainable weights to be optimized; (ii) the cost function increases in complexity (that is, polynomial degree) proportionally to N_{ptt} , hence a learning rate that is appropriate for lower complexity surfaces might not capture new “ruggedities” (in fact, the number of critical points) that appear as N_{ptt} increases.

It is also interesting to analyze parameters varying in the opposite direction (that is, of diminishing the partition cardinality) and its impact on model’s accuracy, although the overall effect in such cases is less dramatic, for accuracy does not degrade as much as in the above case. If we follow the previous paragraph’s reasoning, in this case the cost manifold is less complex (in polynomial order), the number of critical points decrease, and the learning rate used for $N_{\text{ptt}} = 196$ still works well, as shown in Figure 14. It is worthwhile to highlight that high accuracy is achieved even in the case of a non-subordinate

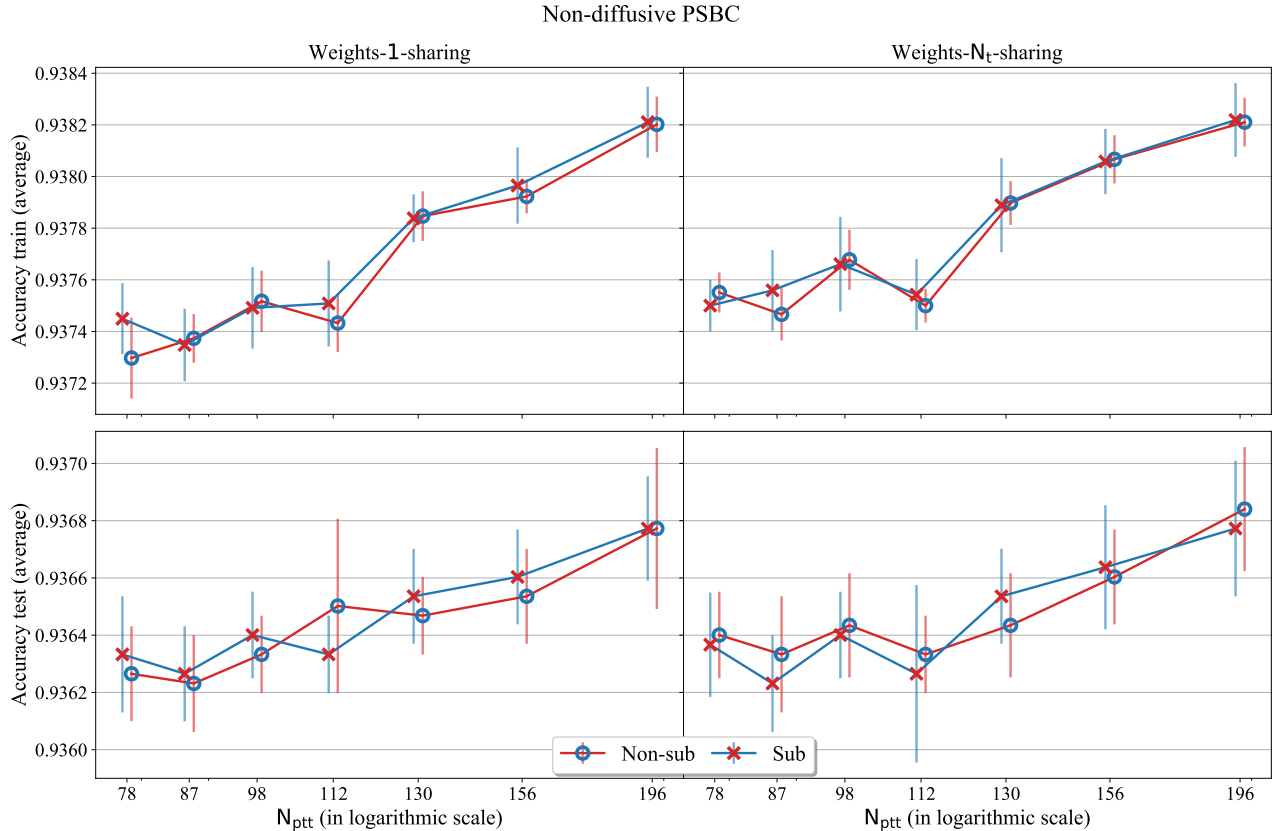


Figure 14: Using a non-diffusive PSBC, we study the effect of varying partition cardinality N_{ptt} on model accuracy, applied to the MNIST database. Hyperparameters were weights- K -sharing for $K \in \{1, N_t\}$, $N_t = 2$, $\Delta_t^u = 0.1$ (initial), $\Delta_t^p = 0.1$ (initial). Learning rates were chosen according to Appendix A, at $N_{\text{ptt}} = 196$. Statistics were taken from a sample space of 10 simulations for each set of hyperparameters. Vertical bars with the same colors as lines denote 1 standard deviation. For the table with numerical data, see Table 4.

PSBC with weights- N_t -sharing and $N_{\text{ptt}} = 78$, where less than 80 trainable weights are been used for model fitting (see Table 4), a remarkable manifestation of PSBC’s model compression qualities and an impossible milestone for ANNs, where the minimum number of nodes is always bigger than the dimension of the input space (784); cf. (Bishop, 2006, Chapter 5).

Figure 14 provides a comparison between the model’s behavior when one adopts weights-1-sharing and weights- N_t -sharing, indicating no substantial difference in their accuracy results and generalization properties. A notable difference, however, is hidden in their computational cost: training non-subordinate PSBCs with weights- N_t -sharing is computationally much cheaper than training a subordinate PSBC with weights-1-sharing, which once again touches on model compression properties of the classifier.

5. The diffusive PSBC

Our discussion in this final part ends in the PSBC in its full form (1.7). Most of the machinery necessary for the presentation has already been derived in the previous section, therefore we shall focus on the role of the diffusive term.

5.1 On feedforward networks, the Allen-Cahn equation, and the PSBC

If we scrutinize the assumption (4.2) on the Energy function - which leads to non-diffusive PSBC (4.9) - we are faced with an immediate objection to the non-diffusive PSBC, mostly because features do not “interact” during forward propagation (see, however, Remark 4.1). We can mitigate this lack of interaction by adding to (4.2) a penalization term of form $\frac{\varepsilon}{2} \sum_{m=1}^{N_u} \left| U_m^{[\cdot]} - U_{m+1}^{[\cdot]} \right|^2$, with due adjustments to account for boundary conditions; the strength of this penalization is controlled by a diffusion parameter ε . Clearly, such a term is only added to the variable $U^{[\cdot]}$'s equations.

Adding diffusion introduces feature interaction and, in passing, features correlation into the model.¹⁶ Obviously, the diffusive PSBC as shown below agrees with the non-diffusive PSBC (4.9) when $\varepsilon = 0$. In essence, both variables $U^{[\cdot]}$ and $P^{[\cdot]}$ still evolve in tandem: the variable $U^{[\cdot]}$ as a semi-implicit discretization of the Allen-Cahn equation, whereas $P^{[\cdot]}$ remains as before, evolving as an ODE,¹⁷

$$\frac{U_m^{[n+1]} - U_m^{[n]}}{\Delta_t^u} = \varepsilon^2 \left(U_{m+1}^{[n+1]} - 2U_m^{[n+1]} + U_{m-1}^{[n+1]} \right) + f(U_m^{[n]}; \alpha_m^{[n]}), \quad \text{for } 1 \leq m \leq N_u, \quad (5.1a)$$

$$\frac{P_j^{[n+1]} - P_j^{[n]}}{\Delta_t^p} = f(P_j^{[n]}; \beta_j^{[n]}), \quad \text{for } 1 \leq j \leq N_p, \quad (5.1b)$$

where $f(u, w) = u(1-u)(u-w)$.

As before, $\alpha^{[n]}$ is constructed using a fixed ordered cover $\pi_1^*, \dots, \pi_{N_{\text{ptt}}}^*$, as described in (4.8). Moreover, the model can be either subordinate ($N_p = 1$) or non-subordinate ($N_p = N_{\text{ptt}}$), as we recall from Definition 4.6.

With (5.1a) as a discretization of a parabolic PDE, boundary conditions must be taken into account. For now we shall limit ourselves to homogeneous boundary conditions of Neumann type,¹⁸

$$U_0^{[n]} := U_{+2}^{[n]}, \quad \text{and} \quad U_{N_u+1}^{[n]} := U_{N_u-1}^{[n]}, \quad \forall n \in \mathbb{N},$$

pointing the reader to Section 6.3 for the case of Periodic boundary conditions.

The connection between the PSBC and the feedforward network description in Figure 1 becomes more pronounced if we rewrite (5.1a) in vectorial form,

$$\mathcal{L}_{N_u} U^{[n+1]} = U^{[n+1]} - \varepsilon^2 \Delta_t^u D_{N_u} U^{[n+1]} = U^{[n]} + \Delta_t^u f(U^{[n]}; \alpha^{[n]}), \quad (5.2)$$

where

$$\mathcal{L}_{N_u} := \text{Id}_{N_u} - \varepsilon^2 \Delta_t^u D_{N_u}, \quad \text{with} \quad D_{N_u} = \begin{bmatrix} -2 & 2 & 0 & \dots & 0 \\ 1 & -2 & 1 & \dots & 0 \\ 0 & 1 & -2 & \dots & 0 \\ \vdots & \ddots & \ddots & -2 & 1 \\ 0 & & 0 & 2 & -2 \end{bmatrix} \in \mathbb{R}^{N_u \times N_u}; \quad (5.3)$$

a similar formula holds for (5.1b), with $\mathcal{L}_{N_p} := \text{Id}_{N_p}$. A direct application of Gershgorin's Theorem (Dym, 2007, Theorem 20.12) implies that \mathcal{L}_{N_u} is invertible for all $\Delta_t^u \geq 0$, $\varepsilon \geq 0$. Therefore, (5.2) reads as

$$U^{[n+1]} = \mathcal{L}_{N_u}^{-1} \cdot \left(U^{[n]} + \Delta_t^u f(U^{[n]}; \alpha^{[n]}) \right). \quad (5.4)$$

16. As we shall see later, our model is still fully connected, but the strength of the interaction decays the farther away features are; see discussion below.

17. This ODE can also be seen as a reaction model, with degenerate diffusion.

18. We readily see that this is consistent with boundary conditions of Neumann type, since $f(x+h) = f(x-h) = f(x) + O(h^2)$ whenever $f(\cdot) \in \mathcal{C}^2(\mathbb{R}; \mathbb{R})$.

Now, writing

$$Z^{[n]} := \begin{pmatrix} U^{[n]}(X, \alpha^{[n]}) \\ P^{[n]}(\frac{1}{2}\mathbf{1}, \beta^{[n]}) \end{pmatrix}, \quad W^{[n]} := \begin{pmatrix} W_U^{[n]} \\ W_P^{[n]} \end{pmatrix} = \begin{pmatrix} \alpha_1^{[n]} \\ \vdots \\ \alpha_{N_u}^{[n]} \\ \beta_1^{[n]} \\ \vdots \\ \beta_{N_p}^{[n]} \end{pmatrix}, \quad \text{with } \alpha^{[n]} = \mathcal{B}^* \cdot \begin{bmatrix} w_1^{[n]} \\ \vdots \\ w_{N_{\text{ptt}}}^{[n]} \end{bmatrix},$$

we define the activation function $\sigma^{[n]}(\cdot, \cdot, \cdot, \cdot)$ as a map from $\mathbb{R}^{N_u} \times \mathbb{R}^{N_u} \times \mathbb{R}^{N_p} \times \mathbb{R}^{N_p}$ to itself,

$$\sigma^{[n]}(U, W_U, P, W_P) := \begin{pmatrix} (\mathcal{L}_{N_u})^{-1} \cdot (U + \Delta_t^u f(U, W_U)) \\ P + \Delta_t^p f(P, W_P) \end{pmatrix}. \quad (5.5)$$

Thus, we can write the discrete evolution (1.7) using the general framework presented in (1.3),

$$Z^{[n+1]} = \begin{pmatrix} U^{[n+1]} \\ P^{[n+1]} \end{pmatrix} = \sigma^{[n]}(U^{[n]}, W_U^{[n]}, P^{[n]}, W_P^{[n]}) = \sigma^{[n]}(Z^{[n]}, W^{[n]}) \quad (5.6)$$

Obviously, this structure persists for the non-diffusive PSBC case (with $\mathcal{L}_{N_u} = \text{Id}_{N_u}$).

Remark 5.1 (The PSBC and ANNs) *It is important to contrast (5.6) with the standard artificial neural networks model,*

$$\tilde{Z}^{[n+1]} = \tilde{\sigma}^{[n]}(\tilde{W}^{[n]} \cdot \tilde{Z}^{[n]} + \tilde{b}^{[n]}), \quad (5.7)$$

where $\tilde{Z}^{[n]} \in \mathbb{R}^{z_n \times 1}$, trainable weights are $\tilde{W}^{[n]} \in \mathbb{R}^{z_{n+1} \times z_n}$ and $\tilde{b}^{[n]} \in \mathbb{R}^{z_{n+1} \times 1}$, and $\tilde{\sigma}^{[n]}(\cdot) \in \mathbb{R}^{z_{n+1}} \rightarrow \mathbb{R}^{z_{n+1}}$ is an activation function that can be for instance a nonlinearity of type $\tanh(\cdot)$ in each entry. Since $\tilde{W}^{[n]}$ acts on all entries of $\tilde{Z}^{[n]}$ this type of layers are called fully-connected, or dense.

The relation (5.7) shows that the entries of $\tilde{Z}^{[n]}$ are linearly recombined through left multiplication by $\tilde{W}^{[n]}$, and are later on amplified by the nonlinearity (activation function) $\tilde{\sigma}^{[n]}$. In contrast, in (5.6) each feature gets amplified by the nonlinearity $f(\cdot, \cdot)$, to afterwards be linearly recombined through left multiplication by $(\mathcal{L}_{N_u})^{-1}$.

We also remark that $f(\cdot; \cdot)$ is linear on trainable weights and a cubic polynomial in $Z^{[n]}$, in remarking contrast to activation functions used in ANNs and CNNs; see (Bishop, 2006, Section 5.1) and also Section 6.9.

Now that the diffusive PSBC has been finally built, we discuss its forward propagation, generalizing Proposition 2.2 and Corollary 4.8.

Proposition 5.2 (Global existence of forward propagation; diffusive PSBC (4.9)) *Let $N_t \in \mathbb{N} \cup \{+\infty\}$ and $U^{[0]} := X \in [0, 1]^{N_u}$. Given trainable weights $(\alpha^{[n]})_{0 \leq n \leq N_t-1} \in \mathbb{R}$ and $(\beta^{[n]})_{0 \leq n \leq N_t-1}$, augmented by $\alpha^{[-1]} := \mathbf{1} \in \mathbb{R}^{N_u}$ and $\beta^{[-1]} := \mathbf{1} \in \mathbb{R}^{N_p}$, define for any $-1 \leq k \leq N_t - 1$ the quantities*

$$L_\alpha^{[k]} := \inf_{-1 \leq n \leq k} \left(\min_{1 \leq m \leq N_u} \left\{ \alpha_m^{[n]}, 0 \right\} \right), \quad R_\alpha^{[k]} := \sup_{-1 \leq n \leq k} \left(\max_{1 \leq m \leq N_u} \left\{ \alpha_m^{[n]}, 1 \right\} \right),$$

and, similarly, $L_\beta^{[k]}$ and $R_\beta^{[k]}$. Assume that

$$-\infty < L_\gamma^{[N_t-1]}, \quad \text{and} \quad R_\gamma^{[N_t-1]} < +\infty, \quad \text{for } \gamma \in \{\alpha, \beta\},$$

and take the Invariant Region Enforcing Condition (1.14) in the form

$$0 \leq \Delta_t^u \leq \frac{1}{\sqrt{3} \left(|L_\alpha^{[N_t-1]}| + |R_\alpha^{[N_t-1]}| \right)^2},$$

with similar conditions imposed on Δ_t^p .

Then, the sequence $U^{[k]}(X, \alpha^{[k]})$ and $P^{[k]}(\frac{1}{2} \cdot \mathbf{1}, \beta^{[k]})$ obtained using (5.6) remains bounded for all $0 \leq k \leq N_t$. More precisely, defining $M_\alpha^{[k]} := |L_\alpha^{[k]}| + |R_\alpha^{[k]}|$, for any $0 \leq k \leq N_t$ it holds that

$$\left(L_\alpha^{[k-1]} - \Delta_t^u M_\alpha^{[k-1]} \right) \mathbf{1} \leq U^{[k]}(X, \alpha^{[k]}) \leq \left(R_\alpha^{[k-1]} + \Delta_t^u M_\alpha^{[k-1]} \right) \mathbf{1}. \quad (5.8)$$

Similar bounds hold true for $P^{[k]}(\frac{1}{2} \cdot \mathbf{1}, \beta^{[k]})$, $L_\beta^{[k-1]}$, $R_\beta^{[k-1]}$, and $M_\beta^{[k-1]}$, Δ_t^p replacing, respectively, $U^{[k]}(X, \beta^{[k]})$, $L_\alpha^{[k-1]}$, $R_\alpha^{[k-1]}$, $M_\alpha^{[k-1]}$, and Δ_t^u in (5.8).

5.2 The diffusive PSBC applied to the MNIST database

Once more we apply the PSBC model - now in its diffusive form (5.1) - to the MNIST database. We are specially interested in studying the impact of viscosity on model's accuracy, therefore, as explained earlier, model selection with regards to learning rates is carried out in the non-diffusive PSBC, whereafter the diffusive parameter ε is increased and model's accuracy assessed; see further discussion in Section A.

Simulations were done in subordinate models with weights-1-sharing and weights- N_t -sharing parameters, where $N_t \in \{1, 2, 4, 8\}$; obviously, both models coincide when $N_t = 1$.

Figure 15 indicates that all models with $N_t \geq 2$ have their accuracy deteriorated when viscosity is large, with a more pronounced effect on training than on testing performance. Interestingly, the model seems to be spared of accuracy deterioration when $N_t = 1$.

A graph of the accuracy in terms of viscosity is shown in Figure 15, indicating that for large values of viscosity training accuracy drops substantially in both models whenever N_t is high, an effect that is not felt as intensely in the test set. We also point out that standard deviation is larger in weights- N_t -sharing than in weights-1-sharing models. Unlike the non-diffusive PSBC of Section 4, where weights- N_t -sharing models presented a slightly better accuracy, in presence of viscosity this fact is not uniformly true for all values of N_t : observe that weights-1-sharing have higher accuracy in training than weights- N_t -sharing models with $N_t = 8$, whereas the opposite happens when $N_t = 2$.

Another interesting fact, whose discussion we postpone to Section 6.8, is the growth of trainable weights. Extra data are available in the supplementary material.

6. Discussion, some extensions, and open questions

As we recall from Section 1, binary classification concerns the construction of approximations $\tilde{h}(\cdot)$ to an unknown hypothesis map $h(\cdot)$. Some of these methods can be motivated by biological mechanisms: for instance, the design and structure of Convolution Neural Networks (CNNs) bears similarity to how cortical neurons are scattered throughout the brain, and CNNs functioning resembles cortical neurons orientation selectivity to visual stimuli; cf. (Hubel and Wiesel, 1962, Part 3). Likewise, the design of Artificial Neural Networks (ANNs) is reminiscent of brain's networks; cf. (Goodfellow et al., 2016, Chapters 1, and 9.10). Nevertheless, in terms of mathematical or physical modeling this resemblance is mostly metaphoric, and the same criticism applies to the PSBC and to the analogy made in this paper, even though, to the author's knowledge, likening binary classification to phase separation processes seems to be new. Nonetheless, we have been inspired by many of these ideas (specially by those we oppose): first, by introducing a model that is not based on brain-like phenomenon we just reiterate

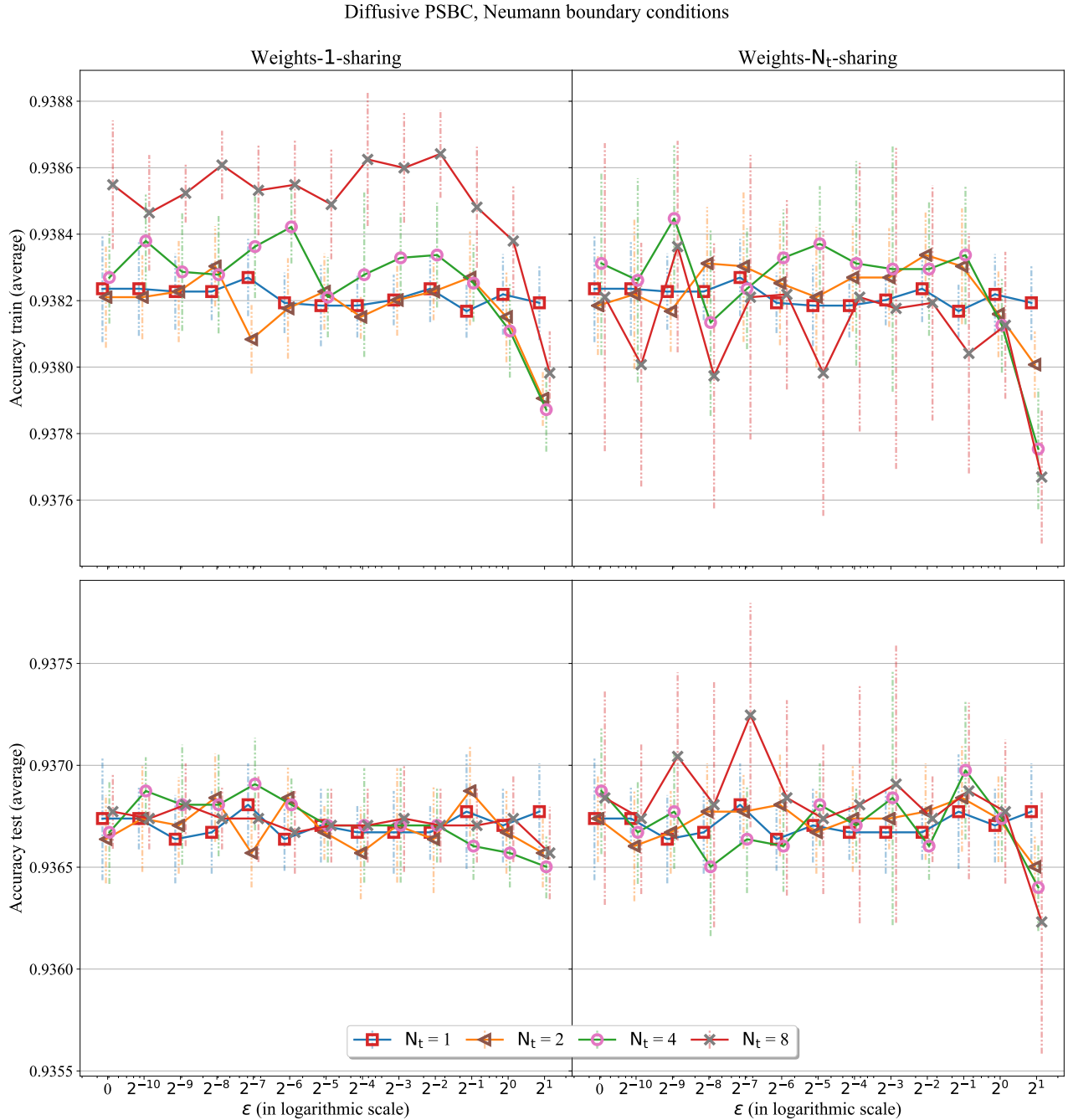


Figure 15: Using a diffusive PSBC with Neumann boundary conditions, we study the effect of varying diffusion ε on model accuracy, applied to the MNIST database. Hyperparameters were weights- K -sharing for $K \in \{1, N_t\}$, subordinate, $N_t \in \{1, 2, 4, 8\}$, $\Delta_t^u = 0.1$ (initial), $\Delta_t^p = 0.1$ (initial). Learning rates were chosen according to Appendix A, at $\varepsilon = 0$. Statistics were taken from a sample space of 10 simulations for each set of hyperparameters. Vertical bars with the same colors as lines denote 1 standard deviation. We remark that models coincide when $N_t = 1$. For statistical data, see Tables 4 and 5 in the Supplementary material.

our belief that such quality is simply unnecessary; and second, by likening binary classification to the process of phase separation in binary fluids, touching the classification problem in supervised learning with mathematical techniques from the field of PDEs.

In recent years there has been a substantial interest in studying ML models through the lenses of PDEs, an approach that gained even more momentum since the paper (Mei et al., 2018), where it has been shown that trainable weights in two-layer ANNs with large number of nodes evolve approximately as a gradient flow on a probability space endowed with a Wasserstein metric. In practical terms it is not yet clear whether such an asymptotic result shed useful bounds on trainable weights: accuracy is asserted in a probabilistic fashion, with arguments based on the theory of “propagation of chaos” and concentration of measures; furthermore, the quality of the mean-field approximation improves algebraically as the number of nodes grow but deteriorate exponentially fast on the time interval’s length (see (Mei et al., 2018, Theorem 3)), a side-effect of deriving evolution estimates based on Gronwall type of inequalities ¹⁹ (Mei et al., 2018, Lemma 3.5, Supplementary Information)).

Still, the results in (Mei et al., 2018) are a milestone in our understanding of ANNs’ nodes interaction and an important step to elucidate the evolutionary behavior of training. In fact, it is reasonable to assume that Gradient flow might bring a relevant point of view in unveiling long time behavior of trainable weights in different ML models that fall in their scope, being one of the reasons we had in mind upon designing the PSBC model. Note that even in the presence of discretization the asymptotic behavior of solutions and dissipation effects in semi and fully discrete models may be successfully estimated, as done in the interesting work (Porretta and Zuazua, 2017) using hypocoercivity techniques.

There are many questions related to properties of the PSBC that we did not even try touch upon: for instance, a study of the impact (if any) that different boundary conditions have on trainable weights, a study using confusion matrices to address misclassification of individuals, an answer to why the model never achieves more than 95% accuracy (is it a “simple” optimization issue, or is there a true mathematical obstruction?), its behavior if applied to other pairs of MNIST digits, and many other questions. Data are available at (Monteiro, 2020a), and their statistical analysis would help to clarify many aspects of the model, but such an analysis shall be pursued elsewhere.

In the sequel we make a few remarks concerning the PSBC. The topics addressed point out to directions in which the model can be improved, investigated, or extended in manners that we did not, at least in this first paper, exploited in depth. Naturally, throughout the discussion many open problems are found.

6.1 Model Parallelization of non-diffusive PSBC with subordinate phase

In real applications of ML, due to the growing size of datasets, nearly all models rely on some sort of data parallelization (processing data in parts) using techniques like (Minibatch) Stochastic Gradient Descent (see Appendix A). However, achieving model parallelization (in which the model itself is split in fully independent parts) is much more complicated and an intense topic of research, with important practical implications to Engineering and Computer Science; cf. (Huang et al., 2019).

It turns out that the non-diffusive PSBC described in Section 4 is model parallelizable. Indeed, we know from Remark 4.3 that the maps $u \mapsto \Pi_j[u] := u \circledast e_{\pi_j}$ displayed in (4.6) are orthogonal projections. An immediate consequence of this result is the Pythagoras Theorem, $\|v\|^2 = \sum_{j=1}^{N_{\text{ptt}}} \|\Pi_j^*[v]\|^2$, of which model parallelism is a direct consequence, as observed in the following result.

19. As we shall see in Section 6.8, Gronwall-type estimates (in a discrete form) also hampers our understanding of trainable weights’ growth, yielding bounds on trainable weights ℓ^∞ -norm that are not useful when the number of epochs is too large.

Proposition 6.1 (Non-diffusive PSBC with subordinate phase: model parallelization) *Consider the non-diffusive, subordinate, PSBC (1.7) (explicitly written in (4.9)), with $1 \leq N_{\text{ptt}} \leq N_{\text{u}}$, weights- K -sharing, and basis matrix \mathcal{B}^* as in (4.7). Then, the following relation holds,*

$$\Pi_j^* \left[U^{\lfloor N_t \rfloor} \left(X_{(i)}; \alpha^{\lfloor N_t - 1 \rfloor} \right) \right] = U^{\lfloor N_t \rfloor} \left(\Pi_j^*[X_{(i)}]; \Pi_j^*[\alpha^{\lfloor N_t - 1 \rfloor}] \right) = U^{\lfloor N_t \rfloor} \left(\Pi_j^*[X_{(i)}]; w_j^{\lfloor N_t \rfloor} e_{\pi_j^*} \right). \quad (6.1)$$

Thus, for any X in a feature space \mathcal{X} , two features X_a and X_b are only interact when $a, b \in \pi_j^*$ for some $1 \leq j \leq N_{\text{ptt}}$. Moreover, the cost function $\text{Cost}_{\mathcal{D}}$ as described in (4.11) can be split as a summation of N_{ptt} functions whose parameters are independent, namely,

$$\begin{aligned} \text{Cost}_{\mathcal{D}}(W) &= \sum_{j=1}^{N_{\text{ptt}}} \left(\frac{1}{2N_d} \sum_{i=1}^{N_d} \left\| (2P_j^{\lfloor N_t \rfloor} - 1) \Pi_j^* \left[U^{\lfloor N_t \rfloor} \left(X_{(i)}; \alpha^{\lfloor N_t - 1 \rfloor} \right) \right] + (1 - P_j^{\lfloor N_t \rfloor} - \tilde{Y}_{(i)}) e_{\pi_j^*} \right\|^2 \right) \\ &=: \sum_{j=1}^{N_{\text{ptt}}} \text{Cost}_{\mathcal{D}}^{(j)}(\Pi_j^*[W_U], \beta_j^{\lfloor \cdot \rfloor}), \end{aligned}$$

where $\Pi_j^*[W_U] := \left(\Pi_j^*[W_U^{\lfloor n \rfloor}] \right)_{0 \leq n \leq N_t - 1}$. Therefore, in view of (6.1), minimizing $\text{Cost}_{\mathcal{D}}(W)$ is equivalent to minimizing each $\text{Cost}_{\mathcal{D}}^{(j)}(\Pi_j^*[W_U], \beta_j^{\lfloor \cdot \rfloor})$ for $1 \leq j \leq N_{\text{ptt}}$ separately.

According to this result, it is possible to split the training process in N_{ptt} different optimization problems. In fact, it reduce matters even further by showing that optimization of a PSBC with the above qualities is mathematically equivalent to optimizing independent PSBC models, each one of them with partition cardinality 1.²⁰ Obviously, in the extreme case $N_{\text{ptt}} = N_{\text{u}}$ features are minimized independently without any possible correlations being taken into account.

6.2 The Multi-class case

Once binary classification is in hands, there are a few possible approaches to treat classification in more than two classes. For instance, using *one-versus-all* method one fixes a class k and relabel the dataset as

$$\tilde{\mathcal{D}} := \{(X_{(i)}, (-1)^{Y_{(i)}=k})\},$$

and then applying the binary classification method for all pairs; cf. (Shalev-Shwartz and Ben-David, 2014, Chapter 17.1). When the number of classes is too large simple combinatorics shows that this approach is mathematically coherent, but computationally not feasible.

Similar ideas involve tensorization of the model, leading to what is known as *one-hot-encodings*: in this case, classes are represented as a vectors with one unique nonzero element 1, $(0, \dots, 1, \dots, 0)$, which gives orthogonal elements in the space $\ell^2(\mathbb{R}^K)$, where K denotes the number of classes considered. In general, discrimination rules for multi-classes (as in (1.6)) can be achieved using soft-max units (Goodfellow et al., 2016, Chapter 6.2.2.3) or other forms of activation functions; in such case it seems unclear to the author how any form of Maximum Principle and Invariant Regions techniques can be applied.

6.3 On diffusion matrices and boundary conditions

It is also possible to study the PSBC model with periodic boundary conditions when $N_{\text{u}} \geq 3$. If one look to (1.7a), one has

$$U_0^{\lfloor n \rfloor} := U_{N_{\text{u}}}^{\lfloor n \rfloor}, \quad \text{and} \quad U_{N_{\text{u}}+1}^{\lfloor n \rfloor} := U_1^{\lfloor n \rfloor}, \quad \forall n \in \mathbb{N}; \quad (6.2)$$

²⁰. In such case, both subordinate and non-subordinate PSBC are the same.



Figure 16: Using a diffusive PSBC with Periodic boundary conditions, we study the effect of varying diffusion ϵ on model accuracy, applied to the MNIST database. Hyperparameters were weights- K -sharing for $K \in \{1, N_t\}$, $N_t \in \{1, 2, 4, 8\}$, subordinate, $\Delta_t^u = 0.1$ (initial), $\Delta_t^p = 0.1$ (initial). Learning rates were chosen according to Appendix A, at $\epsilon = 0$. Statistics were taken from a sample space of 10 simulations for each set of hyperparameters. Vertical bars with the same colors as lines denote 1 standard deviation. We remark that models coincide when $N_t = 1$. For statistical data, see Tables 8 and 9 in the Supplementary material.

consequently, different diffusion matrix is obtained,

$$D_{N_u}^{(\text{per})} = \begin{bmatrix} -2 & 1 & 0 & \dots & 1 \\ 1 & -2 & 1 & \dots & 0 \\ 0 & 1 & -2 & \dots & 0 \\ \vdots & \ddots & \ddots & \ddots & \vdots \\ 1 & & 0 & 1 & -2 \end{bmatrix} \in \mathbb{R}^{N_u \times N_u}. \quad (6.3)$$

Our simulation for the PSBC with periodic boundary conditions show similar accuracies to those of the PSBC with Neumann boundary conditions; see Figure 16 and the tables in the Supplementary material.

Besides different boundary conditions, other modifications in the diffusion matrix can be envisioned if one observes that the matrix D_{N_u} represents a first-order accurate finite difference scheme for the operator ∂_x^2 ; cf. (Strikwerda, 1989, Chapter 3). One could also consider finite difference schemes of higher order of accuracy, to which new diffusion matrices are associated. We highlight that all results related to the Invariant Region Enforcing Condition remain valid as long as Maximum Principles hold (see Appendix C); this turns out to be the case for both operators D_{N_u} in (5.3) and $D_{N_u}^{(\text{per})}$ in (6.3).

With regards to forward propagation, each step (5.6) from a layer to the next one is linear in ε^2 and that the matrix \mathcal{L}_{N_u} in (5.2) is invertible for all $\varepsilon^2 \geq 0$ in both boundary condition cases, Neumann or Periodic. Overall, varying ε is legitimate and does not affect the Invariant Region Enforcing Condition, which does not depend on ε . It is therefore plausible, at least in principle, that the parameter ε^2 can also be trained using Backpropagation, namely, the model can learn “on-the-fly” the best diffusion to use.

Last, it is unclear from our numerical results whether adding diffusion can enhance accuracy or not: our results only indicate that, given a trained non-diffusive PSBC, adding diffusion to it neither improve nor decrease its accuracy for small values of ε (during training and test), but may be deteriorate it for large values of ε ; in such a case, the model should be retrained with a different learning rate. We observe that it could be the case that the form of the diffusion matrices we have considered is too limited: indeed, it is not reasonable to assume that features should be coupled in the same way between them, and this is somehow what the “rigid” matrix D_{N_u} (or, more precisely, $(\mathcal{L}_{N_u})^{-1}$) does. Designing a heuristics to search for a viscosity matrix in a set that also contains anisotropic diffusion matrices would be highly interesting, although there are many caveats, for viscosity matrices must comply with some restrictive conditions in order to satisfy well-posedness conditions of the Cauchy problem (like semi-positivity).

6.4 Extending the PSBC model using a multi-d diffusion operator

A deeper analysis of the representation of the PSBC model in the form (5.6) helps to explain our claim in Section 5 that the diffusion term ε controls the strength of interaction between features. Indeed, a Neumann series expansion of the first term in (5.3) yields

$$\mathcal{L}_N^{-1} = (I - \varepsilon^2 D_N)^{-1} = \sum_{n=0}^{\infty} \varepsilon^{2n} D_N^n,$$

and is valid for sufficiently small values of ε ; cf. (Kato, 1995, I-§4-4, Example 4.5). Two consequences of the above equality are readily available: first, it shows that \mathcal{L}_N^{-1} is diagonal dominant. Second, due to the band-limited structure of D_N (and, consequently, of its powers), it implies that elements of \mathcal{L}_N^{-1} decay polynomially in ε the farther away from the diagonal they are. Now, allying the latter fact with the vectorial representation (5.6), one concludes that in the PSBC features interact more strongly with others that have “nearby index”.

It is important to stress that, since ANNs have fully connected layers, flattening is not immediately concerning (at least in regards to feature interaction). However, in light of the above discussion, this is not the case for the PSBC model. If we bear in mind that flattening destroys spatial properties of an individual’s features, asserting that features interaction strength is based on their entry proximity in an array is somewhat concerning, specially if spatial interaction matter, as in images (and their pixels) it locally does.²¹ To some extent this objection is minimized if we only look at the model’s

21. A thorough modeling of pixels in terms of their spatial interaction motivates the use of stochastic techniques like Markov Random Fields, and has been used in the seminal paper (Geman and Geman, 1984).

accuracy, which remains higher than 90%, as seen in applications to the MNIST database carried out in Sections 4 and 5. Nevertheless, removing the PSBC’s dependence on flattening is a tangible direction of improvement, which can be attained if one extends the model by changing (1.7a) to a multi-d spatial diffusion: intuitively, this corresponds to substituting the 1D Laplacian ∂_x^2 in (1.9) to a 2D Laplacian $\partial_x^2 + \partial_y^2$. As mentioned before, any discretization of the 2D Laplacian that is consistent with the Maximum Principles as developed in Appendix C and D yields a model with similar mathematical properties - Invariant Regions, Invariant Region Enforcing Condition etc. In such a case, one might expect that accuracy improves when image classification problems are dealt with (in particular, in the MNIST database problem).

6.5 The Hessian for the full model in the shallow case

One of the biggest issues in optimization in ML is the lack of convexity of the cost function, which can be plagued with local minima. Quantitative characterization of such information can be based on the cost function’s Hessian, allowing for a better understanding of its landscape: its flatness, spatial clustering of critical points, Hessian eigenvalues’ distribution, etc. Similar questions have been investigated for ANNs in (Choromanska et al., 2015; Sagun et al., 2016; LeCun et al., 2012). In fact, having this question in mind, one can exploit the fact that the activation function (5.6) is linear on the trainable weights to prove the following result.

Proposition 6.2 (Polynomial complexity of cost on trainable weights) *Consider the PSBC - diffusive or non-diffusive - with N_t layers and weights- N_t -sharing parameters (that is, all weights are shared across layers). Then, the cost function is a polynomial in the entries of W_U and W_P with degree at most $2 \cdot 3^{(N_t-1)}$ in each variable.*

We omit the proof of this result, which is easily reproduced by induction on the number of layers. The result can be easily generalized to other hyperparameter configurations, with more cumbersome calculations to obtain the polynomial degree of the cost function.

The above result is somewhat cautionary, showing how quickly cost landscape’s complexity can grow to prohibitive values as the number of layers increase. Yet, a direct application of it to the shallow case $N_t = 1$ implies that the cost function is a second order non-negative polynomial, it is a convex surface. In that case, is plausible that normal forms exist, yielding explicit solutions to the minimization problem (for instance, in the non-subordinate case), but the author did not pursue this matter further.

6.6 Model selection (for K) in weights- K -sharing models

In this paper only two extreme cases of weight sharing have been contemplated: weights- K -sharing parameters models with $K = 1$ or $K = N_t$. Evidently, any value $K \in G_{N_t}$ can be taken, yielding different results.

For the 1D toy problem of Section 3 we studied the average accuracy behavior of the PSBC with weights- K -sharing for all $K \in G_{N_t}$, with $N_t = 20$; this is shown in Figure 17. Interestingly, neither weights-1-sharing nor weights- N_t -sharing are the best models. Recall that the lower the value of k the large the number of variables to be optimized; thus, the smallest number of variables to optimize consists of $K = 20$ which is not more accurate $k = 3$, although yielding better accuracy in training and test sets than the case with weights-1-sharing parameters. Note that we cannot directly associate these observations with the bias-variance trade-off, for the model complexity is not growing in k : indeed, the PSBC model with weights- k -sharing does not contain the PSBC model with weights- $k + 1$ -sharing when $K \geq 2$.

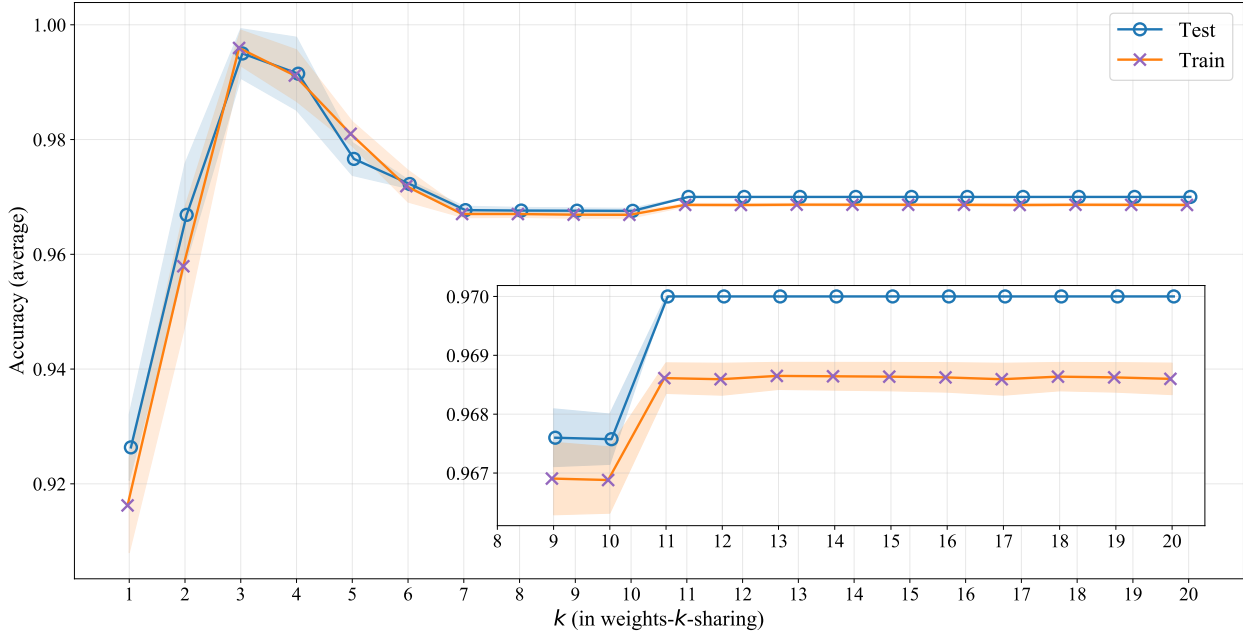


Figure 17: Accuracy of training and test sets for the PSBC (3.4) for different weights- K -sharing models. Data consists of the 1D toy problem in Section 3, partitioned using a train-test split of 80%-20%, and is made of 2000 points following an i.i.d. uniform distribution on $[0, 1]$ with labels (2.9). For each value of where $K \in G_{20}$ statistics were computed from a sample space of 100 simulations for each set of hyperparameters. Shaded areas with the same colors as lines denote 1 standard deviation. Hyperparameters were $N_t = 20$, $\Delta_t = 0.1$ and learning rates $0.1 + 0.08 \cdot (0.93)^{\text{epoch}}$.

6.7 Varying the number of parameters in each layer, and low dimensional feature spaces

A remarkable property of the PSBC is that of model compression, in some cases allowing for the number of trainable weights to be much smaller than the dimension of the feature space. One can further exploit this observation considering different partitions of unity for each layer, giving more flexibility to the model. This process is similar to that of defining the number of nodes in each layer of an ANN, which in a system with N_t layers and N_u features amounts to defining

$$1 \leq N_{\text{ptt}}^{[n]} \leq N_u, \quad \text{with } 0 \leq n \leq N_t - 1, \quad (6.4)$$

and an ordered partition $\{\pi_j^{*,[k]}\}_{1 \leq j \leq N_{\text{ptt}}^{[k]}}$, to which one associates a basis matrix $\mathcal{B}^{*,[k]}$ constructed as in (4.7). We remark that (6.4) is a constraint that comes from Linear Algebra, because the column space of the matrix $\mathcal{B}^{*,[k]}$ has maximal dimension N_u ; (Dym, 2007, Theorem 2.9).

The above constraint is a manifestation of the intrinsic model compression that the PSBC displays, whose implications are twofold:

- (i) It can be too restrictive in a low dimensional feature space, as pointed out in Section 3.1.
- (ii) On the other hand, it can be particularly useful in very high dimensional feature spaces, as illustrated by our applications of the ePSBC on the MNIST database.

It is conceivable that a hybrid approach, using polynomial (see Equation (1.8)) and other types of activation function (see Section 6.9) in the same network, may give better results, specially if we

observe that the output of a sigmoid activation function lies in the normalized condition region (N-C). In that regard, polynomial activation functions can also be used to reduce the dimension of trainable weights space, playing a similar role to that of pooling and averaging layers in CNNs; cf. (Goodfellow et al., 2016, Chapter 9.3). Further simulations that contemplate these questions would be an interesting direction of investigation.

Turning our attention again to (6.4), we see that all parameters $N_{\text{ptt}}^{[k]}$ are defined a priori, as static hyperparameters. However, a more interesting approach consists of allowing the model to learn them dynamically, allowing the basis matrices $\mathcal{B}^{*,[l]}$ (and their associated partition of unity $(\pi_j)_{1 \leq j \leq N_{\text{ptt}}^{[k]}}$) to vary throughout the training process. This yields a combinatorial optimization problem that may not be computationally feasible but, heuristically, could be dealt with by exploration of the associated search space using stochastic methods. It is worthwhile to remark that varying $\mathcal{B}^{*,[l]}$ brings about deep consequences to the model, not only in terms of accuracy improvement: variations in $\mathcal{B}^{*,[l]}$ change the architecture of the network, thereby distorting the approximation space where the prediction map is build; an example of this can be seen in the interesting paper (Hinton and Nowlan, 1987), where different architectures of an ANN have been exploited using Genetic Algorithms with purpose of investigating the duality “evolution” and “learning”. Evidently, especially if we consider the PSBC in the form presented in this paper, exploring variation in $\mathcal{B}^{*,[l]}$ does not seem that interesting from the topological point of view, for patches (partitions of unity supports) are always “intervals”; this question becomes more interesting once the model is extended to higher spatial dimensions, as contemplated in Section 6.4.

6.8 Invariant regions, growth of trainable weights in ℓ^∞ -norm, and the enforced invariant region condition

As discussed in Section 1, training an ML model using a feedforward network consists of iterating the following three steps: given trainable weights W , obtain a sequence Z using (1.3), update W using (1.5). In many practical applications these steps do not unfold without obstructive issues, the most severe of them possibly being the blow-up of trainable weights in ℓ^∞ -norm, with consequences that go beyond floating number overflow: blow-up leads to deterioration of results, vanishing of derivatives, and saturation of nodes (which slows down training speed); cf. (Glorot and Bengio, 2010, §3), (Goodfellow et al., 2016, Chapter 8.2).

In practice, taming the growth of trainable weights is an ubiquitous difficulty in ML and Deep learning that has been achieved in many ways, with varying degree of sophistication and, of course, side effects to model’s accuracy and generalization: by penalization of trainable weights norm (sometimes called regularization; cf. (Goodfellow et al., 2016, Chapter 7)), or ad-hoc ways like trimming (cut-offs), where large values of trainable weights are truncated (Goodfellow et al., 2016, Chapter 10.11.1); see also (LeCun et al., 2015). Similarly, feedforward models with a large number of layers - called Deep-layered models- are often avoided due to the prohibitive complexity of their associated cost function landscapes (Bengio, 2009, Sec. 1.1), bringing about several difficulties in model’s training; see (Sutton and Barto, 2018, Sec. 9.7) for a short and interesting discussion.

We have shown in Propositions 2.2, 4.7, and 5.2 that $U^{[l]}$ and $P^{[l]}$ do not blow-up during forward propagation under appropriate assumptions.²² These results are important to the extent that it establishes and secures one of the basic mechanisms used in the construction of the prediction map (1.6). Our results give a careful description of both $U^{[l]}$ and $P^{[l]}$ range in terms of the PSCB’s trainable weights (W_U, W_P) , being proved with the help of the technique of invariant regions in the spirit of (Chueh et al., 1977) but closer, within the context of finite-difference schemes, to the way it is employed in (Hoff, 1978). On the other hand, the question of blow-up on trainable weights remains unattended;

22. As pointed out before, in doing so we achieve some sort of stability in the model in the ℓ^∞ -norm, which is enough to address the issue of floating point overflow of $U^{[l]}$ and $P^{[l]}$. Nevertheless, the result does not give control of oscillatory behavior; for that, other techniques should be used, like entropy methods (Desvillettes and Villani, 2005).

note that there is a synergy between the ℓ^∞ -norm growth of $(U^{\lfloor \cdot \rfloor}(X, \alpha^{\lfloor \cdot \rfloor}), P^{\lfloor \cdot \rfloor}(X, \beta^{\lfloor \cdot \rfloor}))$ and that of $(W_U, W_P) = (\alpha^{\lfloor \cdot \rfloor}, \beta^{\lfloor \cdot \rfloor})$ due to Gradient Descent, specifically in virtue of the trainable weights update equation (1.5). The connection between these quantities can be quantified as follows.

Proposition 6.3 (Growth of trainable weights) *Denote by $W_q = (W^{[0]}, \dots, W^{[N_t-1]})_q$ be a sequence of trainable weights: assume that W_0 is given, and for $q \in \{1, \dots, Q\}$ has been generated through training, that is, using iteration (1.5). Assume the existence of a function $C_q = C_q(\text{Cost}_{\mathcal{D}}(W_q))$ and an exponent $K \geq 1$ such that*

$$\left\| \frac{\partial \text{Cost}_{\mathcal{D}}(W_q)}{\partial W} \right\|_{\ell^\infty} \leq C_q \|W_q\|_{\ell^\infty}^K.$$

Let $\gamma > 0$ such that $\eta_q C_q (\max\{\|W_q\|_{\ell^\infty}, 1\})^{K-1} \leq \gamma$ hold for all $0 \leq q \leq Q$. Then,

$$\max\{\|W_{Q+1}\|_{\ell^\infty}, 1\} \leq e^{Q\gamma} \max\{\|W_0\|_{\ell^\infty}, 1\}. \quad (6.5)$$

Furthermore, in the PSBC case we can take $K = 1$.

This result is proven in Appendix D.4.

Proposition 6.3 has a local (in “time”) nature, in the sense that it only gives reasonable understanding of trainable weights growth in the short term (small number of epochs Q); this is typical of local estimates derived using Gronwall inequalities. To give a comparative order of magnitude, parameters in the MNIST database simulation have order $\eta_q = \mathcal{O}(10^{-4})$, $Q = \mathcal{O}(10^4)$ (because we are using mini-batches; see Section A), yielding bounds that are not very useful. Note that $\text{Cost}_{\mathcal{D}}(W_q)$ is explicit and observable at the end of each epoch, and is usually decaying (for it is the quantity being minimized); such decay would have to be sufficiently pronounced in order to counterbalance the cumulative growth of trainable weights stemming from Gradient descent iteration. In fact, our simulations indicate that these bounds are too conservative, as one can be seen in Figures 18 and 19. See also the statistical data available in Table 4 of the Supplementary material.

There are many open questions about the asymptotic behavior of trainable weights:

- (i) Is there an invariant region for trainable weights in terms of hyperparameters and quantitative estimates on the dataset \mathcal{D} used for its training?
- (ii) Is it possible to find bounds in (6.5) that are uniform in the number of epochs, that is, bounds that do not depend on Q ?
- (iii) If uniform bounds on Q exist, how do they depend on the distribution of $X \in \mathcal{X}$, and on other parameters of the model, in particular the number of layers N_t ?
- (iv) If trainable weights are uniformly bounded, with bounds independent of Q , do they converge as “ $q \uparrow Q$ ”, or as Q grows?

In a certain way, all these questions touch upon the issue of compactness. We remark that simply controlling the growth of the cost function is not enough to control the parameters W_P and W_U , for the cost is not coercive on $U^{[N_t]}$ nor $P^{[N_t]}$: for instance, $U^{[N_t]} = \frac{1}{2}\mathbf{1}$ implies that $\text{Cost}_{\mathcal{D}}$ is independent of $P^{[N_t]}$. In such case, at the q -th epoch, the last term in (1.5) gives $\frac{\partial \text{Cost}_{\mathcal{D}}(W)}{\partial W_P} = \mathbf{0}$, whence $(W_P)_{q+1} = (W_P)_q$. It is not clear if randomly initializing trainable weights is sufficient to prevent such things; by the same token, it is also unclear if the Invariant Region Enforcing Condition (1.14) is sufficient to control the blow-up of trainable weights.

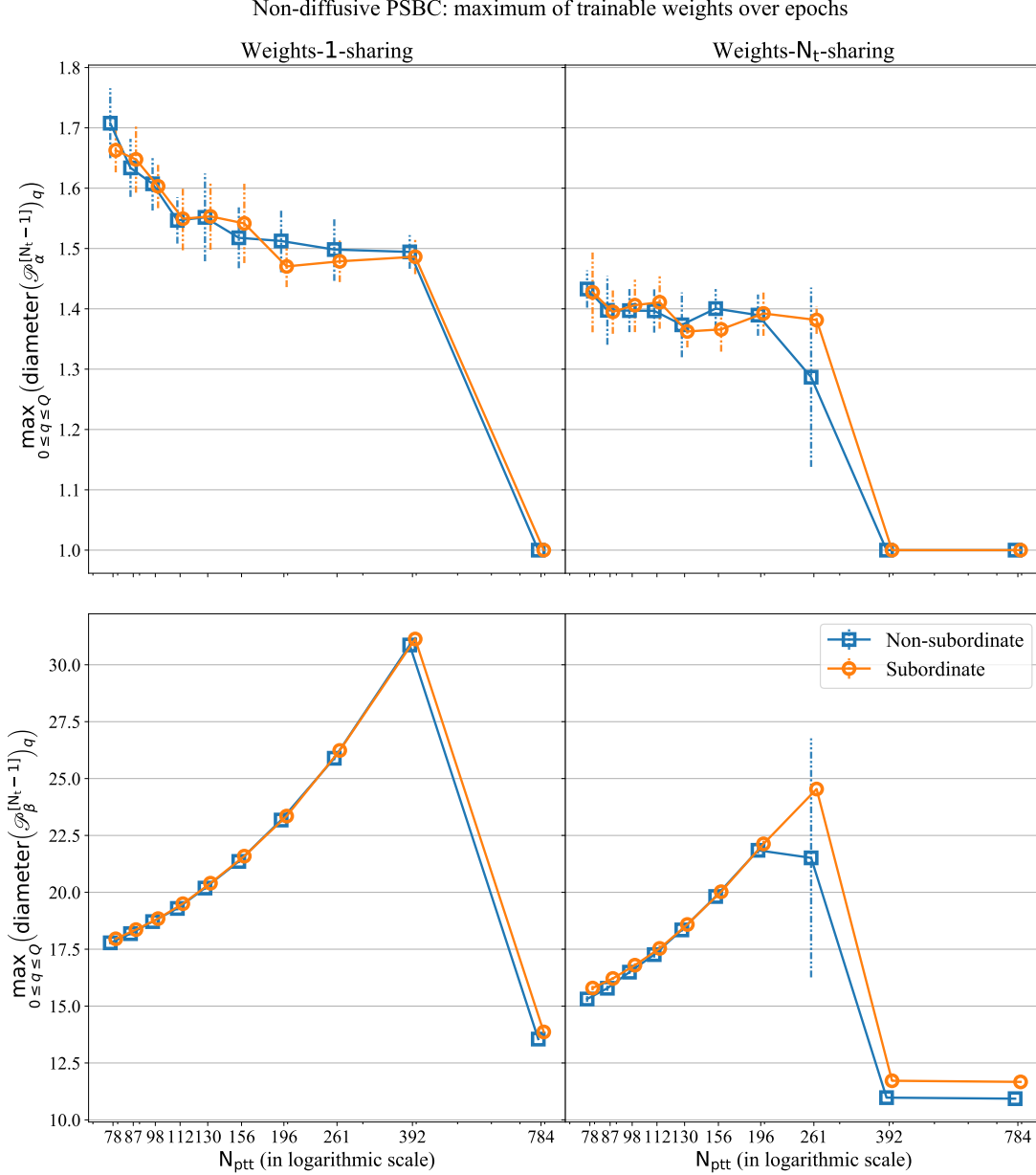


Figure 18: Average and standard deviation for the maximum value attained by the diameter of the set $\mathcal{P}_\alpha^{[N_t-1]} := \text{conv}(\{0, 1\} \cup_{m=0}^{N_t-1} \{\alpha^{[m]}\})$ over epochs, for different values of partition cardinality N_{ptt} ; $\mathcal{P}_\beta^{[N_t-1]}$ is defined similarly. This quantity immediately gives an estimate on the size of trainable weights (in ℓ^∞ -norm) thanks to the relation $\max_{0 \leq n \leq N_t-1} \{\|\alpha^{[n]}\|_{\ell^\infty}, 1\} \leq \text{diam}(\mathcal{P}_\alpha^{[N_t-1]}) \leq 2 \max_{0 \leq n \leq N_t-1} \{\|\alpha^{[n]}\|_{\ell^\infty}, 1\}$. The model in display is a non-diffusive PSBC with parameters $N_t = 2$, $\Delta_t^u = 0.1$ (initial), $\Delta_t^p = 0.1$ (initial), and patience = 50. Learning rates were chosen according to Appendix A at $N_{\text{ptt}} = 196$. The classifier is applied to the MNIST database. For the table with numerical data, see Table 3 in the Supplementary material.

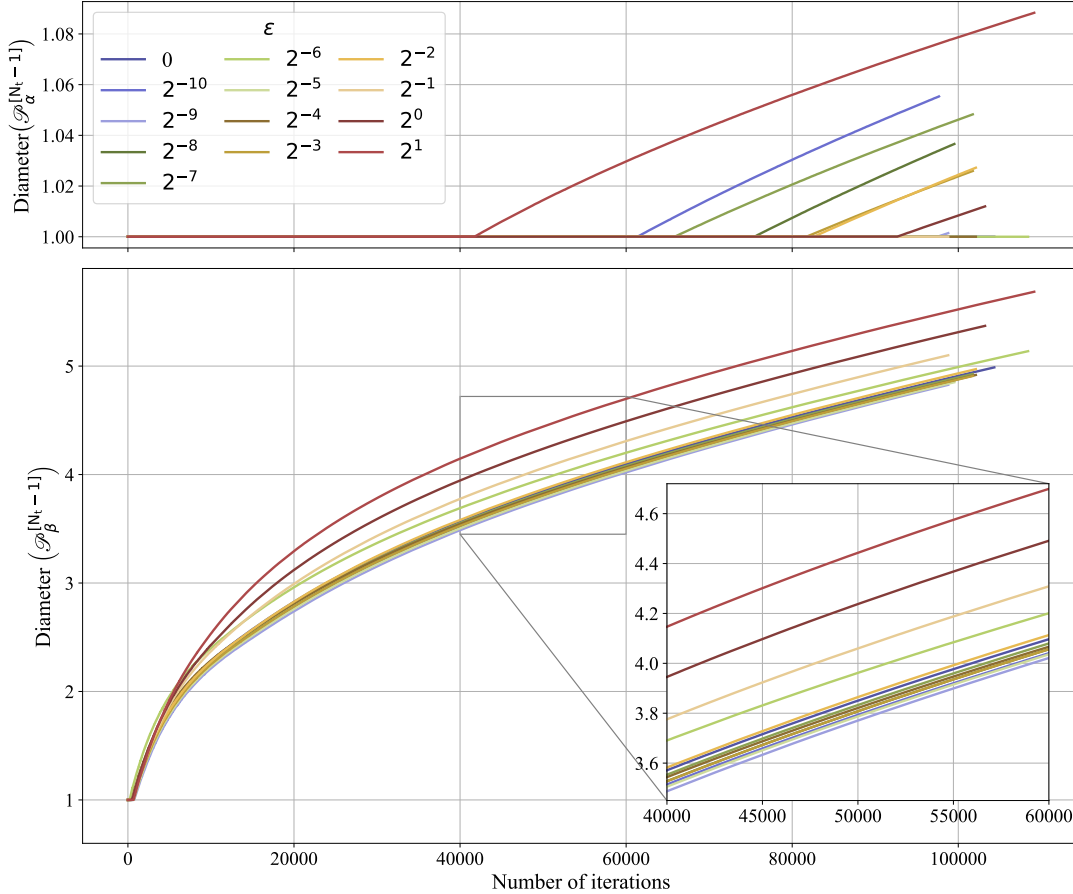


Figure 19: An example of growth of trainable weights over iterations for several realizations of a PSBC with different values of diffusion parameter ε . Here, $\mathcal{P}_\alpha^{[N_t-1]} := \text{conv}(\{0, 1\} \cup_{m=0}^{N_t-1} \{\alpha^{[m]}\})$ with $\mathcal{P}_\beta^{[N_t-1]}$ being defined similarly; see Corollary D.4. The model in display is a PSBC with parameters weights-1-sharing, Neumann boundary conditions, subordinate, $N_t = 8$, $\Delta_t^u = 0.1$ (initial), $\Delta_t^p = 0.1$ (initial), $N_{\text{ptt}} = 196$, and patience = 50. Learning rates were chosen according to Appendix A, at $\varepsilon = 0$. The classifier is applied to the MNIST database. Note that different parameters yield simulations with different number of iterations, due to Early stopping; see Section A. Number of iterations is larger than the number of maximal epochs (600) because minibatches are used.

6.9 Comparison with other ML models

Throughout the paper we have pointed out resemblances between ANNs and the PSBC. There are also some similarities when we compare the PSBC and Convolutional Neural Networks (CNNs). For instance, in the periodic case one can see the matrix \mathcal{L}_N^{-1} as a Toeplitz matrix that plays the role of a convolution in (5.4); cf. (Goodfellow et al., 2016, Chapter 9.1). The comparison becomes more explicit when we consider the fully explicit model (see footnote 6)

$$U^{[n+1]} = \left(\text{Id}_{N_u} + \varepsilon^2 D_{N_u}^{(\text{per})} \right) U^{[n]} + \Delta_t^u f(U^{[n]}; \alpha^{[n]}), \quad (6.6)$$

where the matrix $\text{Id}_{N_u} + \varepsilon^2 \mathbf{D}_{N_u}^{(\text{per})}$ has finite band and, when left multiplied with a column vector, acts as a convolution with a compact kernel. Similarly, one observes that regression on the range of \mathcal{B} is similar to average pooling with the appropriate strides and no padding (Goodfellow et al., 2016, Chapter 9.3); see also Figure 12.²³

It is well known that the type of activation function has a huge impact in qualities of the model, its optimization (Glorot and Bengio, 2010), and mathematical properties concerning approximation theory (Daubechies et al., 2019). The fact that the PSBC’s cost function is polynomial on the trainable weights is in evident contrast to standard ANN and CNN models, where activation functions introduce a strong nonlinearity into the model.

Sigmoid $\sigma(z) = \frac{1}{1+e^{-z}}$	$\sigma(z) = \tanh(z)$	ReLU $\sigma(z) = \max\{0, z\}$	PSBC, Eq. (5.5) $\sigma(z = (u, w)) = f(u; w)$
$\sigma(\mathbb{R})$ bounded	$\sigma(\mathbb{R})$ bounded	$\sigma(\mathbb{R})$ unbounded	$f(\mathbb{R}; w)$ unbounded
$\partial_z \sigma(\mathbb{R})$ bounded	$\partial_z \sigma(\mathbb{R})$ bounded	$\partial_z \sigma(\mathbb{R})$ bounded ²⁴	$\partial_u f(\mathbb{R}; w)$ unbounded

Table 5: A few types of activation functions and some of their properties.

We have focused mostly on properties of activation functions’ 0th and 1st order derivatives, where they differ substantially from the polynomial activation function used in the PSBC. Indeed, first order derivatives of both sigmoid and hyperbolic tangent activation functions decay fast towards zero, making the learning process slow when trainable weights are too large; for years this was a major issue in Recurrent Neural Networks (Bengio et al., 1994; LeCun et al., 2015). The case of ReLU’s in contrast differs because its (almost everywhere) derivative is bounded, whereas in the PSBC case it is not necessarily the case. See (Goodfellow et al., 2016, Chapters 6 and 9) for discussion of different types of activation functions

6.10 Data normalization and model’s symmetries

Data normalization is also a common practice in ANNs, cf. (Hastie et al., 2001, Chapter 11.5.3), as well as breaking the symmetry in the model by random initialization of its trainable weights; cf. (Goodfellow et al., 2016, Chapter 8.4).

In the PSBC normalization takes place in the form (N-C), required in Proposition 2.2, 4.7, and 5.2. Even though normalization only requires initial conditions (individuals) to have its features in a certain range, in our earlier simulations we also shrunk the data with the intent of preventing possible blow-ups in trainable weights. To our surprise we verified then that the PSBC shows some preferences for asymmetric normalizations, which we illustrate next: in a grid search, 5-fold validations were run under the following normalization conditions,

$$\mathcal{N}(X, \gamma, \sigma) = \gamma \mathbf{1} + \sigma f(X), \quad \text{with } X \in \mathcal{X}, \quad \gamma \in \{0, 0.1, \dots, 0.8\}, \quad \sigma = 0.2, \quad (6.7)$$

where $f(X_l) = \frac{X_l - m}{M - m}$, with $m = \min_{1 \leq l \leq N_u} (X_l)$ and $M = \max_{1 \leq l \leq N_u} (X_l)$. Hence, given a fixed grid, σ , and γ , model selection was performed with respect to both learning rates and viscosity parameters. Model’s accuracy is calculated as an average, showing very different behavior along the grid, as shown in Table 6.

It is not clear the why of such a discrepancy, and even if such a discrepancy can be mitigated by increasing the grid over which search has been performed. It is plausible that different normalizations

23. In passing, when comparing the multiplicative role of $(\mathcal{L}_{N_u})^{-1}$ in the PSBC to that of trainable weights $\widetilde{W}^{[n]}$ in (5.7) one could say that ANNs are models that allow (very) non-physical viscosities.

23. Derivative in this case is in almost everywhere sense.

Average Accuracy										
σ	γ									
	0.0	0.1	0.2	0.3	0.4	0.5	0.6	0.7	0.8	0.9
0.1	0.5323	0.5323	0.5323	0.5323	0.5323	0.9397	0.5323	0.5323	0.5330	0.5323
0.2	0.5323	0.5323	0.5323	0.5323	0.5323	0.9403	0.5323	0.5331	0.6004	*

Table 6: Results of a grid search (for learning rate and viscosity ε hyperparameters) using 5-fold cross validation. The model used is a PSBC with parameters $N_t = 2$, $N_{\text{ptt}} = 196$, with subordinate phase and infinite patience. The model has been applied to the MNIST database, normalized as (6.7) with $\sigma \in \{0.1, 0.2\}$ and different values of γ , which varies in such a way that features are always within the range $[0, 1]$.

allow the model to avoid getting stuck in local minima and, consequently, different normalization parameters (here, σ and γ) could be considered as hyperparameters to be optimized. The results are nevertheless inconclusive, and require further investigation. For ANNs, an interesting study along this line of reasoning can be found in (Glorot and Bengio, 2010, Sec. 4.2.1).

In our simulations using the MNIST database we adopt the normalization (6.7) with $\gamma = 0.5$ and $\sigma = 0.2$.

6.11 A remark on optimal control

As pointed out in the introduction, the backbone of the PSBC lies in Problems 1.2 and 1.3, both of which fall in the category of optimal control theory where, roughly speaking, the main goal is that of finding optimal or quasi-optimal parameters (which in our case are trainable weights) to a given control problem. There is a clear parallel between supervised learning and dynamic control theory, as can be seen for instance in (LeCun et al., 1988), where the Backpropagation algorithm has been rederived from optimal control theory principles. It is worthwhile to highlight that our terminology “Maximum Principle” differs from that used in (Li et al., 2017): therein the term is a reference to the Pontryagin Maximum Principle in control theory (Bressan and Piccoli, 2007, Chapter 6), whereas in this paper it denotes a discrete version of Maximum Principles in elliptic and parabolic PDEs theory; see Appendix C for further details.

Supplementary material, Data and Code availability

Supplementary material contains auxiliary results that simplify the vectorization of the PSBC, making it suitable for fast numerical computations, besides tables with accuracy and parameters growth is also available at https://github.com/rafael-a-monteiro-math/Binary_classification_phase_separation.

All the code for this paper has been written in Python and is available on Github (Monteiro, 2020b): https://github.com/rafael-a-monteiro-math/Binary_classification_phase_separation.

All relevant data is available at (Monteiro, 2020a): <https://dx.doi.org/10.5281/zenodo.4005131>.

Acknowledgments

The author would like to thank the hospitality of the Indiana University-Bloomington (U.S.), where he had several interesting conversations about nonlinear stability and gradient flows with Peter Stern-

berg and Kevin Zumbrun, besides getting their criticisms and comments of a preliminary version of this work (January 2020). The semi-implicit “trick” used in (1.7a) was first shown to the author by Arnd Scheel (University of Minnesota, U.S.). *The numerics of the dynamics and the dynamics of the numerics* (as used in Remark 2.5) was a comment taken from an illuminating conversation with André Nachbin (IMPA, Brazil). The author thanks Kartik Sau (MathAM-OIL, Japan) for discussions about parallelization and high performance computations, and also Yueyuan Gao and Natsuhiko Yoshinaga (MathAM-OIL), who made valuable comments on a draft of this paper.

Appendix

In the sequel we adopt the following notation: we denote the Hadamard product (or Schur product)²⁵ of two matrices $A = [a_{ij}], B = [b_{ij}] \in \mathbb{R}^{n \times m}$ as

$$C = A \circledast B = [c_{ij}] \in \mathbb{R}^{n \times m},$$

where $c_{ij} := a_{ij}b_{ij}$ for all $1 \leq i \leq n$, and $1 \leq j \leq m$ (Dym, 2007, Chapter 1.8).

We construct a block matrix with matrices $A_j \in \mathbb{R}^{n_j \times m_j}$, for $1 \leq j \leq M$ in its diagonals as

$$\text{diag}(A_j; 1 \leq j \leq M) = \begin{pmatrix} A_1 & \dots & \dots & \dots \\ \vdots & A_2 & \dots & \dots \\ \vdots & & \ddots & \vdots \\ \vdots & \dots & \dots & A_m \end{pmatrix} \in \mathbb{R}^{l \times r}, \quad \text{where } l = \sum_{j=1}^M n_j, r = \sum_{j=1}^M m_j. \quad (\text{N1})$$

For a given vector $a \in \mathbb{R}^{n \times 1}$, we write $\text{diag}(a) = [b_{ij}]_{1 \leq i, j \leq n}$, where $b_{ij} = a_i$ when $i = j$, $b_{ij} = 0$ otherwise. In the case of vectors or matrices $A, B \in \mathbb{R}^{n \times 1}$, the following properties are easily verified:

$$\begin{aligned} A \circledast B &= B \circledast A = \text{diag}(A) \cdot B = \text{diag}(B) \cdot A; \\ \text{diag}(A \circledast B) &= \text{diag}(A) \circledast \text{diag}(B); \\ \|\text{diag}(A)\|_{\ell^\infty(\mathbb{R}^n) \rightarrow \ell^\infty(\mathbb{R}^n)} &= \|A\|_{\ell^\infty}. \end{aligned} \quad (\text{N2})$$

For all $x \in \mathbb{R}$ it holds that $1 + x \leq e^x$. Hence,

$$\prod_{k=1}^N (1 + a_k) \leq \exp \left\{ \sum_{k=1}^N a_k \right\}, \quad \text{for all } a_k \geq 0. \quad (\text{N3})$$

Last, given a dataset $\mathcal{D} := \{(X_{(i)}, Y_{(i)})_{1 \leq i \leq N_d}\} \subset \mathcal{X} \times \{0, 1\}$ we adopt the convention that $U_{(i)}^{[\cdot, \cdot]} := U^{[\cdot, \cdot]}(X_{(i)}, \alpha^{[\cdot, \cdot]})$, with $1 \leq i \leq N_d$; that is, $U_{(i)}^{[\cdot, \cdot]}$ is the propagation of $X_{(i)}$ using (1.7a). We remark that, in contrast to the previous notation, $U_m^{[\cdot, \cdot]}$ represents the m -th coordinate of a vector $U^{[\cdot, \cdot]}$; see Section 1.3.

25. In the Mathematics literature the Hadamard product between two quantities u and v is commonly represented as $u \circ v$. On the other hand, in many programming languages, the Hadamard product reads as $u * v$. In this paper we shall overlap both notations. In passing, we avoid further issues, like confounding the symbol $*$ with that of convolution, or \circ with composition of functions.

Appendix A. Initialization, optimization, hyperparameter tuning, and hardware

Hardware and computational statistics. All the numerical computations related to the MNIST database were performed on a super computer at MathAM-OIL using a varying numbers of cores (ranging from 5 to 22) over a single node. Other computations were performed using a MacBook Pro with Intel Core i7 processor, 4 Cores, with speed 2.5 GHz.

MNIST database. This database consists of 70000 images of handwritten digits from 0 to 9, each with size 28×28 pixels, stored as matrices of same dimension; we restrict ourselves to the subset of digits “0” and “1”. Following a historical trend, individuals chosen for training purposes were taken from the first 60000 elements, while individuals making up the test set come from the last 10000 elements. There are in total 6903 individuals with label 0 and 7877 individuals with label 1. For further details, see (Lecun et al., 1998) or (Hastie et al., 2001, Section 11.7).

Initialization. Data is rescaled to observe the normalization condition (N-C); as such, each feature of an individual belongs to the range $[0.5, 0.7]$; further discussion can be found in Section 6.10.

Trainable weights $\alpha^{l,j} \in \mathbb{R}^{N_u}$ in (1.7a) and $\beta^{l,j} \in \mathbb{R}^{N_p}$ are initialized randomly, as Normal variables with mean 0.5 and diagonal covariance matrix, with variance σ^2 ; in all the simulations, we took $\sigma = 0.1$.

For the MNIST database, parameters Δ_t^u and Δ_t^p have been initialized as $\Delta_t^* = 0.1$, but evolve independently. Indeed, from the mathematical point of view, it is unnecessary to impose the constraint $\Delta_t^u = \Delta_t^p$ in each epoch, and our simulations on the MNIST database have shown that this does not give good results. Figure 19 corroborates with this fact by showing that $\alpha^{l,j}$ and $\beta^{l,j}$ have different growth rates on their ℓ^∞ -norm, implying that Δ_t^u and Δ_t^p shrink towards zero with different rates in virtue of (1.14). Furthermore, allowing Δ_t^u and Δ_t^p to assume their maximum value gives poor accuracy results, probably because in this way the model’s hyperparameters vary too many times over different epochs. To circumvent such an issue, in each epoch we use the Invariant Region Enforcing Condition (1.14) to define

$$\Delta_t^u := \min \left\{ \Delta_t^*, \frac{1}{\sqrt{3} \operatorname{diameter}(\mathcal{P}_\alpha)^2} \right\},$$

with a similar definition holding for Δ_t^p . For the 1D models, we also initially set Δ_t^u (and Δ_t^p , when it is used) as equal to 0.1.

Model selection (for learning rates) and model assessment. Model selection and model assessment are based on a train-test set split; cf. (Hastie et al., 2001, Chapter 7)). Model selection is performed using 5-fold cross validation on the training set, where the parameter with best accuracy average is the one picked. Afterwards, during model assessment, we train the model again for the chosen parameter (now on the full training set), and accuracy is measured on the test set; cf. (Shalev-Shwartz and Ben-David, 2014, Chap 11).

In our studies to assess the impact of hyperparameters’ variation on models accuracy we have contemplated two different model selection scenarios:

- (i) In non-diffusive PSBCs, for a fixed set of hyperparameters with partition cardinality $N_{\text{ptt}} = \frac{28^2}{4} = 196$, model selection is performed using 5-fold cross validation on the training set to select the learning rate only. Afterwards, once a learning rate is selected and fixed, all hyperparameters are kept fixed except for N_{ptt} , which varies in a certain range of predetermined values. Finally, for each one of these sets of hyperparameters, training is performed doing a train-test set split.
- (ii) In diffusive PSBCs, for a fixed set of hyperparameters with diffusion rate $\varepsilon = 0$, model selection is performed using 5-fold cross validation on the training set to select the learning rate only. Afterwards, once a learning rate is selected and fixed, all hyperparameters are kept fixed but ε ,

which varies in a certain range of predetermined values. Finally, for each one of these sets of hyperparameters, training is performed doing a train-test set split.

An extensive discussion in the Introduction 1.2 and in Section 4.2 gives further explanation on the above matters.

Optimization. Upon training, we rely on several different optimization techniques, several of which are described in (Goodfellow et al., 2016, Chapter 8). The first of them amounts to decaying the learning rate in the Gradient-Descent (1.5), making them smaller throughout epochs (that is, iterations). We do so by describing the learning rate as a family in three parameters,

$$\eta_q = a + b \cdot c^q, \quad (\text{A.1})$$

where $a, b \geq 0$, and $0 \leq c < 1$ are defined in the beginning of the simulation (as hyperparameters) and q denotes the epoch number. In the MNIST database training, these three quantities were chosen by grid search, and on each of them we run a 5-fold validation; see the previous discussion or the numerical implementation in (Monteiro, 2020b).

We use batch processing in the 1D model, but for the bigger MNIST model we use (minibatches) Stochastic Gradient Descent (SGD). There are many reasons to do so, among them limited computer memory, and adding noise to the parameter search (by subsampling the sample space) in order to improve optimization. In effect, stochastic methods can be beneficial for global optimization purposes and, depending on the method used, in many cases yielding converge with probability one to global optima (Van Laarhoven and Aarts, 1987, Chapter 3). When SGD is used, we adopt minibatches of size 32. This choice is based on empirical studies that study several ML models' accuracies according to the size of minibatches used in their training, pointing out that small size minibatches yield better performance; cf. (Masters and Luschi, 2018; Hoffer et al., 2017). In fact, whenever we used large minibatches we obtained very poor performance. We have not tried smaller minibatch sizes, for model selection on minibatch size was not among our goals.

We also employ an optimization technique called *early stopping* (Prechelt, 1998; Girosi et al., 1995; Yao et al., 2007): at each epoch q a monitored quantity M_q that measures the best performance of the model since the begin of simulations. Whenever M_q does not improve for an extent of p^* iterations, the parameter search halts (that is, there exists a sequence such that $M_q = M_{\tilde{q}}$ for $\tilde{q} \leq q \leq \tilde{q} + p^*$); the quantity p^* receives the name *patience*. In the models studies in Section 2 and 3, we use infinite patience (that is, the model never halts due to early stopping), and adopt $p^* = 50$ for all the simulations involving the MNIST database. In all the simulations, accuracy (1.2) was used as the monitored quantity.

Other optimization methods have not been tested, mostly because they are easy to implement, but not necessarily amenable to direct mathematical analysis. In addition to that, SGD is the base for many of them, and serves as a starting point in the search for answers to other relevant questions related to training and convergence. Nevertheless, adopting more robust training methods in the PSBC is an important direction of investigation, and is left for future research.

Appendix B. Backpropagation

B.1 Auxiliary analytical calculations for the Backpropagation

Before we start, we recall some details of Section 4. The model (1.7) is written in (5.6) as

$$\begin{pmatrix} U^{[n+1]} \\ P^{[n+1]} \end{pmatrix} = \sigma^{[n]} \left(U^{[n]}, W_U^{[n]}, P^{[n]}, W_P^{[n]} \right) = \begin{pmatrix} (\mathcal{L}_{N_u})^{-1} \cdot (U + \Delta_t^u f(U, W_U)) \\ P + \Delta_t^p f(P, W_P) \end{pmatrix}, \quad (\text{B.1})$$

with $f(u, w) = u(1 - u)(u - w)$ and \mathcal{L}_{N_u} as in (5.3). We have used partitions of unity to construct $\alpha^{[n]}$, decomposing \mathbb{G}_{N_u} as an ordered cover $\pi_1^*, \dots, \pi_{N_{\text{ptt}}}^*$ of degree N_{ptt} , yielding

$$\alpha^{[n]} = \mathcal{B}^* \cdot \begin{bmatrix} w_1^{[n]} \\ \vdots \\ w_{N_{\text{ptt}}}^{[n]} \end{bmatrix}, \quad \text{with } \mathcal{B}^* := \begin{bmatrix} | & | & \dots & | \\ e_{\pi_1^*} & e_{\pi_2^*} & \dots & e_{\pi_{N_{\text{ptt}}}^*} \\ | & | & \dots & | \end{bmatrix} \in \mathbb{R}^{N_u \times N_{\text{ptt}}}. \quad (\text{B.2})$$

Recall from Definition 4.6 that

$$\widetilde{P^{[N_t]}} = \begin{cases} P^{[N_t]} \mathbf{1}_{N_u} = \mathcal{B}^* \cdot (P^{[N_t]} \mathbf{1}_{N_{\text{ptt}}}), & (\text{non-subordinate, } N_u = 1), \\ \mathcal{B}^* \cdot P^{[N_t]}, \text{ for } P^{[N_t]} = \begin{bmatrix} P_1^{[N_t]} \\ \vdots \\ P_{N_{\text{ptt}}}^{[N_t]} \end{bmatrix} \in \mathbb{R}^{N_{\text{ptt}}}, & (\text{subordinate, } N_u = N_{\text{ptt}}), \end{cases} \quad (\text{B.3})$$

where in both cases $\widetilde{P^{[N_t]}} \in \mathbb{R}^{N_u}$. Last, with $\mathcal{S}_{N_u}^{(0)}(u) = u$ and $\mathcal{S}_{N_u}^{(1)}(u) = \mathbf{1} - u$ as maps from \mathbb{R}^{N_u} to itself, define

$$\mathbb{R}^{N_u} \times \mathbb{R}^{N_u} \ni (p, u) \mapsto \mathcal{S}_{N_u}^{(p)}(u) := (\mathbf{1} - p) \circledast \mathcal{S}_{N_u}^{(0)}(u) + p \circledast \mathcal{S}_{N_u}^{(1)}(u). \quad (\text{B.4})$$

and a cost function

$$\text{Cost}_{\mathcal{D}} = \frac{1}{2N_d} \sum_{i=1}^{N_d} \left\| \mathcal{S}_{N_u}^{(\widetilde{P^{[N_t]}})} \left(U^{[N_t]}(X_{(i)}; \alpha) \right) - Y_{(i)} \mathbf{1} \right\|_{\ell^2(\mathbb{R}^{N_u})}^2. \quad (\text{B.5})$$

The following Lemma encompasses all the necessary computations to perform Backpropagation in the PSBC, in all the forms it has been presented.

Lemma B.1 *Consider a sequence $\{(X_{(i)}, Y_{(i)})\}_{1 \leq i \leq N_d} \subset \mathcal{X} \times \{0, 1\}$. Let $1 \leq i \leq N_d$. Given a non-subordinate or subordinate PSBC with specified hyperparameters $(N_u, N_p, N_{\text{ptt}}, N_t)$, denote the flow of $X_{(i)}$ by (3.4) as $U^{[\cdot]}(X_{(i)}, \alpha^{[\cdot]}) =: U_{(i)}^{[\cdot]}$ and $P^{[\cdot]}(\frac{1}{2}; \beta^{[\cdot]}) =: P^{[n]}$. Furthermore, assume that $\widetilde{P^{[N_t]}} \in \mathbb{R}^{N_u}$ is constructed from $P^{[N_t]}$ as in (B.3).*

For a cost function $\text{Cost}_{\mathcal{D}}$ as in (B.5), we have

$$(i) \quad \frac{\partial \mathcal{S}_{N_u}^{(\widetilde{P^{[N_t]}})}}{\partial U_{(i)}^{[N_t]}} = \text{diag} \left(\mathbf{1} - 2\widetilde{P^{[N_t]}} \right) \in \mathbb{R}^{N_u} \times \mathbb{R}^{N_u}.$$

$$(ii) \quad \frac{\partial \text{Cost}_{\mathcal{D}}}{\partial U_{(i)}^{[N_t]}} = \frac{1}{N_d} \left(\mathcal{S}_{N_u}^{(\widetilde{P^{[N_t]}})} \left(U_{(i)}^{[N_t]} \right) - Y_{(i)} \mathbf{1} \right)^T \cdot \text{diag} \left(\mathbf{1} - 2\widetilde{P^{[N_t]}} \right) \in \mathbb{R}^{1 \times N_u},$$

or, using Hadamard products,

$$\frac{\partial \text{Cost}_{\mathcal{D}}}{\partial U_{(i)}^{[N_t]}} = \frac{1}{N_d} \left(\mathcal{S}_{N_u}^{(\widetilde{P^{[N_t]}})} \left(U_{(i)}^{[N_t]} \right) - Y_{(i)} \mathbf{1} \right)^T \circledast \left(\mathbf{1} - 2\widetilde{P^{[N_t]}} \right)^T \in \mathbb{R}^{1 \times N_u}.$$

$$(iii) \quad D_{P^{[N_t]}} \text{Cost}_{\mathcal{D}} = \frac{1}{N_d} \sum_{i=1}^{N_d} \left(\mathcal{S}_{N_u}^{(\widetilde{P^{[N_t]}})} \left(U_{(i)}^{[N_t]} \right) - Y_{(i)} \mathbf{1} \right)^T \cdot D_{P^{[N_t]}} \mathcal{S}_{N_u}^{(\widetilde{P^{[N_t]}})} \left(U_{(i)}^{[N_t]} \right), \text{ where}$$

$$D_{P^{[N_t]}} \mathcal{S}_{N_u}^{(\widetilde{P^{[N_t]}})}(u) = \begin{cases} \text{diag}(\mathbf{1} - 2u) \cdot \mathbf{1} \in \mathbb{R}^{N_u \times 1} & (\text{non-subordinate}), \\ \text{diag}(\mathbf{1} - 2u) \cdot \mathcal{B}^* \in \mathbb{R}^{N_u \times 1} & (\text{subordinate}). \end{cases}$$

(iv) With $\alpha^{[n]} \in \mathbb{R}^{N_u}$ as in (B.2),

$$D_{U_{(i)}^{[n]}} f(U_{(i)}^{[n]}, \alpha^{[n]}) = \text{diag} \left[U_{(i)}^{[n]} \circledast (\mathbf{1} - U_{(i)}^{[n]}) + (U_{(i)}^{[n]} - \alpha^{[n]}) \circledast (\mathbf{1} - 2U_{(i)}^{[n]}) \right] \in \mathbb{R}^{N_u \times N_u}.$$

(v) Whenever $\tilde{\alpha}^{[j]} = \mathcal{K} \cdot \tilde{w}^{[j]}$, with $\mathcal{K} \in \mathbb{R}^{N_u \times N_{\text{ptt}}}$, it holds that

$$D_{\tilde{w}^{[n]}} f(U_{(i)}^{[n]}, \tilde{\alpha}^{[n]}) = D_{\tilde{w}^{[n]}} f(U_{(i)}^{[n]}, \mathcal{K} \cdot \tilde{w}^{[n]}) = -\text{diag} \left[U_{(i)}^{[n]} \circledast (\mathbf{1} - U_{(i)}^{[n]}) \right] \cdot \mathcal{K} \in \mathbb{R}^{N_u \times N_{\text{ptt}}}.$$

(vi) For all $1 \leq j < N_t$ and $\alpha^{[j]} = \mathcal{B}^* \cdot w^{[j]}$, we have

$$\begin{aligned} \frac{\partial U_{(i)}^{[j+1]}}{\partial U_{(i)}^{[j]}} &= \mathcal{L}_{N_u}^{-1} \left(\text{Id}_{N_u} + \Delta_t D_{U_{(i)}^{[j]}} f(U_{(i)}^{[j]}, \alpha^{[j]}) \right) \in \mathbb{R}^{N_u \times N_u}, \\ \frac{\partial U_{(i)}^{[j+1]}}{\partial w^{[j]}} &= \Delta_t \mathcal{L}_{N_u}^{-1} D_{w^{[j]}} f(U_{(i)}^{[j]}, \alpha^{[j]}) \in \mathbb{R}^{N_u \times N_{\text{ptt}}}, \\ \frac{\partial P^{[j+1]}}{\partial P^{[j]}} &= \text{Id}_{N_u} + \Delta_t D_{P^{[j]}} f(P^{[j]}, \beta^{[j]}) \in \mathbb{R}^{N_p \times N_p}, \\ \frac{\partial P^{[j+1]}}{\partial \beta^{[j]}} &= \Delta_t D_{\beta^{[j]}} f(P^{[j]}, \beta^{[j]}) \in \mathbb{R}^{N_p \times N_{\text{ptt}}}. \end{aligned}$$

The proof is a standard Calculus exercise and therefore omitted.

B.2 Algorithms

In this section we present an implementation of the PSBC; further remarks concerning practical aspects of the numerical implementation (like code vectorization) are given in the Supplementary material. In the sequel, we refer to \mathbb{H} as a variable containing halting parameters in methods like Early Stopping, Drop SGD, among others, that one checks at each epoch in order to decide whether the optimization process is complete or not; cf. Appendix A. In this manner, the training process ends if \mathbb{H} is true, and continues otherwise. The set $\tilde{\mathcal{D}}$ can be the same as \mathcal{D} and is used to define an accuracy

metric; this is particularly important for model assessment. Recall that in the latter appendix one also discusses the initialization of W_U and W_P , that we shall refer to below.

Algorithm 1: PSBC.

Result: Trains the PSBC model.

Data: Dataset $\mathcal{D} = (X_{(i)}, Y_{(i)})_{1 \leq i \leq N_d}$, and $\tilde{\mathcal{D}} = (\tilde{X}_{(j)}, \tilde{Y}_{(j)})_{1 \leq j \leq \tilde{N}_d}$ ($\tilde{\mathcal{D}}$ and \mathcal{D} can be the same).

Input: PSBC parameters, number of epochs Q , Halting conditions \mathbb{H} , Jump in parameters $K^* \in \mathbb{G}_{N_t}$, diffusion ε , Partition Cardinality N_{ptt} , Subordination type, number of minibatches M , initial time discretization Δ_t^* .

Initialize

$$W = (W_U, W_P) = (W_U^{[0]} \dots W_U^{[N_t-1]}, W_P^{[0]}, \dots W_P^{[N_t-1]});$$

$q \leftarrow 0$;

while $q \leq Q$ and \mathbb{H} is False **do**

$\eta \leftarrow \eta_q$; // Shrink the learning rate

Split \mathcal{D} into disjoint sets \mathcal{D}_j , for $1 \leq j \leq M$; // Minibatch SGD

for $1 \leq j \leq M$ **do**

Compute $\text{diam}_A := \max\{1, \|W_A^{[0]}\|_{\ell^\infty}, \dots, \|W_A^{[N_t-1]}\|_{\ell^\infty}\}$, for $A \in \{P, U\}$;

Assign

$$\Delta_t^u \leftarrow \min \left\{ \Delta_t^*, \frac{0.57}{(\text{diam}_U)^2} \right\} \quad \text{and} \quad \Delta_t^p \leftarrow \min \left\{ \Delta_t^*, \frac{0.57}{(\text{diam}_P)^2} \right\}$$

to comply with the Invariant Region Enforcing Conditions (1.14);

Forward propagate elements in \mathcal{D}_j ;

Backpropagate using weights- K^* -sharing; /* See Algorithm 2 */

Update W using Gradient descent (1.5);

end

$q \leftarrow q + 1$; Compute accuracy using $\tilde{\mathcal{D}}$;

end

return PSBC with trained parameters.

Finally, we implement Backpropagation using model compression, that is, weights- K -sharing, where every K successive layers assume the same values; see Definition 1.5. An application of this technique to the Backpropagation Algorithm yields the algorithm given below. For a descriptive diagram, see Figure 5.

Algorithm 2: Backpropagation with weights- K -sharing.

Result: Compute the derivative of cost function using weights- K -sharing.

Data: $Z = (Z^{[0]}, \dots, Z^{[N_t]})$, $W = (W^{[0]}, \dots, W^{[N_t-1]})$, $\text{Cost}_{\mathcal{D}}(W) = \text{Cost}_{\mathcal{D}}(W, Z)$.

Input: PSBC parameters, $K \in \mathbb{G}_{N_t}$ (weights- K -sharing parameters).

Compute $\frac{\partial \text{Cost}_{\mathcal{D}}}{\partial Z^{[N_t]}}$;

$n \leftarrow N_t - 1$;

while $0 \leq n$ **do**

Calculate $\frac{\partial Z^{[n+1]}}{\partial Z^{[n]}}$ and $G = \frac{\partial Z^{[n+1]}}{\partial W^{[n]}}$;

Assign $\frac{\partial \text{Cost}_{\mathcal{D}}}{\partial W^{[n]}} \leftarrow \frac{\partial \text{Cost}_{\mathcal{D}}}{\partial Z^{[n+1]}} \cdot G$;

if $n \in K\mathbb{Z}$ **then**

$\frac{\partial \text{Cost}_{\mathcal{D}}}{\partial W^{[n]}} \leftarrow \sum_{j=n}^{\min\{n+K-1, N_t-1\}} \frac{\partial \text{Cost}_{\mathcal{D}}}{\partial W^{[j]}}$;

$n \leftarrow n - 1$;

end

return $\left(\frac{\partial \text{Cost}_{\mathcal{D}}}{\partial W^{[n]}} \right)_{n \in K\mathbb{Z}}$.

Appendix C. Some discrete maximum principles

The results in this section are all standard: they are discrete counterparts to classical results in elliptic PDE theory (Gilbarg and Trudinger, 1983, Chapter 3). We prove them here for the sake of completion, since we could not find an exposition close enough to our purposes.²⁶

In what follows, let $V \in \mathbb{R}^N$, for $N \geq 3$. For any $j \in \{1, \dots, N\}$, define

$$\text{Average}_{\partial\{j\}}(V) := \begin{cases} V_2, & \text{if } j = 1; \\ \frac{V_{j-1} + V_{j+1}}{2}, & \text{if } 1 < j < N; \\ V_{N-1}, & \text{if } j = N. \end{cases} \quad (\text{C.1})$$

We begin by proving an auxiliary result:

Lemma C.1 *Let $V \in E = \mathbb{R}^N$. Consider D_N be the diffusion finite difference matrix as in (5.3). Then the following statements are true:*

(i) *The condition $(D_N V)_j \leq 0$ is equivalent to $\text{Average}_{\partial\{j\}}(V) \leq V_j$.*

(ii) *The condition $(D_N V)_j \geq 0$ is equivalent to $\text{Average}_{\partial\{j\}}(V) \geq V_j$.*

(iii) *If $V_m = \min_{1 \leq j \leq N} \{V_j\}$, then $(D_N V)_m \geq 0$. Likewise, if $V_M = \max_{1 \leq j \leq N} \{V_j\}$, then $(D_N V)_M \leq 0$.*

(iv) *(Invariant positive cone) Given $U \in \mathbb{R}_+^N$ and $\alpha \geq 0$ then*

$$(\text{Id}_N - \alpha D_N)^{-1} U \in \mathbb{R}_+^N.$$

(v) $\|(\text{Id}_N - \alpha D_N)^{-1}\|_{\ell^\infty \rightarrow \ell^\infty} \leq 1$.

Note that (iv) and (v) are important results used in the study of invariant regions: the former is related to the elliptic maximum principle, and the latter to the parabolic maximum principle. They have been stated for more general finite difference operators in (Hoff, 1978, Lemma 3.2.).

Proof. The proof of (i)-(ii) are straightforward, hence omitted. Assertion (iii) is a direct consequence of (i) and (ii). We then prove (iv), arguing by contradiction. Assume the existence of $V \in \mathbb{R}_+^N \neq \mathbf{0}$ such that

$$(\text{Id}_N - \alpha D_N)^{-1} U \notin \mathbb{R}_+^N.$$

Taking $j = \text{argmin}(U)$, we must have that $\{(\text{Id}_N - \alpha D_N)^{-1} U\}_j = U_j < 0$. Equivalently,

$$V_j = \{(\text{Id}_N - \alpha D_N) U\}_j.$$

As $V \in \mathbb{R}_+^N$ we get from the left hand side in non-negative. Therefore,

$$(\alpha D_N U)_j \leq U_j < 0.$$

However, Lemma C.1(iii) implies that $(D_N U)_j \geq 0$. This contradiction finishes the proof.

The proof of (v) is also by contradiction. Assume that $\|(\text{Id}_N - \alpha D_N)^{-1}\|_{\ell^\infty \rightarrow \ell^\infty} > 1$. Hence, there exists a V and U in E such that $\|U\|_{\ell^\infty} = 1$, $\|V\|_{\ell^\infty} > 1$ and

$$(\text{Id}_N - \alpha D_N)^{-1} U = V.$$

²⁶ The closest, in (Strikwerda, 1989, Theorem 12.5.1).

Without loss of generality, let $M = \operatorname{argmax}(V)$ be so that $V_M = \|V\|_{\ell^\infty} > 1$. Then, using (C.1(i)), $(D_N V)_M \leq 0$. However, $U = (\operatorname{Id}_N - \alpha D_N) V$ implies that

$$U_M = ((\operatorname{Id}_N - \alpha D_N) V)_M = V_M - \alpha (D_N V)_M \stackrel{\alpha \geq 0}{\geq} V_M > 1,$$

which is in contradiction to the fact that $\|U\|_{\ell^\infty} = 1$, and this finishes the proof of (v). \blacksquare

Remark C.2 (Periodic Boundary Conditions) *The proofs in this session rely essentially on the Maximum Principle. They extend naturally to the case of periodic boundary conditions, substituting D_N in Lemma C.1 by $D_N^{(\text{per})}$ given in 6.3 and modifying the average operator C.1 to*

$$\widetilde{\operatorname{Average}}_{\partial\{j\}}(V) := \begin{cases} \frac{V_2 + V_N}{2}, & \text{if } j = 1; \\ \frac{V_{j-1} + V_{j+1}}{2}, & \text{if } 1 < j < N; \\ \frac{V_{N-1} + V_1}{2}, & \text{if } j = N. \end{cases} \quad (\text{C.2})$$

Appendix D. Proofs and auxiliary results

Throughout this section we shall use the following notation: for any $p \in \mathbb{R}$ and any set $\mathcal{A} \subset \mathbb{R}$, define

$$\operatorname{dist}(p, \mathcal{A}) := \inf_{q \in \mathcal{A}} |p - q|, \quad \text{and} \quad \operatorname{diam}(\mathcal{A}) := \sup_{a, b \in \mathcal{A}} |a - b|.$$

Recall that a set \mathcal{A} is convex if for any $p, q \in \mathcal{A}$ we have that $\lambda p + (1 - \lambda)q \in \mathcal{A}$, for all $\lambda \in [0, 1]$. Hence, it is easy to show that for any $C > 0$ and any two points p, q , we have

$$\operatorname{dist}(p, \mathcal{A}) \leq C, \quad \text{and} \quad \operatorname{dist}(q, \mathcal{A}) \leq C, \quad \text{implies} \quad \operatorname{dist}(\lambda p + (1 - \lambda)q, \mathcal{A}) \leq C, \quad (\text{D.1})$$

therefore the set $\widetilde{\mathcal{A}} = \{p \in \mathbb{R} \mid \operatorname{dist}(p, \mathcal{A}) \leq C\}$ is also a convex set.

We write $\operatorname{conv}(S)$ to denote the convex hull of a set S , which corresponds to the intersection of all convex sets containing S ; one can easily prove that the latter set is also convex.

D.1 An abstract invariant region lemma

Throughout the training process it is important to control the ℓ^∞ norm of trainable weights. Thanks to (1.5), we approach this problem by showing global existence²⁷ of the dynamics (1.7), proving that $\|U^{[\cdot, \cdot]}(X, \alpha^{[\cdot, \cdot]})\|_{\ell^\infty}$ and $\|P^{[\cdot, \cdot]}(\frac{1}{2}, \beta^{[\cdot, \cdot]})\|_{\ell^\infty}$ can both be controlled by the ℓ^∞ -norm of the trainable weights $\alpha^{[\cdot, \cdot]}$ and $\beta^{[\cdot, \cdot]}$, independently of N_t .

As trainable weights $\alpha^{[\cdot, \cdot]}$ and $\beta^{[\cdot, \cdot]}$ vary along the training, we would like to understand how they affect the growth of $U^{[\cdot, \cdot]}(X, \alpha^{[\cdot, \cdot]})$ and $P^{[\cdot, \cdot]}(\frac{1}{2}, \beta^{[\cdot, \cdot]})$ as the latter propagate through (1.7a) and (1.7b), respectively. Using the technique of invariant regions, dividing it in two parts: one that is the convex hull of the trainable weights $\alpha^{[\cdot, \cdot]}$ and $\beta^{[\cdot, \cdot]}$, the other an “excess” region, whose existence is a side effect of numerical discretization.

Remark D.1 (Continuum versus discrete III) *It is important to contrast the techniques we use and those of the Invariant region theory, mostly applied in the continuum setting; cf. Chueh et al. (1977) and Smoller, 1994, Chapter 14). In the sequel, assume that $\partial_t v = F(v)$ represents a reaction-diffusion PDE, and $v_{n+1} = \widetilde{F}(v_n)$ its discretization. Roughly speaking, the (continuum) theory looks*

27. We keep the term “global” even when $N_t < \infty$, because the result is easily extended to the case $N_t = +\infty$. Furthermore, because $\operatorname{dist}(p, \mathcal{P}) = \operatorname{dist}(p, \widetilde{\mathcal{P}})$ in the $\ell^\infty(\mathbb{R})$ topology, the result in Lemma D.3 still holds when $\mathcal{S}^{[N_t, \cdot]}$ has infinitely many points.

for sufficient conditions on a set Ω and on the behavior of $F|_{\partial\Omega}(\cdot)$, in such a way that initial conditions for the Cauchy problem that start on Ω remain on it for all $t \geq 0$. Notably, none of these conditions directly apply to the discrete problem, but have been adapted in some cases, as developed in the work Hoff (1978).

In showing that forward propagation is well-defined our goals are the same as those in the continuum theory: we prove that obstructive conditions prevent solutions to leave a certain bounded set (which is analogous to the aforementioned set Ω). In that regards, the results in this section and that of (Hoff, 1978, Theorem 3.3) are similar, although the techniques we employ differ in two ways: (i) due to training, our model's coefficients are mostly changing over iterations, therefore such variation (especially those between different layers) should be taken into account; (ii) we have the advantage of knowing both the range of initial conditions (due to the normalization condition (N-C)) and the structure of the reaction term. Thus, given n th layer's trainable weights (or, equivalently, coefficients in n -th time step), we can combine (i) and (ii) to dynamically adapt the invariant region at the $n+1$ -th layer. In Hoff (1978) the meshgrid is fixed, therefore such an estimate can be obtained using Lipschitz bounds, which is equivalent to what we do in Lemma D.3 and Corollary D.4. It is important to emphasize that, in scope, the result in Hoff (1978) is more general, for it applies to a wider range of reaction diffusion models.

We begin with an auxiliary result.

Lemma D.2 *The polynomial $p(z) = -z^4 + z^3 + 2z - 1$ is non-negative in the range $1 \leq z \leq 1 + \frac{1}{\sqrt{3}}$.*

Proof. Rewrite the polynomial as $p(z) = z - (1-z)^2(z^2 + z + 1)$. Then the result follows from $p(z) \geq z - \frac{(z^2+z+1)}{3} =: q(z) \geq q(1) = 0$ in $1 \leq z \leq 1 + \frac{1}{\sqrt{3}}$. ■

The next result is fundamental in the rest of this Appendix. We remark that when compared to classical global existence results in PDEs, Lemma D.3(i) and Lemma D.3(ii) are, roughly speaking, equivalent to showing local existence (and associated bounds), and then applying a feedback argument, respectively; cf. (Rauch and Smoller, 1978, Theorems 2.1 and 3.9).

Lemma D.3 (Abstract invariant region) *Let $\mathcal{P} \subset \mathbb{R}$ be a convex set of parameters satisfying $\{0, 1\} \subset \mathcal{P}$. For a fixed $\beta \in \mathcal{P}$, let*

$$U^{[n+1]} = U^{[n]} + \Delta_t U^{[n]}(1 - U^{[n]})(U^{[n]} - \beta). \quad (\text{D.2})$$

Then, the following properties hold:

(i) *If $U^{[n]} \in \mathcal{P}$, then $\text{dist}(U^{[n+1]}, \mathcal{P}) \leq \Delta_t \text{diam}(\mathcal{P})^3$.*

(ii) *For any $0 \leq \Delta_t \leq \frac{1}{\sqrt{3} \text{diam}(\mathcal{P})^2}$, the set*

$$\mathcal{S} := \left\{ X \in \mathbb{R} \mid \text{dist}(X, \mathcal{P}) \leq \Delta_t \text{diam}(\mathcal{P})^3 \right\}$$

is convex and positively invariant under (D.2).

Proof. [of Lemma D.3] Throughout the proof we write $D = \text{diam}(\mathcal{P})$. To begin with, (D.2) gives

$$|U^{[n+1]} - U^{[n]}| = \Delta_t |U^{[n]}| \cdot |1 - U^{[n]}| \cdot |U^{[n]} - \beta|. \quad (\text{D.3})$$

Because $\{0, 1, \beta, U^{[n]}\} \subset \mathcal{P}$ we can majorize the right hand side by $\Delta_t D^3$. As $U^{[n]} \in \mathcal{P}$, the left hand side is bounded from below by $\text{dist}(U^{[n+1]}, \mathcal{P})$, and this completes the proof.

Now we turn to the proof of (ii). We prove positive invariance using an induction argument on n . The result is clearly true for $n = 0$, since $U^{[0]} = X \in \mathcal{S}$ due to the normalization condition (N-C). Thus, assuming that $U^{[k]} \in \mathcal{S}$ for all $0 \leq k \leq n$, we must prove that $U^{[n+1]} \in \mathcal{S}$.

A simplification is readily available: it suffices to consider the case $U^{[n]} \in \mathcal{S} \setminus \mathcal{P}$, for (i) contemplates the other case. To begin with, observe that \mathcal{S} is convex, which it inherits from the convexity of the set \mathcal{P} allied to convexity of the ℓ^∞ norm (see discussion below (D.1)). Thus, from $0 \in \mathcal{P} \subset \mathcal{S}$ we conclude that $\{-\Delta_t D^3, +\Delta_t D^3\} \subset \mathcal{S}$. Furthermore, as we also have that $U^{[n]} \in \mathcal{S}$, the result follows if we show that $U^{[n+1]}$ belongs to the interval $[-\Delta_t D^3, U^{[n]}]$ when $U^{[n]} \geq 0$, or that $U^{[n+1]}$ belongs to the interval $[U^{[n]}, +\Delta_t D^3]$ when $U^{[n]} \leq 0$. We shall prove only the former assertion, the proof of the latter being similar.

Since $U^{[n]} \in \mathcal{S} \setminus \mathcal{P} \subset \mathbb{R}$ is non-negative, we must have $U^{[n]} \geq \max\{1, \beta\}$ and, consequently, that $\Delta_t U^{[n]}(1 - U^{[n]})(U^{[n]} - \beta) \leq 0$; inspecting (D.2), this implies that $U^{[n+1]} \leq U^{[n]}$. Therefore, in order to finalize the proof it suffices to show that $-\Delta_t D^3 \leq U^{[n+1]}$ or, equivalently, that

$$-\Delta_t D^3 \leq U^{[n]} \left(1 + \Delta_t(1 - U^{[n]})(U^{[n]} - \beta) \right) \quad (\text{D.4})$$

holds, where the equivalence is due to (D.2). Since $U^{[n]}$ and $U^{[n+1]}$ have the same sign, it holds that $0 \leq U^{[n+1]} \leq U^{[n]}$, therefore both 0 and $U^{[n]}$ belong to the convex set \mathcal{S} . Consequently, we only need to consider the cases in which both quantities $U^{[n]}$ and $U^{[n+1]}$ have different signs.

It is easy to conclude by triangle inequality that $\text{dist}(U^{[n]}, p) \leq \text{dist}(U^{[n]}, q) + \text{diam}(\mathcal{P})$ for any $p, q \in \mathcal{P}$. By optimization on q and the induction hypothesis, this yields

$$\text{dist}(U^{[n]}, p) \leq \text{dist}(U^{[n]}, \mathcal{P}) + \text{diam}(\mathcal{P}) \leq D(1 + \Delta_t D^2). \quad (\text{D.5})$$

Thus, we can bound $(1 + \Delta_t(1 - U^{[n]})(U^{[n]} - \beta))$ from below by $(1 - \Delta_t(D + \Delta_t D^3)^2)$, since $\{1, \beta\} \subset \mathcal{P}$. Consequently,

$$\min \left\{ (D + \Delta_t D^3) (1 - \Delta_t(D + \Delta_t D^3)^2), 0 \right\} \leq U^{[n]} \left(1 + \Delta_t(1 - U^{[n]})(U^{[n]} - \beta) \right).$$

It is evident that $-\Delta_t D^3 \leq 0$, therefore it suffices to study the values of Δ_t for which the inequality

$$-\Delta_t D^3 \leq (D + \Delta_t D^3) (1 - \Delta_t(D + \Delta_t D^3)^2),$$

holds, which we claim to hold whenever $\Delta_t D^2 \leq \frac{1}{\sqrt{3}}$ is satisfied. Indeed, we shall use a rearrangement of the above inequality as

$$-\Delta_t D^2 \leq (1 + \Delta_t D^2) (1 - \Delta_t D^2(1 + \Delta_t D^2)^2).$$

Plugging $Z = 1 + \Delta_t D^2$ into the previous inequality and expanding gives

$$-Z^4 + Z^3 + 2Z - 1 \geq 0.$$

The above inequality holds in the range $1 \leq Z \leq 1 + \frac{1}{\sqrt{3}}$, thanks to the result of Lemma D.2. Unpacking, this gives the equivalent statement $\Delta_t D^2 \leq \frac{1}{\sqrt{3}}$, proving the claim. We have then established (D.4), and with this we conclude the proof. \blacksquare

Corollary D.4 *For any sequence $(\alpha^{[k]})_{-1 \leq k \leq N_t - 1}$, with $\alpha^{[-1]} = 1$, define the sets*

$$\mathcal{P}^{[k]} := \text{conv} \left(\{0, 1\} \cup_{m=-1}^k \{\alpha^{[m]}\} \right),$$

for $-1 \leq k \leq N_t - 1$. Let

$$U^{[k+1]} = U^{[k]} + \Delta_t U^{[k]}(1 - U^{[k]})(U^{[k]} - \alpha^{[k]}),$$

with $U^{[0]} \in [0, 1]$, $0 \leq k \leq N_t - 1$. Thus, whenever $0 \leq \Delta_t \leq \frac{1}{\sqrt{3} \text{diam}(\mathcal{P}^{[N_t-1]})^2}$, we have

$$\text{dist}(U^{[k]}, \mathcal{P}^{[k-1]}) \leq \Delta_t \text{diam}(\mathcal{P}^{[k-1]})^3, \quad \text{for all } 0 \leq k \leq N_t.$$

Remark D.5 (the case of parameter range on a symmetric set) In the case of \mathcal{P}_{sym} being a symmetric set about the origin (that is, $\beta \in \mathcal{P}_{\text{sym}}$ if and only if $-\beta \in \mathcal{P}_{\text{sym}}$), then it is possible to extend the previous proof to show that, whenever $0 \leq \Delta_t \leq \frac{1}{\text{diam}(\mathcal{P}_{\text{sym}})^2}$, the set

$$\mathcal{S} := \left\{ X \in \mathbb{R} \mid \text{dist}(X, \mathcal{P}_{\text{sym}}) \leq \frac{\Delta_t}{2} \text{diam}(\mathcal{P}_{\text{sym}})^3 \right\}$$

is a convex, positively invariant set through (D.2). In such a case, Corollary D.4 applies to

$$\mathcal{P}_{\text{sym}}^{[k]} := \text{conv} \left(\{0, 1, -1\} \cup_{m=-1}^k \{\alpha^{[m]}\} \cup_{m=-1}^k \{-\alpha^{[m]}\} \right).$$

D.2 Proof of results in Section 2

Proof. [of Proposition 2.2] For $\mathcal{P}^{[k]}$ as in Corollary D.4, define

$$\mathcal{S}^{[k]} := \left\{ X \in \mathbb{R} \mid \text{dist}(X, \mathcal{P}^{[k]}) \leq \Delta_t^u \text{diam}(\mathcal{P}^{[k]})^3 \right\}.$$

The equivalence between the interval $[L^{[k]} - \Delta_t^u M^{[k]}, R^{[k]} + \Delta_t^u M^{[k]}]$ and the set $\mathcal{S}^{[k]}$ is clear. Applying Corollary D.4 then gives the result. \blacksquare

Proof. [of Proposition 2.7] We argue by contradiction. Assume that for all $j \in \{0, \dots, N_t\}$ the assertion

$$U^{[j]}(X; \alpha^{[j]}) \geq U^{[j]}(\tilde{X}; \alpha^{[j]})$$

holds, but at $n+1$ we get for the first time

$$U^{[n+1]}(X; \alpha^{[n+1]}) < U^{[n+1]}(\tilde{X}; \alpha^{[n+1]}). \quad (\text{D.6})$$

From Proposition 2.2, we immediately obtain the bound $|U^{[n]}| \leq 1 + \Delta_t^u$, for all $n \in \{0, \dots, N_t\}$. Now, as $\alpha^{[n]} \in [0, 1]$ and $0 \leq \Delta_t^u \leq \frac{1}{10}$, a straightforward computation shows that

$$\max_{|U| \leq 2, \alpha \in [0, 1]} |D_U f(U, \alpha^{[n]})| \leq 8 \left(1 + \frac{\Delta_t^u}{2}\right)^2 \leq 9. \quad (\text{D.7})$$

Using (2.1), a simple application of the Intermediate Value Theorem gives

$$\begin{aligned} U^{[n+1]}(X, \alpha^{n+1}) - U^{[n+1]}(\tilde{X}, \alpha^{n+1}) &= U^{[n]}(X, \alpha^{[n]}) - U^{[n]}(\tilde{X}, \alpha^{[n]}) \\ &\quad + \Delta_t^u (D_U f) \left(\theta, \alpha^{[n]} \right) \left(U^{[n]}(X, \alpha^{[n]}) - U^{[n]}(\tilde{X}, \alpha^{[n]}) \right). \end{aligned}$$

for some $U^{[n]}(\tilde{X}, \alpha^{[n]}) \leq \theta \leq U^{[n]}(X, \alpha^{[n]})$. From (D.6) we conclude that the left hand side of the above equality is strictly negative. However, the bound in (D.7) and the assumption $0 \leq \Delta_t^u \leq \frac{1}{10}$ imply that the right hand side is non-negative. This contradiction implies that (D.6) cannot happen, and the result is therefore established. \blacksquare

D.3 Proof of results in Section 5

Proof. [of Proposition 5.2] The proof is essentially a reprise of that in Lemma D.3, with some subtle changes due to the presence of the diffusion operator; the main argument invokes Lemma C.1(iv), an idea we learned from (Hoff, 1978, Theorem 3.3).

To begin with, observe that there is no diffusion in the component $P^{[k]}(\frac{1}{2}, \beta^{[k]})$, hence the proof of this case is contemplated by Corollary 4.8. Therefore, in the rest of the proof we are left with estimates for the component $U^{[k]}(X, \alpha^{[k]})$ only. For all $-1 \leq n \leq N_t - 1$, define

$$L_*^{[n]} := L_\alpha^{[n]} - \Delta_t^u M^{[n]}, \quad R_*^{[n]} := R_\alpha^{[n]} + \Delta_t^u M^{[n]}.$$

We have to show that $L_*^{[n-1]} \mathbf{1} \leq U^{[n]} \leq R_*^{[n-1]} \mathbf{1}$ holds for every $0 \leq n \leq N_t$. Once more, we shall use an induction argument on n . The result is clearly true for $n = 0$, because of the normalization conditions (N-C). Hence, assume that the result holds for all $0 \leq j \leq n$.

Recall from (5.3) that $\mathcal{L}_{N_u} = \text{Id}_{N_u} - \varepsilon^2 \Delta_t^u D_{N_u}$. A simple inspection shows that, for all $\gamma \in \mathbb{R}$, it holds

$$\mathcal{L}_N \cdot (\gamma \mathbf{1}) = \gamma \mathbf{1}, \quad \text{and} \quad (\mathcal{L}_N)^{-1} \cdot (\gamma \mathbf{1}) = \gamma \mathbf{1}. \quad (\text{D.8})$$

In other words, the vector $\gamma \mathbf{1}$ is an eigenvector to $(\mathcal{L}_{N_u})^{-1}$ with associated eigenvalue 1.

First, it is clear from the monotonicity of $L_*^{[n-1]}$ and $R_*^{[n-1]}$ that it suffices to show that

$$U^{[n+1]} - L_*^{[n-1]} \mathbf{1} \geq 0, \quad \text{and} \quad R_*^{[n-1]} \mathbf{1} - U^{[n+1]} \geq 0.$$

We shall prove the case on the left hand side, the other case having a similar proof. We remark that the discretization of the Laplacian (5.3) implies that $D_N \mathbf{1} = 0$. From (5.4), we subtract $L_*^{[n-1]} \mathbf{1}$ on both sides and apply (D.8), getting

$$U^{[n+1]} - L_*^{[n-1]} \mathbf{1} = \mathcal{L}_{N_u}^{-1} \left[U^{[n]} - L_*^{[n-1]} \mathbf{1} + \Delta_t^u f(U^{[n]}, \beta^{[n]}) \right].$$

Thanks to invariance of the positive cone in Lemma C.1(iv), the result follows if we prove that the bracketed term in the above equation is in the non-negative cone. But this is true, thanks to Proposition 4.8. With this assertion, we complete the induction argument, concluding the proof. \blacksquare

D.4 Proof of results in Section 6

In this session, we abuse notation deliberately: for any operator $A = [A_{i,j}] : \mathbb{R}^n \rightarrow \mathbb{R}^m$, we write $\|A\|_{\text{op}} := \|A\|_{\ell^\infty(\mathbb{R}^n) \rightarrow \ell^\infty(\mathbb{R}^m)}$. Further, for a given vector $V \in \mathbb{R}^n$ we write $\|V\|_{\ell^p}$ to denote $\|V\|_{\ell^p(\mathbb{R}^n)}$.

The main goal of this session is proving Proposition 6.3. A quick digression is necessary before we do so. Let $Z \in \mathbb{R}^N$. Consider the functional $\mathcal{F}(Z) = \frac{1}{2} \|Z\|_{\ell^2}^2 = \frac{1}{2} \langle Z, Z \rangle_{\ell^2}$, with $Z = Z(W) : \mathbb{R}^M \rightarrow \mathbb{R}^N$.

Then $\frac{\partial \mathcal{F}}{\partial W_l} = \left\langle Z, \frac{\partial Z}{\partial W_l} \right\rangle_{\ell^2}$, with $1 \leq l \leq m$. A direct application of the Cauchy-Schwarz inequality, followed by the trivial inequality $\|Z\|_{\ell^2} \leq \sqrt{N} \|Z\|_{\ell^\infty}$, gives

$$\left\| \frac{\partial \mathcal{F}}{\partial W_l} \right\|_{\ell^\infty} \leq \|Z\|_{\ell^2} \cdot \left\| \frac{\partial Z}{\partial W_l} \right\|_{\ell^2} = \sqrt{2\mathcal{F}} \cdot \left\| \frac{\partial Z}{\partial W_l} \right\|_{\ell^2} \leq \sqrt{2N\mathcal{F}} \cdot \left\| \frac{\partial Z}{\partial W_l} \right\|_{\ell^\infty}. \quad (\text{D.9})$$

Hence,

$$\left\| \frac{\partial \mathcal{F}}{\partial W} \right\|_{\ell^\infty} \leq \sqrt{2N\mathcal{F}} \cdot \left\| \frac{\partial Z}{\partial W} \right\|_{\text{op}}. \quad (\text{D.10})$$

The next result establishes some auxiliary estimates to be used in the proof of Proposition D.7.

Lemma D.6 (Energy estimates) *Given fixed numbers $N_u, N_{\text{ptt}}, N_p \in \mathbb{N}$ such that $1 \leq N_p \leq N_{\text{ptt}} \leq N_u$, and $\varepsilon \geq 0$, consider the associated PSBC model (1.7) with $N_t \in \mathbb{N}$ layers, weights- k^* -sharing. Recall that $\alpha^{\lfloor \cdot \rfloor} = \mathcal{B}^* \cdot w^{\lfloor \cdot \rfloor} \in \mathbb{R}^{N_u}$ and $\beta^{\lfloor \cdot \rfloor} \in \mathbb{R}^{N_p}$.*

Let $\text{Cost}_{\mathcal{D}} = \frac{1}{N_d} \sum_{i=1}^{N_d} \text{Cost}_{(i)}$, with $\text{Cost}_{(i)} = \frac{\|Z_{(i)}\|_{\ell^2}^2}{2}$, and $Z_{(i)} = \mathcal{S}_{N_u}^{(\widehat{P}^{\lfloor N_t \rfloor})} \left(U_{(i)}^{\lfloor N_t \rfloor} \right) - Y_{(i)} \mathbf{1}$. Define $\Gamma := \frac{1+\sqrt{3}}{\sqrt{3}}$, and the set

$$\mathcal{P}_{\alpha}^{\lfloor n \rfloor} = \text{conv} \left(\{0, 1\} \cup_{m=0}^{N_u} \{\alpha_m^{\lfloor 0 \rfloor}\} \cup \dots \cup_{m=0}^{N_u} \{\alpha_m^{\lfloor n \rfloor}\} \right),$$

with a similar definition holding for $\mathcal{P}_{\beta}^{\lfloor n \rfloor}$. Accordingly, one writes the Invariant Region Enforcing Condition (1.14) on Δ_t^p and Δ_t^u ,

$$0 \leq \Delta_t^u \leq \frac{1}{\sqrt{3} \text{diam} \left(\mathcal{P}_{\alpha}^{\lfloor N_t-1 \rfloor} \right)^2} \quad \text{and} \quad 0 \leq \Delta_t^p \leq \frac{1}{\sqrt{3} \text{diam} \left(\mathcal{P}_{\beta}^{\lfloor N_t-1 \rfloor} \right)^2}. \quad (\text{D.11})$$

Then, the following bounds hold:

- (i) $\left\| \frac{\partial \text{Cost}_{\mathcal{D}}}{\partial U_{(i)}^{\lfloor N_t \rfloor}} \right\|_{\text{op}} \leq \Gamma \text{diam}(\mathcal{P}_{\beta}^{\lfloor N_t-1 \rfloor}) \frac{\sqrt{8N_u \text{Cost}_{(i)}}}{N_d}$.
- (ii) $\left\| \frac{\partial \text{Cost}_{\mathcal{D}}}{\partial P^{\lfloor N_t \rfloor}} \right\|_{\text{op}} \leq \Gamma \text{diam}(\mathcal{P}_{\alpha}^{\lfloor N_t-1 \rfloor}) \sqrt{8N_u \text{Cost}_{\mathcal{D}}}$.
- (iii) $\max \left\{ \left\| \frac{\partial U_{(i)}^{\lfloor k+l \rfloor}}{\partial U_{(i)}^{\lfloor k \rfloor}} \right\|_{\text{op}}, \left\| \frac{\partial P^{\lfloor k+l \rfloor}}{\partial P^{\lfloor k \rfloor}} \right\|_{\text{op}} \right\} \leq \left(1 + \sqrt{3} \Gamma^2 \right)^l$, for all $0 \leq k \leq N_t$, $0 \leq k+l \leq N_t$.
- (iv) $\max \left\{ \left\| \frac{\partial U_{(i)}^{\lfloor k+1 \rfloor}}{\partial w^{\lfloor k \rfloor}} \right\|_{\text{op}}, \left\| \frac{\partial P^{\lfloor k+1 \rfloor}}{\partial \beta^{\lfloor k \rfloor}} \right\|_{\text{op}} \right\} \leq \frac{\Gamma^2}{\sqrt{3}}$, for all $0 \leq k \leq N_t - 1$.
- (v) $\left\| \frac{\partial \text{Cost}_{\mathcal{D}}}{\partial U_{(i)}^{\lfloor k \rfloor}} \right\|_{\text{op}} \leq \Gamma \cdot \left(1 + \sqrt{3} \Gamma^2 \right)^{N_t-k} \cdot \frac{\sqrt{8N_u \text{Cost}_{(i)}}}{N_d} \cdot \text{diam}(\mathcal{P}_{\beta}^{\lfloor N_t-1 \rfloor})$, for any $k \in k^* \mathbb{Z}$, $k \leq N_t$.
- (vi) $\left\| \frac{\partial \text{Cost}_{\mathcal{D}}}{\partial P^{\lfloor k \rfloor}} \right\|_{\text{op}} \leq \Gamma \cdot \left(1 + \sqrt{3} \Gamma^2 \right)^{N_t-k} \cdot \sqrt{8N_u \text{Cost}_{\mathcal{D}}} \cdot \text{diam}(\mathcal{P}_{\alpha}^{\lfloor N_t-1 \rfloor})$, for any $k \in k^* \mathbb{Z}$, $k \leq N_t$.
- (vii) $\left\| \frac{\partial \text{Cost}_{\mathcal{D}}}{\partial w^{\lfloor k \rfloor}} \right\|_{\text{op}} \leq k^* \cdot \frac{\Gamma^3}{\sqrt{3}} \cdot \left(1 + \sqrt{3} \Gamma^2 \right)^{N_t-k-1} \cdot \sqrt{8N_u \text{Cost}_{\mathcal{D}}} \cdot \text{diam}(\mathcal{P}_{\beta}^{\lfloor N_t-1 \rfloor})$, for any $k \in k^* \mathbb{Z}$, $k \leq N_t$.
- (viii) $\left\| \frac{\partial \text{Cost}_{\mathcal{D}}}{\partial \beta^{\lfloor k \rfloor}} \right\|_{\text{op}} \leq k^* \cdot \frac{\Gamma^3}{\sqrt{3}} \cdot \left(1 + \sqrt{3} \Gamma^2 \right)^{N_t-k-1} \cdot \sqrt{8N_u \text{Cost}_{\mathcal{D}}} \cdot \text{diam}(\mathcal{P}_{\alpha}^{\lfloor N_t-1 \rfloor})$, for any $k \in k^* \mathbb{Z}$, $k \leq N_t$.
- (ix) $\text{Cost}_{\mathcal{D}} \leq \frac{N_u}{2} \cdot \left(2\Gamma^2 \cdot \text{diam}(\mathcal{P}_{\alpha}^{\lfloor N_t-1 \rfloor}) \cdot \text{diam}(\mathcal{P}_{\beta}^{\lfloor N_t-1 \rfloor}) + 1 \right)^2$.

Proof. We begin with a few remarks. Let $0 \leq k \leq N_t - 1$. First, it is immediate that $\frac{\partial \text{Cost}_{\mathcal{D}}}{\partial U_{(i)}} = \frac{1}{N_d} \frac{\partial \text{Cost}_{(i)}}{\partial U_{(i)}}$. Obviously,

$$\alpha_m^{[k]} \in \mathcal{P}_\alpha^{[k]} \subset \mathcal{P}_\alpha^{[N_t-1]}, \quad \forall 1 \leq m \leq N_u, \quad \text{and} \quad \beta_j^{[k]} \in \mathcal{P}_\beta^{[k]} \subset \mathcal{P}_\beta^{[N_t-1]}, \quad \forall 1 \leq j \leq N_p.$$

Using the constraints (D.11), we argue as in (D.5) to obtain

$$\text{dist}(U_m^{[k]}, p_\alpha) \leq \Gamma \text{diam}(\mathcal{P}_\alpha^{[N_t-1]}) \quad \text{and} \quad \text{dist}(P_j^{[k]}, p_\beta) \leq \Gamma \text{diam}(\mathcal{P}_\beta^{[N_t-1]}), \quad (\text{D.12})$$

for all $1 \leq m \leq N_u$ and $1 \leq j \leq N_p$, whenever $p_\alpha \in \mathcal{P}_\alpha^{[N_t-1]}$ and $p_\beta \in \mathcal{P}_\beta^{[N_t-1]}$.

We are ready to prove (i). Thanks to (D.10), we have

$$\left\| \frac{\partial \text{Cost}_{\mathcal{D}}}{\partial U_{(i)}^{[N_t]}} \right\|_{\text{op}} \leq \frac{1}{N_d} \left\| \frac{\partial \text{Cost}_{(i)}}{\partial U_{(i)}^{[N_t]}} \right\|_{\text{op}} \leq \frac{\sqrt{2N_u \text{Cost}_{(i)}}}{N_d} \left\| \frac{\partial Z_{(i)}}{\partial U_{(i)}^{[N_t]}} \right\|_{\ell^\infty}.$$

Lemma B.1(ii) in combination with (D.12) then gives

$$\left\| \frac{\partial Z_{(i)}}{\partial U_{(i)}^{[N_t]}} \right\|_{\ell^\infty} = \left\| \text{diag} \left(\mathbf{1} - 2P^{[N_t]} \right) \right\|_{\ell^\infty} \leq 2 \text{dist} \left(\mathcal{P}_\beta^{[N_t-1]}, \frac{1}{2} \right) \leq 2 \Gamma \text{diam}(\mathcal{P}_\beta^{[N_t-1]}),$$

since $\frac{1}{2} \in \mathcal{P}_\alpha^{[N_t-1]} \cap \mathcal{P}_\beta^{[N_t-1]}$. Combining the last two inequalities establishes (i).

To prove (ii), it is clear from the construction (4.7) that $\|\mathcal{B}\|_{\text{op}} = 1$. Thus,

$$\left\| \frac{\partial Z_{(i)}}{\partial P^{[N_t]}} \right\|_{\text{op}} \leq \left\| \text{diag} \left(\mathbf{1} - 2U_{(i)}^{[N_t]} \right) \right\|_{\ell^\infty} \|\mathcal{B}\|_{\ell^\infty} \leq \left\| \text{diag} \left(\mathbf{1} - 2U_{(i)}^{[N_t]} \right) \right\|_{\ell^\infty}.$$

Triangle inequality then gives,

$$\left\| \frac{\partial \text{Cost}_{\mathcal{D}}}{\partial P_{(i)}^{[N_t]}} \right\|_{\text{op}} \leq \sum_{i=1}^{N_d} \left\| \frac{\partial \text{Cost}_{\mathcal{D}}}{\partial P_{(i)}^{[N_t]}} \right\|_{\text{op}},$$

and the result follows arguing as in case item (i).

To prove (iii), we use Lemma B.1(v) and the convexity of $\mathcal{P}_\alpha^{[k]}$ to get

$$\begin{aligned} \left\| D_{U_{(i)}^{[k]}} f(U_{(i)}^{[k]}, \alpha^{[k]}) \right\|_{\text{op}} &\leq \left\| \text{diag} \left[(U_{(i)}^{[k]} \circledast (\mathbf{1} - U_{(i)}^{[k]}) + (U_{(i)}^{[k]} - \alpha^{[k]}) \circledast (\mathbf{1} - 2U_{(i)}^{[k]}) \right] \right\|_{\text{op}} \\ &\leq 3 \Gamma^2 \text{diam} \left(\mathcal{P}_\alpha^{[N_t-1]} \right)^2. \end{aligned}$$

Lemma C.1(v) and the constraining (D.11) then imply

$$\begin{aligned} \left\| \frac{\partial U_{(i)}^{[k+1]}}{\partial U_{(i)}^{[k]}} \right\|_{\text{op}} &\leq \|\mathcal{L}_{N_u}^{-1}\|_{\text{op}} \cdot \left\| \left(\text{Id} + \Delta_t^u D_{U_{(i)}^{[k]}} f(U_{(i)}^{[k]}, \alpha^{[k]}) \right) \right\|_{\text{op}} \\ &\leq 1 + 3 \Delta_t^u \text{diam} \left(\mathcal{P}_\alpha^{[N_t-1]} \right)^2 \\ &\leq 1 + \sqrt{3} \Gamma^2. \end{aligned}$$

Finally, we apply the Chain rule,

$$\left\| \frac{\partial U_{(i)}^{[k+l]}}{\partial U_{(i)}^{[k]}} \right\|_{\text{op}} = \left\| \frac{\partial U_{(i)}^{[k+l]}}{\partial U_{(i)}^{[k+l-1]}} \circ \dots \circ \frac{\partial U_{(i)}^{[k+1]}}{\partial U_{(i)}^{[k]}} \right\|_{\text{op}} \leq \prod_{j=0}^{l-1} \left\| \frac{\partial U_{(i)}^{[k+j+1]}}{\partial U_{(i)}^{[k+j]}} \right\|_{\text{op}} \leq \left(1 + \sqrt{3}\Gamma^2\right)^l,$$

finishing the proof of the first inequality in (iii); the proof for the derivative with respect to $P^{[k]}$ is similar.

In order to derive (iv), we recall that $\|\mathcal{B}\|_{\text{op}} = 1$, invoking Lemma B.1(v) and (D.12) to get

$$\begin{aligned} \left\| D_{w^{[k]}} f(U_{(i)}^{[k]}, \alpha^{[k]}) \right\|_{\text{op}} &\leq \left\| \text{diag} \left[U_{(i)}^{[k]} \circledast (\mathbf{1} - U_{(i)}^{[k]}) \right] \right\|_{\text{op}} \cdot \|\mathcal{B}\|_{\text{op}} \\ &\leq \left\| U_{(i)}^{[k]} \circledast (\mathbf{1} - U_{(i)}^{[k]}) \right\|_{\ell^\infty} \\ &\leq \Gamma^2 \text{diam} \left(\mathcal{P}_\alpha^{[N_t-1]} \right)^2, \end{aligned}$$

Now we invoke Lemma C.1(v) and use the constraint (D.11), obtaining

$$\left\| \frac{\partial U_{(i)}^{[k+1]}}{\partial \alpha^{[k]}} \right\|_{\text{op}} \leq \Delta_t^u \|\mathcal{L}_{N_u}^{-1}\|_{\text{op}} \left\| D_{w^{[j]}} f(U_{(i)}^{[j]}, w^{[j]}) \right\|_{\text{op}} \leq \frac{\Gamma^2}{\sqrt{3}},$$

and we are done. The proof of the other case is similar, and this completes the proof of (iv).

In light of the Chain Rule, assertions (iv) and (v) are direct consequences of (i) and (ii); in the same fashion, assertions (vi) and (vii) are direct consequences of (i) and (iii).

Estimate in (ix) is established arguing as in the previous cases, and with this we finish the proof of the Lemma. \blacksquare

In practice, the estimate in Lemma D.6(ix) is not directly useful, for the cost is a quantity that is observable throughout the numerics. Moreover, the relevance of the estimates lie on the fact that they are controlled by Cost, η_q , and the parameters, being linear in each one of them whenever other variables are frozen. This is the content of the next Lemma.

Lemma D.7 (Growth of trainable weights in terms of epochs) *Given W_0 , let W_q be a sequence generated using (1.5), for $q \in \{1, \dots, Q\}$. Assume the existence of a constant C_q and an exponent K such that*

$$\left\| \frac{\partial \text{Cost}_\varphi(W_q)}{\partial W} \right\|_{\ell^\infty} \leq C_q \|W_q\|_{\ell^\infty}^K.$$

Given any sequence $\gamma_q \geq 0$, choose $\eta_q \geq 0$ in such a way that $\eta_q C_q (\|W_q\|_{\ell^\infty})^{K-1} \leq \gamma_q$ is satisfied. Hence,

$$\|W_{q+1}\|_{\ell^\infty} \leq (1 + \gamma_q) \|W_q\|_{\ell^\infty}. \quad (\text{D.13})$$

In particular, it holds that

$$\|W_Q\|_{\ell^\infty} \leq \prod_{q=0}^{Q-1} (1 + \gamma_q) \|W_0\|_{\ell^\infty} \leq e^{\sum_{q=0}^{Q-1} \gamma_q} \|W_0\|_{\ell^\infty}. \quad (\text{D.14})$$

Furthermore, since (D.13) implies $\|\max\{W_{q+1}, 1\}\|_{\ell^\infty} \leq (1 + \gamma_q) \|\max\{W_q, 1\}\|_{\ell^\infty}$, we can rewrite (D.14) as

$$\max\{\|W_Q\|_{\ell^\infty}, 1\} \leq \prod_{q=0}^{Q-1} (1 + \gamma_q) \max\{\|W_0\|_{\ell^\infty}, 1\} \leq e^{\sum_{q=0}^{Q-1} \gamma_q} \max\{\|W_0\|_{\ell^\infty}, 1\}. \quad (\text{D.15})$$

We omit the proof, since it follows by standard induction argument and using (D.13). Now we are ready to prove our last result.

Proof. [of Proposition 6.3] Considering the PSBC model with weights- k^* -sharing parameter, let

$$W = \left(W^{[0]}, W^{[k^*]}, \dots, W^{[k^* \lfloor \frac{N_t}{k^*} \rfloor]} \right)^T =: (\alpha^{[\cdot]}, \beta^{[\cdot]})^T.$$

By construction, it holds that

$$\begin{aligned} \max_{0 \leq n \leq N_t - 1} \left\{ \|\alpha^{[n]}\|_{\ell^\infty}, 1 \right\} &\leq \text{diam}(\mathcal{P}_\alpha^{[N_t - 1]}) \leq 2 \max_{0 \leq n \leq N_t - 1} \left\{ \|\alpha^{[n]}\|_{\ell^\infty}, 1 \right\}, \\ \max_{0 \leq n \leq N_t - 1} \left\{ \|\beta^{[n]}\|_{\ell^\infty}, 1 \right\} &\leq \text{diam}(\mathcal{P}_\beta^{[N_t - 1]}) \leq 2 \max_{0 \leq n \leq N_t - 1} \left\{ \|\beta^{[n]}\|_{\ell^\infty}, 1 \right\}. \end{aligned}$$

Thus, $\max \left\{ \text{diam}(\mathcal{P}_\alpha^{[N_t - 1]}), \text{diam}(\mathcal{P}_\beta^{[N_t - 1]}) \right\} \leq 2 \max \{ \|W\|_{\ell^\infty}, 1 \}$. A direct application of Lemma D.6 then gives

$$\begin{aligned} &\left\| \frac{\partial \text{Cost}_{\mathcal{D}}(W)}{\partial W} \right\|_{\ell^\infty} \\ &\leq \frac{\Gamma^3}{\sqrt{3}} \cdot \left(1 + \sqrt{3} \Gamma^2 \right)^{N_t - n - 1} \cdot \sqrt{8N_u \text{Cost}_{\mathcal{D}}} \cdot \max \left\{ \text{diam}(\mathcal{P}_\alpha^{[N_t - 1]}), \text{diam}(\mathcal{P}_\beta^{[N_t - 1]}) \right\} \\ &\leq 2 \cdot \frac{\Gamma^3}{\sqrt{3}} \cdot \left(1 + \sqrt{3} \Gamma^2 \right)^{N_t - n - 1} \cdot \sqrt{8N_u \text{Cost}_{\mathcal{D}}} \cdot \max \{ \|W\|_{\ell^\infty}, 1 \}. \end{aligned}$$

Finally, an application of Lemma D.7 with

$$K = 1, \quad \text{and} \quad C_q = 2 \cdot \frac{\Gamma^3}{\sqrt{3}} \cdot \left(1 + \sqrt{3} \Gamma^2 \right)^{N_t - n - 1} \cdot \sqrt{8N_u \text{Cost}_{\mathcal{D}}(W_q)}$$

establishes the result. ■

References

- Samuel M Allen and John W Cahn. A microscopic theory for antiphase boundary motion and its application to antiphase domain coarsening. *Acta metallurgica*, 27(6):1085–1095, 1979.
- S. B. Angenent, J. Mallet-Paret, and L. A. Peletier. Stable transition layers in a semilinear boundary value problem. *J. Differential Equations*, 67(2):212–242, 1987. ISSN 0022-0396. doi: 10.1016/0022-0396(87)90147-1. URL [https://doi.org/10.1016/0022-0396\(87\)90147-1](https://doi.org/10.1016/0022-0396(87)90147-1).
- D. G. Aronson and H. F. Weinberger. Multidimensional nonlinear diffusion arising in population genetics. *Adv. in Math.*, 30(1):33–76, 1978. ISSN 0001-8708. doi: 10.1016/0001-8708(78)90130-5. URL [https://doi.org/10.1016/0001-8708\(78\)90130-5](https://doi.org/10.1016/0001-8708(78)90130-5).
- Y. Bengio. Learning deep architectures for ai. *Foundations*, 2:1–55, 01 2009. doi: 10.1561/22000000006.
- Yoshua Bengio, Patrice Simard, and Paolo Frasconi. Learning long-term dependencies with gradient descent is difficult. *IEEE transactions on neural networks*, 5(2):157–166, 1994.
- Christopher M. Bishop. *Pattern recognition and machine learning*. Information Science and Statistics. Springer, New York, 2006. ISBN 978-0387-31073-2; 0-387-31073-8. doi: 10.1007/978-0-387-45528-0. URL <https://doi.org/10.1007/978-0-387-45528-0>.

- Stéphane Boucheron, Olivier Bousquet, and Gábor Lugosi. Theory of classification: a survey of some recent advances. *ESAIM Probab. Stat.*, 9:323–375, 2005. ISSN 1292-8100. doi: 10.1051/ps:2005018. URL <https://doi.org/10.1051/ps:2005018>.
- Alberto Bressan and Benedetto Piccoli. *Introduction to the mathematical theory of control*, volume 2 of *AIMS Series on Applied Mathematics*. American Institute of Mathematical Sciences (AIMS), Springfield, MO, 2007. ISBN 978-1-60133-002-4; 1-60133-002-2.
- Steven L Brunton and J Nathan Kutz. *Data-driven science and engineering: Machine learning, dynamical systems, and control*. Cambridge University Press, 2019.
- José A Carrillo, Robert J McCann, and Cédric Villani. Contractions in the 2-wasserstein length space and thermalization of granular media. *Archive for Rational Mechanics and Analysis*, 179(2):217–263, 2006.
- Richard G. Casten and Charles J. Holland. Instability results for reaction diffusion equations with Neumann boundary conditions. *J. Differential Equations*, 27(2):266–273, 1978. ISSN 0022-0396. doi: 10.1016/0022-0396(78)90033-5. URL [https://doi.org/10.1016/0022-0396\(78\)90033-5](https://doi.org/10.1016/0022-0396(78)90033-5).
- Nathaniel Chafee. Asymptotic behavior for solutions of a one-dimensional parabolic equation with homogeneous Neumann boundary conditions. *J. Differential Equations*, 18:111–134, 1975. ISSN 0022-0396. doi: 10.1016/0022-0396(75)90084-4. URL [https://doi.org/10.1016/0022-0396\(75\)90084-4](https://doi.org/10.1016/0022-0396(75)90084-4).
- Pratik Chaudhari, Adam Oberman, Stanley Osher, Stefano Soatto, and Guillaume Carlier. Deep relaxation: partial differential equations for optimizing deep neural networks. *Res. Math. Sci.*, 5(3): Paper No. 30, 30, 2018. ISSN 2522-0144. doi: 10.1007/s40687-018-0148-y. URL <https://doi.org/10.1007/s40687-018-0148-y>.
- Anna Choromanska, Mikael Henaff, Michael Mathieu, Gérard Ben Arous, and Yann LeCun. The loss surfaces of multilayer networks. In *Artificial intelligence and statistics*, pages 192–204, 2015.
- K. N. Chueh, C. C. Conley, and J. A. Smoller. Positively invariant regions for systems of nonlinear diffusion equations. *Indiana Univ. Math. J.*, 26(2):373–392, 1977. ISSN 0022-2518. doi: 10.1512/iumj.1977.26.26029. URL <https://doi.org/10.1512/iumj.1977.26.26029>.
- Felipe Cucker and Steve Smale. On the mathematical foundations of learning. *Bulletin of the American mathematical society*, 39(1):1–49, 2002.
- Ingrid Daubechies, Ronald DeVore, Simon Foucart, Boris Hanin, and Guergana Petrova. Nonlinear approximation and (deep) relu networks. *arXiv preprint arXiv:1905.02199*, 2019.
- Mark R. Dennis, Paul Glendinning, Paul A. Martin, Fadil Santosa, and Jared Tanner, editors. *The Princeton companion to applied mathematics*. Princeton University Press, Princeton, NJ, 2015. ISBN 978-0-691-15039-0. doi: 10.1515/9781400874477. URL <https://doi.org/10.1515/9781400874477>.
- L. Desvillettes and C. Villani. On the trend to global equilibrium for spatially inhomogeneous kinetic systems: the Boltzmann equation. *Invent. Math.*, 159(2):245–316, 2005. ISSN 0020-9910. doi: 10.1007/s00222-004-0389-9. URL <https://doi.org/10.1007/s00222-004-0389-9>.
- Luc Devroye, László Györfi, and Gábor Lugosi. *A probabilistic theory of pattern recognition*, volume 31 of *Applications of Mathematics (New York)*. Springer-Verlag, New York, 1996. ISBN 0-387-94618-7. doi: 10.1007/978-1-4612-0711-5. URL <https://doi.org/10.1007/978-1-4612-0711-5>.

- Harry Dym. *Linear algebra in action*, volume 78 of *Graduate Studies in Mathematics*. American Mathematical Society, Providence, RI, 2007. ISBN 978-0-8218-3813-6; 0-8218-3813-X.
- David J Eyre. An unconditionally stable one-step scheme for gradient systems. *Unpublished article*, pages 1–15, 1998.
- Paul C. Fife. *Mathematical aspects of reacting and diffusing systems*, volume 28 of *Lecture Notes in Biomathematics*. Springer-Verlag, Berlin-New York, 1979. ISBN 3-540-09117-3.
- Walter Gautschi. How (un) stable are vandermonde systems. *Asymptotic and computational analysis*, 124:193–210, 1990.
- Stuart Geman and Donald Geman. Stochastic relaxation, gibbs distributions, and the bayesian restoration of images. *IEEE Transactions on pattern analysis and machine intelligence*, (6):721–741, 1984.
- David Gilbarg and Neil S. Trudinger. *Elliptic partial differential equations of second order*, volume 224 of *Grundlehren der Mathematischen Wissenschaften [Fundamental Principles of Mathematical Sciences]*. Springer-Verlag, Berlin, second edition, 1983. ISBN 3-540-13025-X. doi: 10.1007/978-3-642-61798-0. URL <http://dx.doi.org/10.1007/978-3-642-61798-0>.
- Federico Girosi, Michael Jones, and Tomaso Poggio. Regularization theory and neural networks architectures. *Neural Computation*, 7(2):219–269, 1995. doi: 10.1162/neco.1995.7.2.219. URL <https://doi.org/10.1162/neco.1995.7.2.219>.
- Xavier Glorot and Yoshua Bengio. Understanding the difficulty of training deep feedforward neural networks. In *Proceedings of the thirteenth international conference on artificial intelligence and statistics*, pages 249–256, 2010.
- Gene H. Golub and Charles F. Van Loan. *Matrix computations*. Johns Hopkins Studies in the Mathematical Sciences. Johns Hopkins University Press, Baltimore, MD, third edition, 1996. ISBN 0-8018-5413-X; 0-8018-5414-8.
- Ian Goodfellow, Yoshua Bengio, and Aaron Courville. *Deep learning*. Adaptive Computation and Machine Learning. MIT Press, Cambridge, MA, 2016. ISBN 978-0-262-03561-3.
- Jack K. Hale. *Asymptotic behavior of dissipative systems*, volume 25 of *Mathematical Surveys and Monographs*. American Mathematical Society, Providence, RI, 1988. ISBN 0-8218-1527-X.
- Trevor Hastie, Robert Tibshirani, and Jerome Friedman. *The elements of statistical learning*. Springer Series in Statistics. Springer-Verlag, New York, 2001. ISBN 0-387-95284-5. doi: 10.1007/978-0-387-21606-5. URL <https://doi.org/10.1007/978-0-387-21606-5>. Data mining, inference, and prediction.
- Geoffrey E Hinton and Steven J Nowlan. How learning can guide evolution. *Complex systems*, 1(3): 495–502, 1987.
- Morris W. Hirsch and Stephen Smale. *Differential equations, dynamical systems, and linear algebra*. Academic Press [A subsidiary of Harcourt Brace Jovanovich, Publishers], New York-London, 1974. Pure and Applied Mathematics, Vol. 60.
- David Hoff. Stability and convergence of finite difference methods for systems of nonlinear reaction-diffusion equations. *SIAM J. Numer. Anal.*, 15(6):1161–1177, 1978. ISSN 0036-1429. doi: 10.1137/0715077. URL <https://doi.org/10.1137/0715077>.

- Elad Hoffer, Itay Hubara, and Daniel Soudry. Train longer, generalize better: closing the generalization gap in large batch training of neural networks. In I. Guyon, U. V. Luxburg, S. Bengio, H. Wallach, R. Fergus, S. Vishwanathan, and R. Garnett, editors, *Advances in Neural Information Processing Systems 30*, pages 1731–1741. Curran Associates, Inc., 2017. URL <http://papers.nips.cc/paper/6770-train-longer-generalize-better-closing-the-generalization-gap-in-large-batch-training-of-neural-networks.pdf>.
- Yanping Huang, Youlong Cheng, Ankur Bapna, Orhan Firat, Dehao Chen, Mia Chen, HyoukJoong Lee, Jiquan Ngiam, Quoc V Le, Yonghui Wu, and zhifeng Chen. Gpipe: Efficient training of giant neural networks using pipeline parallelism. In H. Wallach, H. Larochelle, A. Beygelzimer, F. Alché-Buc, E. Fox, and R. Garnett, editors, *Advances in Neural Information Processing Systems 32*, pages 103–112. Curran Associates, Inc., 2019. URL <http://papers.nips.cc/paper/8305-gpipe-efficient-training-of-giant-neural-networks-using-pipeline-parallelism.pdf>.
- D. H. Hubel and T. N. Wiesel. Receptive fields, binocular interaction and functional architecture in the cat’s visual cortex. *The Journal of Physiology*, 160(1):106–154, 1962. doi: 10.1113/jphysiol.1962.sp006837. URL <https://physoc.onlinelibrary.wiley.com/doi/abs/10.1113/jphysiol.1962.sp006837>.
- Arieh Iserles. *A first course in the numerical analysis of differential equations*. Cambridge Texts in Applied Mathematics. Cambridge University Press, Cambridge, second edition, 2009. ISBN 978-0-521-73490-5.
- Tosio Kato. *Perturbation theory for linear operators*. Classics in Mathematics. Springer-Verlag, Berlin, 1995. ISBN 3-540-58661-X. Reprint of the 1980 edition.
- Joseph B. Keller. Inverse problems. *The American Mathematical Monthly*, 83(2):107–118, 1976. doi: 10.1080/00029890.1976.11994053. URL <https://doi.org/10.1080/00029890.1976.11994053>.
- Yann LeCun, D Touresky, G Hinton, and T Sejnowski. A theoretical framework for back-propagation. In *Proceedings of the 1988 connectionist models summer school*, volume 1, pages 21–28. CMU, Pittsburgh, Pa: Morgan Kaufmann, 1988.
- Yann Lecun, Léon Bottou, Yoshua Bengio, and Patrick Haffner. Gradient-based learning applied to document recognition. In *Proceedings of the IEEE*, pages 2278–2324, 1998.
- Yann LeCun, Yoshua Bengio, and Geoffrey Hinton. Deep learning. *Nature*, 521(7553):436–444, 2015. ISSN 1476-4687. doi: 10.1038/nature14539. URL <https://doi.org/10.1038/nature14539>.
- Yann A. LeCun, Léon Bottou, Genevieve B. Orr, and Klaus-Robert Müller. *Efficient BackProp*, pages 9–48. Springer Berlin Heidelberg, Berlin, Heidelberg, 2012. ISBN 978-3-642-35289-8. doi: 10.1007/978-3-642-35289-8_3. URL https://doi.org/10.1007/978-3-642-35289-8_3.
- Qianxiao Li, Long Chen, Cheng Tai, and Weinan E. Maximum principle based algorithms for deep learning. *J. Mach. Learn. Res.*, 18:Paper No. 165, 29, 2017. ISSN 1532-4435.
- Dominic Masters and Carlo Luschi. Revisiting small batch training for deep neural networks. *arXiv preprint arXiv:1804.07612*, 2018.
- Song Mei, Andrea Montanari, and Phan-Minh Nguyen. A mean field view of the landscape of two-layer neural networks. *Proceedings of the National Academy of Sciences*, 115(33):E7665–E7671, 2018.
- Mehryar Mohri, Afshin Rostamizadeh, and Ameet Talwalkar. *Foundations of machine learning*. Adaptive Computation and Machine Learning. MIT Press, Cambridge, MA, 2018. ISBN 978-0-262-03940-6. Second edition of [MR3057769].

- Martin Fodslette Møller. A scaled conjugate gradient algorithm for fast supervised learning. *Neural Networks*, 6(4):525–533, 1993.
- Rafael Monteiro. Data repository for the paper “Binary classification as a phase separation process”. <https://dx.doi.org/10.5281/zenodo.4005131>, September 2020a.
- Rafael Monteiro. Source code for the paper “Binary classification as a phase separation process”. https://github.com/rafael-a-monteiro-math/Binary_classification_phase_separation, September 2020b.
- David Mumford. Issues in the mathematical modeling of cortical functioning and thought. In *The Legacy of Norbert Wiener: A Centennial Symposium (Cambridge, MA, 1994)*, volume 60 of *Proc. Sympos. Pure Math.*, pages 235–260. Amer. Math. Soc., Providence, RI, 1997. doi: 10.1090/pspum/060/1460286. URL <https://doi.org/10.1090/pspum/060/1460286>.
- János Neumann, Arthur W Burks, et al. *Theory of self-reproducing automata*, volume 1102024. University of Illinois Press Urbana, 1966.
- Wei-Ming Ni. *The mathematics of diffusion*, volume 82 of *CBMS-NSF Regional Conference Series in Applied Mathematics*. Society for Industrial and Applied Mathematics (SIAM), Philadelphia, PA, 2011. ISBN 978-1-611971-96-5. doi: 10.1137/1.9781611971972. URL <https://doi.org/10.1137/1.9781611971972>.
- Yasumasa Nishiura. *Far-from-equilibrium dynamics*, volume 209 of *Translations of Mathematical Monographs*. American Mathematical Society, Providence, RI, 2002. ISBN 0-8218-2625-5. Translated from the 1999 Japanese original by Kunimochi Sakamoto, Iwanami Series in Modern Mathematics.
- Steven J. Nowlan and Geoffrey E. Hinton. Simplifying neural networks by soft weight-sharing. *Neural Computation*, 4(4):473–493, 1992. doi: 10.1162/neco.1992.4.4.473. URL <https://doi.org/10.1162/neco.1992.4.4.473>.
- Alessio Porretta and Enrique Zuazua. Numerical hypocoercivity for the kolmogorov equation. *Mathematics of Computation*, 86(303):97–119, 2017.
- Lutz Prechelt. *Early Stopping - But When?*, pages 55–69. Springer Berlin Heidelberg, Berlin, Heidelberg, 1998. ISBN 978-3-540-49430-0. doi: 10.1007/3-540-49430-8_3. URL https://doi.org/10.1007/3-540-49430-8_3.
- Jeffrey Rauch and Joel Smoller. Qualitative theory of the FitzHugh-Nagumo equations. *Advances in Math.*, 27(1):12–44, 1978. ISSN 0001-8708. doi: 10.1016/0001-8708(78)90075-0. URL [https://doi.org/10.1016/0001-8708\(78\)90075-0](https://doi.org/10.1016/0001-8708(78)90075-0).
- Robert D. Richtmyer and K. W. Morton. *Difference methods for initial-value problems*. Second edition. Interscience Tracts in Pure and Applied Mathematics, No. 4. Interscience Publishers John Wiley & Sons, Inc., New York-London-Sydney, 1967.
- Carlos Rocha. Examples of attractors in scalar reaction-diffusion equations. *J. Differential Equations*, 73(1):178–195, 1988. ISSN 0022-0396. doi: 10.1016/0022-0396(88)90124-6. URL [https://doi.org/10.1016/0022-0396\(88\)90124-6](https://doi.org/10.1016/0022-0396(88)90124-6).
- David E. Rumelhart, Geoffrey E. Hinton, and Ronald J. Williams. Learning representations by back-propagating errors. *Nature*, 323(6088):533–536, 1986. ISSN 1476-4687. doi: 10.1038/323533a0. URL <https://doi.org/10.1038/323533a0>.

- Levent Sagun, Leon Bottou, and Yann LeCun. Eigenvalues of the hessian in deep learning: Singularity and beyond. *arXiv preprint arXiv:1611.07476*, 2016.
- Carola-Bibiane Schönlieb and Andrea Bertozzi. Unconditionally stable schemes for higher order inpainting. *Commun. Math. Sci.*, 9(2):413–457, 2011. ISSN 1539-6746. URL <http://projecteuclid.org/euclid.cms/1305034461>.
- Shai Shalev-Shwartz and Shai Ben-David. *Understanding Machine Learning: From Theory to Algorithms*. Cambridge University Press, USA, 2014. ISBN 1107057132.
- Linda G Shapiro and George C Stockman. *Computer vision*. Prentice Hall, 2001.
- Joel Smoller. *Shock waves and reaction-diffusion equations*, volume 258 of *Grundlehren der Mathematischen Wissenschaften [Fundamental Principles of Mathematical Sciences]*. Springer-Verlag, New York, second edition, 1994. ISBN 0-387-94259-9. doi: 10.1007/978-1-4612-0873-0. URL <http://dx.doi.org/10.1007/978-1-4612-0873-0>.
- John C. Strikwerda. *Finite difference schemes and partial differential equations*. The Wadsworth & Brooks/Cole Mathematics Series. Wadsworth & Brooks/Cole Advanced Books & Software, Pacific Grove, CA, 1989. ISBN 0-534-09984-X.
- Richard S. Sutton and Andrew G. Barto. *Reinforcement learning: an introduction*. Adaptive Computation and Machine Learning. MIT Press, Cambridge, MA, second edition, 2018. ISBN 978-0-262-03924-6.
- Lloyd N. Trefethen. *Spectral methods in MATLAB*, volume 10 of *Software, Environments, and Tools*. Society for Industrial and Applied Mathematics (SIAM), Philadelphia, PA, 2000. ISBN 0-89871-465-6. doi: 10.1137/1.9780898719598. URL <https://doi.org/10.1137/1.9780898719598>.
- Lloyd N. Trefethen and David Bau, III. *Numerical linear algebra*. Society for Industrial and Applied Mathematics (SIAM), Philadelphia, PA, 1997. ISBN 0-89871-361-7. doi: 10.1137/1.9780898719574. URL <https://doi.org/10.1137/1.9780898719574>.
- Peter JM Van Laarhoven and Emile HL Aarts. Simulated annealing. In *Simulated annealing: Theory and applications*, pages 7–15. Springer, 1987.
- Yuan Yao, Lorenzo Rosasco, and Andrea Caponnetto. On early stopping in gradient descent learning. *Constructive Approximation*, 26(2):289–315, 2007.
- EC Zeeman. Brain modelling. In *Structural Stability, The Theory of Catastrophes, and Applications in the Sciences*, pages 367–372. Springer, 1976.